The neutron resonance reactions in thermal nuclear reactors determined by semi-analytic as well as numerical methods

Mikkelsen, J.

Publication date:
1970

Document Version
Publisher's PDF, also known as Version of record

Risø Report No. 234

Danish Atomic Energy Commission

Research Establishment Risö

The Neutron Resonance Reactions in Thermal Nuclear Reactors Determined by Semi-Analytic as well as Numerical Methods

by Jörn Mikkelsen

November, 1970

Sales distributors: Jul. Gjellerup, 87, Sölvgade, DK 1307 Copenhagen K, Denmark
Available on exchange from: Library, Danish Atomic Energy Commission, Risö, DK-4000 Roskilde, Denmark

The Neutron Resonance Reactions in Thermal Nuclear Reactors Determined by Semi-Analytic as well as Numerical Methods

by

Jörn Mikkelsen

Danish Atomic Energy Commission
Research Establishment Risø
Reactor Physics Department

Abstract

Methods for calculation of the neutron resonance reactions in thermal nuclear reactors are developed, verified against experiments and mutually compared. The intention is partly to demonstrate the potential of modern computation technique in this field and partly to select those methods among the primitive approximations that show the best agreement with sophisticated calculations. The methods investigated comprise intermediate resonance semi-analytic methods, statistical treatment and numerical heterogeneous or homogeneous slowing-down calculation with resonance overlap included or excluded. The influence of detailed spatial flux distribution, the accuracy of the equivalence principles and methods of constructing effective group cross sections from simple resonance integral tabulations have received special attention. It is concluded that the best way to profit from the improved resonance reaction treatments in standard multi-group reactor computation is to make use of tabulations as those just mentioned. Apart from summarizing of these studies the report describes the RESAB programme system developed in connection with the investigation.

This report was written in partial fulfillment of the requirements for obtaining the Ph. D. (lic. techn.) degree.

CONTENTS

Page

1. INTRODUCTION

Modern reactor design shows a tendency towards a reduction in the safety margins with improved economy as a consequence. Among other things this gives rise to a demand for more accurate reactivity predictions and quantities such as temperature and void coefficients must be well known. The epithermal neutron absorption, the so-called resonance absorption, which is the topic of the present work, is one of the effects for which accurate information is of importance in this connection. Furthermore the capture and fission during neutron moderation constitutes a field within neutronic reactor physics where the calculational technique in certain respect is still rather rough.

It has long been common practice to use more or less sophisticated analytic approximations in the description of the flux depression through a resonance with the consequence that the nucleonic and the neutronic calculations are inseparable. This restricts the flexibility of both calculations and therefore reduces the attainable accuracy.

During the last few years the resonance reactions have attracted great attention in connection with fast-reactor research. Here the efforts concentrate on the variation in the resonance reactions with fuel temperature (the Doppler effect) because this effect without delay influences the reactivity after an increase in the neutron flux level. The GENEX/SDR group of programmes produced by Brissenden and Durston constitutes pioneering work in this field. The present treatment, which concerns thermal-reactor calculations, profits by the methods developed in the fast-reactor analysis. Detailed numerical integration of the heterogeneous slowing-down equation is introduced, and accurate cross section calculation completely separated from the neutronic computation is applied.

In 1968 Lewis and Adler showed that for some graphite-moderated reactor lattices resonance integral calculations based on the assumption of constant flux within each homogeneous material region, the so-called flat flux approximation, are not very accurate. By means of the multiregion collision probability technique the validity of the flat flux assumption is investigated below for isolated humps and lattices moderated with graphite, and heavy- and light-water.

Apart from these numerical investigations the frequently used analytic approximation, the intermediate resonance approximation, will studied with emphasis on the scattering interference which is usually more or less neglected in the approximate resonance treatments. The large effect

of the scattering interference for strongly scattering resonances established by the numerical computation was the incitation to this part of the work.

The equivalence principles connecting heterogeneous systems with homogeneous cases were analysed, and the accuracy of the methods for calculation of effective epithermal group cross sections introduced in the WIMS code by Askew was investigated for regular lattices.

Determination of the neutron multiplication factor with an accuracy of about one per cent is frequently desired. Part of the objective of the present treatment of the resonance absorption was to produce effective epithermal cross sections that comply with this accuracy requirement. In a modern light-water reactor with a resonance escape probability, p, of e.g. 0.7, this means that the resonance absorption proportional to 1-p must be determined with an accuracy of at least three per cent, which is of the same order of magnitude as most of the effects neglected in ordinary resonance absorption theory. Contrary to the multiplication factor the variation in the plutonium content during irradiation depends on 1-p rather than on p, for which reason accurate burn-up predictions are even more difficult to obtain. However, the required accuracy is correspondingly smaller.

In connection with the investigation a programme system, RESAB, written in ILLINOIS ALGOL for the IBM 7094 [1] computer was developed.

Certain parts of the work were previously described in four publications (refs. A, B, C and D), and only the outlines are repeated in the present report.

2. CALCULATION PRINCIPLES

2.1. The Resonance Integral and the Resonance Escape Probability

The resonance reaction rate is determined by means of the epithermal energy integral of the detailed reaction cross section multiplied by the detailed flux. If the flux per unit lethargy is normalized to one above the energy interval under consideration, the reaction rate is called the resonance integral, RI. Flux disturbances connected with the over-all reactor problem are neglected here.

Often a modified resonance integral definition is applied (RI'). Instead of taking into account the accumulated reduction in the neutron source during the slowing-down process (due to the resonance absorption itself), the flux between the resonances is forced to reproduce the asymptotic 1/E-flux occurring in the absence of the resonances. The total resonance escape probability, p, may here be calculated by means of a simple formula that from the resonance integral determines the product of the escape probabilities of the individual resonances. In this way the slow variation in flux with energy caused by the accumulated resonance absorption is, nevertheless, taken into account. (This material is discussed in detail in section 4.3.).

In ordinary two-group theory p appears directly in the coupled differential equations that describe the over-all flux distribution in the reactor.

2.2. Effective Group Cross Sections

When multi-group theory is applied, other spectrum effects than those originating in the epithermal absorption itself influence the resonance reaction rate (e.g. the neutron leakage). For this purpose the partial resonance integrals determined in the rather narrow groups are converted into effective group cross sections. In the multi-group treatment these cross sections are then multiplied by the actual reactor fluxes in the groups.

The effective reaction cross sections are obtained by dividing the partial resonance integrals by the academic group fluxes underlying the resonance integral calculation. The resonance integrals are more difficult to determine accurately than the fluxes because the resonance reactions take place just where the flux varies drastically on account of the resonances. A large portion of the report is therefore concerned with the resonance integrals, while the discussion of the conversion into group cross sections is restricted to one chapter (chapter 8).

2.3. Illustration of the Problem

The complexity of the detailed fuel material cross section and the corresponding fluxes in an actual power reactor cell is illustrated in figs. 8.10-8.13. The detailed flux in an experimental arrangement is shown in fig. 8.2. These figures comprise only the lowest part of the resonance region. (For ^{238}U the resolved resonance region extends to 3920 eV).

2.4. A Limitation of the Analysis

Only isolated lumps and regular lattices are investigated in the present report. In cluster-type fuel elements like those of heavy-water reactors a great many of the fuel rods are situated at the boundary of the elements, where the surrounding geometry is greatly different from that surrounding rods in an infinite lattice. Neltrup [2] and Leslie and Jonsson [3] have developed approximations that take the cluster effects into account. Furthermore fast and rather accurate procedures for calculation of the collision probability matrix in annular symmetric clusters now exist [4, 5]. An estimate of the computer time necessary for performance of a numerical slowing-down calculation by means of these collision probabilities combined with the SDP routine mentioned below indicates that such reference calculations are practicable.

In a light-water reactor fuel box rather few fuel pins are situated at the element boundary. In the Swedish CAROL code [6] an effective Dancoff factor for edge pins is obtained by multiplying of the infinite lattice Dancoff factor by 5/8, while a multiplication by 3/8 is used for a corner pin (square lattice). Lindstrøm Jensen [7] has established that in practical use this intuitive method for treating of the finite lattice works satisfactorily.

2.5. The RESAB Programme System

Practically all calculations described in the present report were performed by means of the RESAB programme system. The purpose of collecting so many calculation methods in one programme system was to facilitate a combination of the methods in a practical computation. The methods should be combined in such a way that the calculation accuracy achieved during a reasonable running time is optimized. Also the testing of the methods against each other is facilitated by means of this programme arrangement.

The programme system consists of three programmes named FILE 1, FILE 2 and FILE 3 that communicate with each other via magnetic tapes.

The link structure of the programme system is shown in fig. 2.1, and the relation between deck names and method descriptions is estbalished in appendix A. The composition of the programme system is described in brief below.

FILE 1

This programme performs the slowing-down calculation. It consists of two parts named SDP (chapter 5) and link ALFA (chapter 4). By means of SDP numerical multi-region collision probability slowing-down calculations are performed throughout the resonance region, while link ALFA comprises a simple, homogeneous slowing-down procedure, RESCOLDENS, together with most of the semi-analytic methods in common use for treating of the resonance reactions.

FILE 2

The cross section tabulations and energy mesh structures applied in SDP are produced by FILE 2 (chapter 3 and section 5.4).

FILE 3

Detailed cross sections and flux spectra determined by SDP are (if wanted) printed on magnetic tape. The plan was to produce a series of small programmes that make use of this information, but until now only one such programme has been developed (FILE 3). This programme controls a digital plotter and produces curves by means of the SDP output tapes (section 8.3.5).

3. DETERMINATION OF NEUTRON CROSS SECTIONS

The task of constructing detailed energy- and temperature-dependent cross sections in the resonance region for all reactor materials is very great, and the available formalisms have presumably not attained their final formulations, at least not for the unresolved resonance region. The situation is especially complicated for fissile nuclides because the resonances are found to be only slightly narrower than their spacing with the consequence that the single-level Breit-Wigner formula usually forms a poor basis for cross section calculations. In late years a channel fission theory [8-10] has been set up, and by means of the closely related so-called R-matrix formalism [11, 12] the cross sections of the main fissile nuclides throughout the resolved resonance region have been described in a more or less approximate form [13-17]. Contrary to the R-matrix treatment the method developed by Adler and Adler [18, 19], which is related to the S-matrix theory [20, 21], leads to cross section formulas that are compatible with the same numerical techniques that are applicable to single-level expressions. However, the sampling of parameters from their distribution functions in the unresolved region causes difficulties in this less fundamental theory [22].

In the present work the cross sections used are based partly on single-level formalism, and partly on multi-level R-matrix treatment in the approximative formulation developed by Buckler and Pull [23]. The main topic of the present investigation is, however, the neutron slowing-down and not the detailed resonance cross section calculation, and for this reason the evaluational effort has been confined to a minimum. In many cases known cross section tabulations are used directly. Of the three internationally available data libraries, ENDF/B, KEDAK and UKNDL, the latter was chosen for this purpose.

3.1. Calculation of Cross Sections from Resonance Parameters

Most approximative slowing-down calculations in the resonance region are based on the analytic representation of the energy-dependent cross sections provided by the single-level Breit-Wigner formalism. In order to introduce the symbolism and physical constants used throughout this report the formulas expressing the Doppler-broadened cross sections are presented here.

$$\sigma_R(E) = \sqrt{\frac{E_r}{E}}\,\sigma_o\,\frac{\Gamma_R}{\Gamma}\,\phi(\theta,x) \quad . \tag{3.1}$$

$$\sigma_S(E) = \sigma_o\,\frac{\Gamma_n}{\Gamma}\,\psi(\theta,x) + d\cdot\sqrt{\frac{\sigma_o\sigma_p\Gamma_n}{\Gamma}}\,g_J\cdot\chi(\theta,x) + \sigma_p \quad . \tag{3.2}$$

$$\Gamma = \Gamma_n + \Gamma_\gamma(+\Gamma_f) \quad , \qquad d = \begin{cases} 1 & \text{s-wave neutrons} \\ 0 & \text{all other neutrons.} \end{cases} \tag{3.3}$$

$\sigma_R(E)$ and $\sigma_S(E)$ are microscopic reaction and scattering cross sections as functions of the energy, E. The reaction may be either radiative capture (γ) or fission (f). σ_p, σ_o, Γ_n, Γ_R, Γ, g_J, and E_r are the potential scattering cross section, peak cross section, neutron width, reaction width, total width, statistical spin factor, and resonance energy respectively.

$$\sigma_o = 2.603\cdot 10^6 \left(\frac{1.00897+A}{A}\right)^2 \frac{\Gamma_n}{\Gamma E_r}\,g_J \quad . \tag{3.4}$$

$$g_J = (2J+1)/2(2I+1) \quad . \tag{3.5}$$

The parenthesis containing the isotopic mass, A, corrects for the transformation from centre of mass system to laboratory system. J and I symbolize the spin quantum number of the compound nucleus and of the target nucleus respectively. The square root in front of σ_o in eq. (3.1) takes into account the neutron width energy variation, whereas the quantity Γ_n is considered independent of the energy. $\phi(\theta,x)$ and $\chi(\theta,x)$ express the Doppler-broadened line shapes, which have been thoroughly investigated by, among others, Dresner [24].

$$\theta = \sqrt{\frac{A\Gamma^2}{4kT_e E_r}} \quad , \qquad k = 8.61\cdot 10^5\ \text{eV/K} \quad . \tag{3.6}$$

$$x = \frac{E-E_r}{\Gamma/2} \tag{3.7}$$

T_e is the effective temperature which takes into account the crystal effects.

$$T_e = \frac{3}{2}\,\theta_D \int_0^1 x^3 \coth(x\,\theta_D/2T)\,dx = T\left[1 + \frac{1}{5}\left(\frac{\theta_D}{2T}\right)^2 + O\left(\left(\frac{\theta_D}{2T}\right)^4\right)\right] . \tag{3.8}$$

where T and θ_D equal absolute and Debye temperature respectively [25,26]. Generally the difference between T and T_e can be disregarded (θ_D = 162 K for U-metal [27]). In the limit of zero temperature

$$\psi(\infty, x) = (1+x^2)^{-1} , \qquad \chi(\infty, x) = 2x(1+x^2)^{-1} . \tag{3.9}$$

In the present work ψ and χ are calculated from the (complementary) error integral with complex argument.

$$2(\psi(\theta, x) + i\,\chi(\theta, x)/2) \,/\, (\theta\sqrt{\pi}) =$$

$$e^{-z^2}\,\mathrm{erfc}(-iz) = w(z) , \qquad z = x\,\theta/2 + i\,\theta/2 . \tag{3.10}$$

$$w(z) = \exp(-z^2)\left[1 + \frac{2i}{\sqrt{\pi}} \int_0^z \exp(t^2)\,dt\right] . \tag{3.11}$$

The method developed by S. Christensen [28,29] has been used for the determination of erfc(z). Some investigations have shown that this method is faster and just as accurate as, for example, a recently developed NASA procedure [30].

Apart from this single-level treatment the RESAB programme system comprises a multi-level procedure, DORES [31], which is used when cross sections are generated over energy intervals containing more than one resonance. The method is identical to that developed by Buckler and Pull [23] and later on used in the programme GENEX [32]. The most serious approximation is connected with the inversion of the level matrix. The explicit expressions that are obtained for the Doppler-broadened cross sections are again analytic, containing the complex error integral, which now, however, must be calculated many times for each energy. In addition to the multi-level effects the method includes in fact a more exact treatment of the Doppler-broadening than the single-level formulas above.

In the calculations that have been performed by means of DORES for fertile nuclides, four consecutive resonances are usually included in the

multi-level treatment, while the single-level "tails" of thirty neighbouring resonances are added. This is perhaps more than strictly necessary, but it ensures that the truncation of the resonances does not affect, for example, the Doppler effect. The inclusion of multi-level effects in the treatment of fertile nuclides has the advantage of reducing the troubles caused by the negative total scattering cross section that may occur if the single-level scattering interference cross sections (cf. the second term in eq. (3.2)) of two resonances are added up at energies lower than both resonance energies. Of course complete multi-level treatment would never result in a negative cross section. Single-level resonance parameters are used in the calculations on fertile nuclides, and this is correct because these parameters are determined from the cross sections around the resonance peaks, where the relative influence of the multi-level effects is negligible.

For fissile nuclides DORES has been used in some test calculations where it was demonstrated that the approximation of Buckler and Pull reproduced rather accurately for instance the multi-level fission cross section of ^{239}Pu determined by Farrel [16] in the energy region from 10 to 85 eV. Complete cross section tabulations have not been compiled as is the case with fertile nuclides, and for this reason all the investigations below are built on known tabulations or single-level analysis. Effects as the Doppler effect of the fissile nuclides, which depend directly on all details in the cross section shape, are not at all important in thermal-reactors. Furthermore, multi-level treatments of such effects have in fact not been very successful until now [32, 33].

3.2. Absorption and Fission Cross Section in the Unresolved Resonance Region

In the unresolved resonance region the available experimental quantities are the average cross sections determined in energy intervals which in principle are much wider than the average level spacing. Because of the self-shielding effect, which depends on the detailed cross section structure, it is in reactor calculations necessary to construct some sort of a resonance model that agrees with the measured average characteristics and at the same time provides the most important features of detailed energy-dependent cross sections.

Measurements in the resolved region as well as theoretical considerations support the assumption that the spacing between adjacent levels with the same values for constants of the motion is distributed like the Wigner

frequency function [34]. This distribution comes approximately from the assertion that the level spacing is the same as the spacing of eigenvalues of a real symmetric matrix with random elements. The widths obey the Porter-Thomas[35] distribution defined as the usual Chi-squared frequency function

$$P(x,\nu)\,dx = \left(\frac{\nu x}{2}\right)^{\frac{\nu}{2}-1} \frac{e^{-\frac{\nu x}{2}}}{\Gamma(\nu/2)}\,\nu/2\,dx \qquad (3.12)$$

$$x = \Gamma_P / \langle \Gamma_P \rangle \quad , \quad P = n,\ \gamma \text{ or } f \ .$$

ν is the number of degrees of freedom determined by the number of channels through which the considered process may occur.

The average level spacing is assumed to be proportional to $1/(2J+1)$, but independent of the orbital angular momentum of the incident neutron (quantum number l) and consequently independent of parity. If D^s_{obs} is the observed average level spacing between all resolved s-wave resonances, it follows now immediately that the distance D^{Jl} between levels with equal J and l may be determined by

$$D^{Jl} = \frac{D^s_{obs}\,2(2I+1)}{2J+1} = \frac{D^s_{obs}}{g_J} \ . \qquad (3.13)$$

The J dependence used here is predicted by the Fermi gas model, provided J is small. Some modifications, appearing when J is about 3 or larger [36], have been disregarded because of the approximative character of the whole theory. D^s_{obs} is determined at low energies. The energy dependence of D^{Jl} is approximated by (cf. ref. 10, p. 128)

$$D^{Jl}(E) = \frac{D^s_{obs}}{g_J}\left(\frac{E+B}{B}\right)^{5/4} \exp\left[\sqrt{\frac{2}{3}}\,\pi\left(\sqrt{g_o B} - \sqrt{g_o(E+B)}\right)\right] . \qquad (3.14)$$

$D^{Jl}(E)$ is normalized according to eq. (3.13) at $E = 0$. B is the neutron-binding energy reduced by the pairing correction on account of the odd - even effect. g_o is the sum of the neutron and proton single-particle level density. Approximately we have

$$g_o = 0.4 \cdot A^{2/3} \ \text{MeV}^{-1} \qquad (3.15)$$

provided A is larger than 220 amu [37]. The exponent of the second term in eq. (3.14) is very uncertain, but this term is fortunately very near to one throughout the resonance region.

The only neutron channel that need be considered is the entrance channel. Any other exit channel would have to have an l-value differing by at least 2 owing to parity conservation, and hence a very small width. s- and p-wave neutrons must be considered, while d-wave neutrons are usually not important. The ratio between average reduced neutron width and average level spacing, the strength function, s^{Jl}, is considered independent of the energy. As indicated here and also in eq. (3.14) there exists an independent series of resonances for each pair of the quantum numbers (J, l). The total strength function for a given l is defined by

$$s_T^l = \frac{1}{2(2l+1)} \sum_{S=|I-\frac{1}{2}|}^{I+\frac{1}{2}} \sum_{J=|l-S|}^{l+S} 2 \cdot g_J \cdot s^{Jl} \quad . \tag{3.16}$$

The strength function per channel-spin projection is assumed independent of the channel spin, S. The same weighting of the individual strength functions as in eq. (3.16) appears in the average total cross section, but for the total capture cross section the weighting of the components is different and not even constant with energy [10]. If it is formally assumed that s^{Jl} is independent of J, it follows that

$$s^{Jl} = s_T^l \quad , \tag{3.17}$$

and this is the equation used here because very little information concerning the individual s^{Jl} is available. However, some analyses of s-wave neutron resonances for target nuclei with $I > 0$ indicate in accordance with theoretical studies that [10]

$$s^{I+\frac{1}{2},0} \neq s^{I-\frac{1}{2},0} \quad .$$

For these arguments determination of total strength functions from average total cross sections does not necessarily provide the best estimate of the effective strength function for calculation of capture cross sections by use of eq. (3.17). Eq. (3.16) indicates that for p-wave neutrons two dif-

ferent channel spins (S) may initiate the formation of one and the same compound state defined by J and l. In such cases it is reasonable to sample the neutron widths from a chi-squared distribution function with two degrees of freedom, and according to eqs. (3.16) and (3.17) the average reduced neutron width must be determined from an effective strength function equal to $2 \cdot s_T^l$. In all other cases ($l < 2$) the neutron widths are distributed like the chi-squared frequency function with one degree of freedom.

When the average reduced neutron widths, $\langle \Gamma_n^o \rangle$, have been determined from s^{Jl}, the neutron widths are obtained by means of a penetration factor [10].

$$\text{s-wave} \qquad \langle \Gamma_n \rangle = \langle \Gamma_n^o \rangle \sqrt{E_r} \ . \tag{3.18}$$

$$\text{p-wave} \qquad \langle \Gamma_n \rangle = \langle \Gamma_n^o \rangle \sqrt{E_r} \, \frac{(ka)^2}{1+(ka)^2} \ . \tag{3.19}$$

a is the channel radius. Approximately we have [10]

$$a = (1.23 \cdot A^{1/3} + 0.8) \text{ fm} \ . \tag{3.20}$$

k symbolizes the wave number in the channel.

$$k = 0.21968 \sqrt{E_r} \sqrt{\frac{A \cdot m}{A+m}} \cdot 10^{-3} \text{ fm}^{-1} \tag{3.21}$$

with m equal to the neutron mass and E_r expressed in eV.

In the capture process the number of exit channels is large, and the distribution of Γ_γ is approximated by a delta-function ($\nu \to \infty$). $\langle \Gamma_\gamma \rangle$ is considered independent of J and l.

In accordance with the channel fission theory the fission width distribution function is assumed to be a chi-squared frequency function with 1, 2, 3, or 4 degrees of freedom depending on the target nucleus, J and l. No attempt to reproduce the energy fluctuations of the α-value in the unresolved region has been made because these are not important for thermal reactor calculations. The energy variation of the average fission width is described by the simple formulas [38]

$$\langle \Gamma_f^{Jl} \rangle = \begin{cases} \Gamma_{f1}^{Jl} \log_{10}(E_r/10^6) + \Gamma_{f2}^{Jl}, & E_r > 150 \text{ eV} \\ \Gamma_{f3}^{Jl} & E_r < 150 \text{ eV} \end{cases} \tag{3.22}$$

In the present work the interference between the resonances is neglected in the unresolved region, and consequently the distribution of spacings does not affect the result. The energy integral of the cross section for a certain reaction extended over one single resonance with the parameters

$$\Gamma_n = x_n \langle \Gamma_n^{Jl} \rangle_{E=E_r}, \quad \Gamma_f = x_f \langle \Gamma_f^{Jl} \rangle_{E=E_r}, \quad \Gamma_\gamma = \langle \Gamma_\gamma \rangle$$

is designated by

$$RS_R^{Jl}(E_r, x_n, x_f) .$$

The average total reaction cross section may now be determined by

$$\sigma_R(E) = \sum_{l=0}^{1} \sum_{J} \frac{1}{D^{Jl}(E)} \int_0^\infty \int_0^\infty RS_R^{Jl}(E, x_n, x_f) \cdot P(\nu_f^{Jl}, x_f) \cdot P(\nu_n^{Jl}, x_n)\, dx_f\, dx_n , \tag{3.23}$$

where the sum over J must include all possible values for the given l and L. ν_f^{Jl} and ν_n^{Jl} are the number of degrees of freedom in the fission and scattering process respectively. If fission is not possible, the integration over dx_f vanishes. The way in which the integrations are actually performed is discussed in section 4.5.1, where the self-shielding is investigated.

A different calculation method is that of sampling a so-called ladder of resonances from the different distribution functions by use of a random number generator and then constructing the detailed cross sections from the determined resonance parameters. The advantage of this method is that more complicated effects may be included, but the problem of selecting the best ladder among the many possible ladders is very complicated and to some extent still unsolved.[15, 39-41]

Above 0.2-0.4 MeV the calculation performed by means of RESAB is only formal as the resonances are now strongly interfering. Actually, it

is also assumed that $k \cdot a \ll 1$, and this assumption is certainly not fulfilled at these high energies (cf. eqs. (3.20) and (3.21)). For fissile isotopes the programme should not be used above 10 keV. This is not a serious limitation because above the mentioned energies there is no self-shielding, and the smooth measured average cross sections may therefore be used without modifications as effective cross sections.

3.3. Present Status of the RESAB Resonance Parameter Library

The developed library of resonance parameters is by no means complete. The choice of materials has not been systematic, but directed by the actual demand of effective epithermal cross sections.

For some elements a joint tabulation has been constructed containing all stable isotopes. It is here assumed that the potential scattering cross section and all statistical parameters of the different isotopes in the unresolved region are approximately equal. The statistical spin factors of the resolved resonances are multiplied by the percentage of the individual isotopes (a_i). It is now possible to determine, for instance, self-shielded effective cross sections for the whole element in one calculation, while alternatively a calculation had to be performed for each isotope and the results added up afterwards. If the resonance parameters are determined by measurement on a sample of the naturally occurring element, one of the primarily obtained parameters is in fact $(a_i \cdot g_J)\Gamma_n^o$. From this the total s-wave strength function for the element, s_T^o, may easily be calculated

$$s_T^o = \sum_i a_i s_{T,i}^o = \frac{\sum_i \sum_{J=|I-1/2|}^{I+1/2} (a_i g_J)\, \Gamma_n^o}{\Delta E} \quad , \tag{3.24}$$

where ΔE is the extension of the resolved region (cf. eq. (3.16)). The sum includes all observed (s-wave) resonances. In the s-wave case it is both for pure elements ($a_1 = 1$) and for mixtures common practice to denote the strength function as determined above by

$$"s_T^o = \langle \Gamma_n^o \rangle / \langle D \rangle" \quad . \tag{3.25}$$

The assumption that the different isotopes of the same element show equal behaviour in the unresolved region is certainly not fulfilled when the iso-

topes have different spins. In such cases the isotopes constituting the natural element are divided into groups each representing one spin.

In the frequently occurring case for $I > 0$ in which J for a resolved s-wave resonance has not been determined, the mean value of g_J equal to 0.5 has been applied, and for resonances with undetermined Γ_f or Γ_γ the average values are used as well.

At low energies the cross sections are calculated as the sum of the "1/v-tails" of the positive energy and possibly one negative energy resonance plus a "pure" 1/v cross section if necessary.

The resolved resonance parameters for fissile nuclides are single-level parameters. Smooth energy-dependent contributions are added to the fission cross sections in order to obtain the partial infirite dilution resonance integrals recommended by Hennies [38]. These additional contributions, which are generally small, may be considered as corrections accounting for multi-level effects. The influence of multi-level effects on the capture cross sections is very small [23], for which reason no smooth contributions are added here. In fact, the experimental information concerning the capture cross sections of the fissile nuclides is rather poor.

The contents of the RESAB library has for ^{238}U and ^{232}Th previously been discussed in two reports [C, D]. Recently the value of s_T^1 for ^{238}U has been changed a little on the basis of a new, highly accurate evaluation of the capture cross section in the statistical region [42]. The main features of the library are summarized in table 3.1 together with the most important references. In table 3.2 the infinite dilution resonance integrals are listed. s_T^0, $\langle \Gamma_\gamma \rangle$ and D_{obs}^s are usually calculated from resolved-region data. As a first estimate of the p-wave strength function, values appearing in the literature have been chosen. But as pointed out in section 3.2, it is quite possible that a value may be determined that suits the reaction model used in RESAB better, for which reason s_T^1 is considered some sort of a fitting parameter. The finally obtained capture cross section in the unresolved region is shown for ^{232}Th in ref. D, fig. 1. From this figure it appears that the energy variation of the average level spacing, which is expressed in eq. (3.14), influences the capture cross section by about 35 per cent at 200 keV. This effect is important for the obtained accordance with the measurements. Another example is shown in fig. 3.1 in the present report. In all cases the determined "effective" p-wave strength function is rather near to the first estimate, a fact which supports the statistical model used, because most of the first chosen values are based on total cross section analysis.

Table 3.1.

A summary of the contents of the RESAB resonance parameter library

DFN	Material	Spin (I)	Number of resolved s-wave resonances *)	Negative energy resonance	σ_γ^{2200} (b)	σ_f^{2200} (b)	Upper limit of resolved region (eV)	Average contents of one isotope ($\sum_i a_i^2$)	D_{obs}^s (eV)	$s_T^o \times 10^4$	$s_T^1 \times 10^4$	$\langle \Gamma_\gamma \rangle$ (meV)	Main references
238	^{238}U	0	188(68)	0	2.71	0	3915	1.00	20.8	0.90	2.1	21.1 **)	37,44,46-51
232	^{232}Th	0	223(30)	1	7.45	0	3940	1.00	17.5	0.69	1.95	23.3	37,44,46-48,52
235	^{235}U	7/2	194(80)	1	101.3	582	143	1.00	0.5	1.03	1.76	47.9	37,38,47,48,53-55
239	^{239}Pu	1/2	98(70)	1	289.4	742	252	1.00	2.3	0.92	1.8	41.6	37,38,47,53,56-58
240	^{240}Pu	0	131(33)	0	282	0.05	2090	1.00	14.7	1.05	1.75	23.2	10,37,44,47,59, 60-61
107109	^{nat}Ag	1/2	365(37)	0	63.6	0	4005	0.50	18.8	0.48	4.0	132	37,43,47,59,62-66
113115	^{nat}In	9/5	18(11)	0	194	0	100	0.92	9.0	0.45	3.0	80	37,43,45,47,59, 63,64
110246	$^{(nat)}Cd$ spin = 0	0	16(3)	0	-	0	1200	0.31	178	0.93	3.5	112	37,47,59,63,64,67
111113	$^{(nat)}Cd$ spin=1/2	1/2	42(18)	0	-	0	870	0.50	35	0.54	3.5	112	
14761 ***)	^{147}Pm	7/2	16(4)	1	230	0	230	1.00	6.8	3.1	1.7	73.4	68-70

*) The numbers in parenthesis indicate the numbers of resonances with individually determined Γ_γ.

**) A series of calculations of total self-shielded resonance integrals has shown that a constant Γ_γ = 24.6 meV leads to the same results as the library above. This is due to the actual distribution of Γ_γ. ($\langle \Gamma_\gamma \rangle$ = 24.5 meV for E_r < 850 eV).

***) Data provided by L. Mortensen, Risö (1970).

Table 3.2.

Infinite dilution resonance integrals calculated by use of the RESAB resonance parameter library and the corresponding experimental results (0.5 - ∞ eV)

Material	Resonance integral (b)		
	RESAB	Experimental	References
^{238}U	281	278(± 10)	71)
^{232}Th	79	81(± 3)	72)
^{235}U	fission: 271 α = 0.63	280(± 11) 0.5-0.6	73) 38)
^{239}Pu	fission: 302 (E < 4.65 eV: ref. 38)	310(± 20)	73)
^{240}Pu	8091	8300(± 1100)	74)
^{nat}Ag	766	752(± 40)	75)
^{nat}In	3181	3235(± 200)	75)
^{147}Pm	2180	2100-3220	76, 77)

α is the capture to fission ratio.

The distinction between resolved and unresolved region is in fact not so well defined as has been pretended until now. Generally very few p-wave resonances are observed in the resolved region even though the statistical treatment indicates that their number should be much larger than the number of s-wave levels. Some recent measurements in the lower part of the resolved region show that this prediction is correct [50,51]. The extremely weak p-wave resonances contribute to the resolved region resonance integral by an amount that is by no means negligible compared with the generally strongly shielded s-wave contribution. This is due to the large number and the lacking self-shielding of the p-wave resonances. Contrary to the usual practice, p-wave resonances are, if possible, removed from the resolved-region data, and then the complete p-wave contribution as determined by statistical treatment is added to the resonance integrals and effective cross sections throughout the resolved region. By this procedure a very smooth transition from the resolved s-wave resonance region to the unresolved region is obtained, and this may be considered a verification of the method. For ^{238}U the capture cross section in the transitional zone has in fig. 3.2 been compared with the low resolution measurement of Moxon [78] in the lower keV-region. The calculated curve shows the average cross section determined in groups containing about 25 s-wave resonances each. The corresponding curve calculated from UKNDL by the Danish ILLINOIS ALGOL version of the GALAXY programme [79], SIGMA, is also indicated. In this latter case the transition from the region with smooth cross section to the region containing a detailed tabulation of the resonance cross section is much more pronounced.

4. THE THEORY OF CALCULATION OF RESONANCE INTEGRALS BY MEANS OF EQUIVALENCE PRINCIPLES

Detailed heterogeneous neutron transport calculations in the resonance region are rather time-consuming even on modern high-speed computers because of the complicated energy dependence of the cross sections. In routine calculations, for example in connection with optimization studies, it is necessary, however, to have a fast method at one's disposal. One way of overcoming this difficulty has been to set up equivalence principles by which the problems are reduced to homogeneous cases. In this section the equivalence principles are deduced for isolated rods and lattices, and fast methods for solving of the resulting homogeneous problems are discussed. Finally, various calculational results are presented. An investigation of the limitations of the method is postponed until the heterogeneous reference method has been discussed in chapter 5.

4.1. The Basic Equation

When the neutron balance is considered, and when it is assumed that the neutrons only change energy by elastic scattering, which is isotropic in the CM system, the integral slowing-down equation in a multi-region lattice cell may immediately be written down in the following form:

$$V_i F_i(u) = \sum_{j=1}^{NOR} V_j P_{ij}(u) \sum_{k=1}^{M_j} \int_{u-\Delta_{jk}}^{u} \frac{\Sigma_{Sjk}(u')}{\Sigma_{Tj}(u')} F_j(u') \frac{e^{u'-u}}{1-\alpha_{jk}} du' \quad (4.1)$$

Here

- u = lethargy.
- V_i = volume of region i.
- $\Sigma_{Sjk}(u')$ = macroscopic scattering cross section of isotope k in region j at lethargy u'.
- $\Sigma_{Tj}(u')$ = total macroscopic cross section in region j at lethargy u'.
- $F_i(u)$ = average collision density per unit lethargy in region i at lethargy u ($= \varphi_i(u)\, \Sigma_{Ti}(u)$, where $\varphi_i(u)$ is the average flux per unit lethargy in the same region).

α_{jk} = $\left(\frac{A_{jk}-1}{A_{jk}+1}\right)^2$, A_{jk} = mass of isotope number k in region j.

Δ_{jk} = $\log(1/\alpha_{jk})$.

NOR = number of regions.

M_j = number of isotopes in region j.

$P_{ij}(u)$ = probability that a neutron born in region j at lethargy u will first collide in region i.

In the calculation of the spatial distribution all scattering processes are considered isotropic in the laboratory system. On these assumptions eq. (4. 1) is exact if the collision probabilities depend on the source distribution inside the regions. In practice, however, the calculation is based on the so-called flat flux approximation, and flux variations inside each material region may only be taken into account by introduction of a suitable number of subregions. Such a subdivision is usually not performed in resonance absorption calculations, and one may wonder why reasonable results can, nevertheless, be obtained. Generally it is a requirement in collision probability theory that the optical thickness of each region is in the order of one, and this condition is certainly not fulfilled near a resonance top. However, the source of the flux at the resonance energy originates mainly from the energy regions between the resonances, where the flux is almost flat throughout the cell, and therefore the flat flux assumption for each material region is justifiable. This is also the reason why the anisotropic moderator scattering in the laboratory system may usually be neglected. In chapter 7 the consequences of these approximations are discussed in detail.

Equation (4. 1) is solved with the boundary condition that the flux is unity in all space and at all lethargies down to a certain energy above which it is assumed that no resonance reactions take place. In practice this function approximates the flux in the energy region below the important part of the fission spectrum and above the resonance region very well, but as mentioned it is also a good approximation to the flux between the resonances. From the determined collision densities the resonance integrals, RI_{Rjk}, for a specified lethargy interval may be calculated:

$$N_{jk} \cdot RI_{Rjk} = \int_{u_1}^{u_2} \frac{\Sigma_{Rjk}(u)}{\Sigma_{Tj}(u)} F_j(u)\, du \quad , \qquad (4.2)$$

where N_{jk} is the number density of isotope number k in region j, and $\Sigma_{Rjk}(u)$ is the reaction cross section for the process considered.

4.2. Calculation of Collision Probabilities (P_{ij})

The aim of this section is not only to introduce the formulas which are used to derive the equivalence relations, but also to discuss briefly methods of calculating collision probabilities suitable for numerical slowing-down calculations.

4.2.1. Exact Collision Probabilities

On the assumption of flat sources, the collision probabilities in a cylindricalized cell may be calculated exactly by the so-called Flurig scheme introduced by Carlvik [80].

In the present work a procedure developed by Neltrup [81] on the basis of this method has been applied. In this procedure the white boundary conditions on the outer surface are used. Some resonance integral investigations have shown that five Gauss points must be introduced in each region if subdivision is not performed, while two points suffice when a reasonable number of subregions are used.

The effect of cylindricalization is examined below by means of an infinite square lattice collision probability routine prepared by Kirkegaard [82]. An approach inspired by Carlvik [83] is used.

Finally, an exact multi-region slab-geometry, collision probability procedure has been applied in a few investigations in chapter 6.

4.2.2. The Two-Region Problem

When eq. (4.1) is solved with the flat flux assumption, the reactor cell is usually described by a two-region model. The collision probability matrix contains four elements, but if one of these is known, all the others may easily be calculated by means of the neutron balance and the reciprocity theorem.

$$P_{2j} + P_{1j} = 1, \quad \Sigma_{T2}V_2P_{12} = \Sigma_{T1}V_1P_{21} \ . \tag{4.3}$$

Below it is assumed that region 1 is the fuel zone.

4.2.3. The Isolated Fuel Rod

Besides exact calculation the following rational approximations are

applied.

$$p_o = \frac{\bar{l}}{\bar{l}+a} \tag{4.4}$$

and

$$p_o = k \frac{\bar{l}}{\bar{l}+a} + (1-k) \frac{\bar{l}}{\bar{l}+b} \ . \tag{4.5}$$

$p_o = P_{11}$ for an isolated rod.

$$\bar{l} = 4\Sigma_{T1} V_1 / S_1 = \sigma_t / \sigma_{ex} \ , \tag{4.6}$$

where

$$\sigma_t = \Sigma_{T1}/N_o \quad \text{and} \quad \sigma_{ex} = S_1/(4N_o V_1) \ .$$

$\bar{l}$ is the optical mean chord length of the infinite cylinder, and S_1/V_1 is the surface to mass ratio of the rod. N_o symbolizes the absorber number density. The expression (4.4) is known as Wigner's rational approximation if the so-called Bell factor, a, equals one. Constant Bell factors ranging between 1.16 and 1.27 have previously been proposed [84-86]. Bearwood [87] has determined the best values of a as functions of $\bar{l}$ and the fuel scatter cross section by fitting the effective cross section of ^{238}U to the exact results obtained by numerical slowing-down calculations in two regions. From the graphical representation of a found in reference 87, the following analytic expression may be deduced

$$a = 1 + 0.16 \frac{x^{1.27}}{x^{1.27} + 0.48(1-(x/10)^2) \cdot \delta} \ , \tag{4.7}$$

where

$$x_e = \frac{\sigma_{ex}}{5 + \sigma_s} \ ,$$

$$\delta = \begin{cases} 1 \text{ for } x < 10 \\ 0 \text{ for } x \geq 10 \end{cases} \qquad \text{and} \quad \sigma_s = \begin{cases} 0 \text{ for metal} \\ 7.6 \text{ for } UO_2 \end{cases} \ .$$

The combination of eqs. (4.7) and (4.4) is described as the Bell factor

approximation below, while expression (4.5) is designated Carlvik's approximation if a = 2, b = 3 and k = 2 [86]. Other approximations of the same character as eq. (4.5) have been proposed [85, 88, 89], but Carlvik's approximation is as good as any of these.

The accuracy of the different approximations was investigated, and the results are shown in fig. 4.1. It appears from the figure that the Bell factor approximation is not very accurate. Error cancellations must be the reason why good results can be obtained by this approximation, and therefore it is important to bear in mind that the resonance structure of ^{238}U is underlying eq. (4.7).

4.2.4. Non-Isolated Fuel Rod

In order to calculate collision probabilities in a lattice by means of the above-listed isolated rod expressions, the so-called Nordheim's (or Bell's) approximation [90] can be used.

$$P_{11} = 1 - \frac{(1-C_o)(1-p_o)}{1-(1-\bar{l}(1-p_o))C_o} \quad . \tag{4.8}$$

C_o is the Dancoff correction calculated in the limit of black absorber (zero for distant rods). Many authors have examined the accuracy of this formula [90-93]. The approximation is poorest when the optical mean chord of the moderator region is small, but even in this case the maximum error is insignificant as illustrated for a square cell in fig. 4.2. The exact square lattice Dancoff factor is calculated by the Carlvik routine [83] which is contained in the RESAB programme system. Fig. 4.2 presents the effect of cylindricalization and also Brissenden's square lattice approximation [94] is illustrated. Finally, the result obtained with C_o in eq. (4.8) replaced by C_{oe} defined by

$$1-C_{oe} = \begin{cases} (1-C_o)\left[1+0.05(1-C_o)C_o^2\,\dfrac{(\beta\frac{x}{1+x}-\bar{l}/2)^2(1+x)^2}{x+0.33x^2+0.06x^3}\right] & \text{for } \bar{l}/2 < \beta\frac{x}{1+x} \\ 1-C_o & \text{for } \bar{l}/2 \geq \beta\frac{x}{1+x} \end{cases},$$

$$x = \frac{V_2}{1.25\,V_1} \quad \text{and} \quad \beta = 2.6 \ , \tag{4.9}$$

is indicated in the figure. This rather complicated correction was developed on the basis of a series of calculations on different square lattices. The approximation expressed by eqs. (4.8) and (4.9) is denoted a corrected Nord-

heim approximation.

By introduction of the Bell factor approximation in eq. (4. 7) the following formula is obtained

$$P_{11} = \frac{\bar{l}}{\bar{l} + \frac{a(1-C_0)}{1+C_0(a-1)}} \quad . \tag{4. 10}$$

while the use of Carlvik's approximation results in an expression of the form

$$P_{11} = \frac{d\bar{l}}{\bar{l}+r_1} + \frac{(1-d)\bar{l}}{\bar{l}+r_2} \quad . \tag{4. 11}$$

d, r_1 and r_2 are real numbers. The accuracy of the last approximation appears from fig. 4.2. The equivalence principles deduced below are based on eqs. (4. 10) or (4. 11).

4. 3. The Equivalence Principles

The equivalence between homogeneous systems and infinite lattices or isolated rods has been discussed by several authors on the basis of approximations of limited nature[24,84,85,95,96]. The topic is reviewed here in a rather general manner to clarify the inherent approximations.

Eq. (4. 1) is applied in the two-region formulation, and in order to simplify the considerations the system investigated is composed of one absorber (j, k = 0. Cf. eq. (4. 1)) mixed with one moderator (j, k = 1) and surrounded by only one moderating isotope (j, k = 2). From eqs. (4. 1) and (4. 3) it follows that

$$F_1(u) = \frac{\sigma_{T1}(u)}{\sigma_{T2}} (1 - P_{11}(u)) \frac{V_2}{V_1} K_2 F_2(u)$$

$$+ P_{11}(u) \left[K_1 \frac{\sigma_{S1}}{\sigma_{T1}(u)} + K_0 \frac{\sigma_{S0}(u)}{\sigma_{T1}(u)} \right] F_1(u) \tag{4. 12}$$

and

$$V_2/V_1 F_2(u) = (1 - P_{11}(u)) \left[K_0 \frac{\sigma_{S0}(u)}{\sigma_{T1}(u)} + K_1 \frac{\sigma_{S1}}{\sigma_{T1}(u)} \right] F_1(u)$$

$$+ \frac{V_2}{V_1} \left[1 - \frac{\sigma_{T1}(u)}{\sigma_{T2}} (1 - P_{11}(u)) \right] K_2 F_2(u) \quad . \tag{4. 13}$$

Here σ symbolizes microscopic cross sections per absorbing atom corresponding to the macroscopic cross sections in eq. (4.1), e.g.

$$\sigma_{T2} = (\Sigma_{T2} V_2)/(N_o V_1) \ .$$

K_k is an integral operator defined by

$$K_k \varphi(u) = \int_{u-\Delta_k}^{u} \frac{e^{-(u-u')}}{1-\alpha_k} \varphi(u') \, du' \ . \qquad (4.14)$$

By combining eqs. (4.12) and (4.13) we obtain

$$V_2/V_1 \, F_2(u) = \left(\frac{1}{P_{11}(u)} - 1 \right) F_1(u) + \frac{V_2}{V_1} \left[1 - \frac{\sigma_{T1}(u)}{\sigma_{T2}} \left(\frac{1}{P_{11}(u)} - 1 \right) \right] K_2 F_2(u) \ . \qquad (4.15)$$

Eq. (4.12) cannot be reduced to the slowing-down equation for any homogeneous system if the relationship between $F_1(u)$ and $F_2(u)$ includes an integral operator like the last term in eq. (4.15). Therefore an exact equivalence principle only exists if

$$1 - \frac{\sigma_{T1}(u)}{\sigma_{T2}} \left(\frac{1}{P_{11}(u)} - 1 \right) = 0 \ ,$$

or

$$P_{11}(u) = \frac{\sigma_{T1}(u)}{\sigma_{T1}(u) + \sigma_{T2}} \ . \qquad (4.16)$$

According to eq. (4.10) this is not a good approximation unless

$$\sigma_{T2} = S \ , \qquad (4.17)$$

where S is defined by

$$S = \frac{a(1-C_a)}{1+C_a(a-1)} \cdot \sigma_{ex} = a_1 \sigma_{ex} \ . \qquad (4.18)$$

In this particular case eq. (4.12) takes the form

$$F_1^*(u) = \left[K_0 \frac{\sigma_{S0}(u)}{\sigma_{T1}(u)+S} + K_1 \frac{\sigma_{S1}}{\sigma_{T1}(u)+S} + K_2 \frac{S}{\sigma_{T1}(u)+S} \right] F_1^*(u) \tag{4.19}$$

with

$$F_1^*(u) = F_1(u) \frac{\sigma_{T1}(u)+S}{\sigma_{T1}(u)} \tag{4.20}$$

if the Bell factor approximation for the collision probability is applied. The resonance integral as defined in eq. (4.2) is determined by

$$N_o \cdot RI_{R0} = \int_{u_1}^{u_2} \frac{\sigma_{R0}(u)}{\sigma_{T1}(u)+S} F_1^*(u)\, du \ . \tag{4.21}$$

Eqs. (4.19) and (4.21) describe exactly the homogeneous case where the external moderator and the fuel material are homogenized.

It is now assumed that $\sigma_{T2} \neq S$. Eq. (4.15) is rewritten in the following form:

$$F_2(u) = K_2 F_2(u) + B(u) \ , \tag{4.22}$$

and the order of magnitude of B(u) is estimated by means of the Bell factor approximation.

$$B \simeq \frac{S}{\sigma_{T1}(u)} \frac{V_1}{V_2} F_1(u) - \frac{S}{\sigma_{T2}} K_2 F_2(u) \ .$$

In the asymptotic intervals between the resonances it is obvious that $B = 0$, and if the moderator atoms in region 2 are light, the main source from region 2 in eq. (4.12) originates in these intervals. Generally $\sigma_{T2} \rangle S$ because this condition ensures that the lumping of the fuel material reduces the total resonance absorption owing to the self-shielding. For an isolated rod $\sigma_{T2}/S \to \infty$. Provided $\sigma_{T2} \rangle\rangle S$, the last term in the estimate of B is much smaller than the first term in eq. (4.22), and close to a resonance peak the dominating term in B is generally the last term. Therefore if σ_{T2} is much larger than S, B is also negligible in the environment of a resonance. According to these arguments a large class of problems may be solved by replacing eq. (4.22) by

$$F_2(u) = K_2 F_2(u) .$$

The solution of this equation obeying the demanded boundary condition is

$$F_2(u) = \Sigma_{T2} . \tag{4.23}$$

An abstract moderator, which in the slowing-down equation is described by a source term equal to its cross section, is below named a Narrow-Resonance (NR)-moderator. By defining $S^*(u)$ as

$$\frac{\sigma_{T1}(u)}{\sigma_{T1}(u)+S^*(u)} = P_{11}(u) \tag{4.24}$$

it is deduced from eqs. (4.12) and (4.23) that

$$F_1^*(u) = N_o \cdot S^*(u) + \left[K_0 \frac{\sigma_{S0}(u)}{\sigma_{T1}(u)+S^*(u)} + K_1 \frac{\sigma_{S1}}{\sigma_{T1}(u)+S^*(u)} \right] F_1^*(u) . \tag{4.25}$$

$$F_1^*(u) = F_1(u)/P_{11}(u) .$$

Eq. (4.25) is accepted as the equation describing a homogeneous mixture composed of the fuel material mixed with an NR moderator with the cross section $S^*(u)$ per absorbing atom. It is, however, inconvenient to consider moderators with lethargy-dependent cross sections. If $S^*(u)$ is constant, it is again necessary to use the Bell factor collision probability (cf. eqs. (4.10) and (4.24)) and substitute S as defined by eq. (4.18) for $S^*(u)$. The resonance integral, which may be calculated as indicated in eq. (4.21), is characterized by S, the temperature, T, and the fuel material.

$$RI_{R\theta} = RI_R(S,T)_{u1,u2} . \tag{4.26}$$

An infinite lattice is not equivalent to a homogeneous problem in any other cases than those listed above. It is now, however, the intention to deduce some sort of an approximate equivalence principle based on the Carlvik approximation (cf. eq. (4.11)).

All functions behind the slowing-down operators (cf. eq.

(4.14)) are approximated by means of their asymptotic values. This is the so-called Narrow Resonance approximation. From eq. (4.12) we obtain

$$F_1^{NR}(u) = N_o \left[q_{T1}(u) \, (1-P_{11}(u)) + (\sigma_{S1} + \sigma_p) \, P_{11}(u) \right], \qquad (4.27)$$

where σ_p is the absorber potential scattering cross section. By means of eqs. (4.2), (4.11) and (4.27) it is easily shown that

$$RI_{R0} = d \cdot RI_R(r_1 \sigma_{ex}, T)_{u1,u2} + (1-d) \cdot RI_R(r_2 \sigma_{ex}, T)_{u1,u2} \; . \qquad (4.28)$$

$RI_R(S,T)_{u1,u2}$, which is introduced above, must here be calculated by means of the NR solution of the homogeneous problem. If instead the Absorber is treated as Infinitly heavy, the NRIA-collision density is obtained (the absorber is treated by the Wide-Resonance (WR)-approximation)

$$F_1^{NRIA}(u) = N_o \frac{\sigma_{T1}(u)(1-P_{11}(u)) + \sigma_{S1} P_{11}(u)}{1 - \frac{\sigma_{S0}(u) \, P_{11}(u)}{\sigma_{T1}(u)}} \qquad (4.29)$$

Here a simple formula like (4.28) may not be deduced directly if the Carlvik approximation is applied. However, Neltrup [88] has demonstrated that eq. (4.28) is in fact generally a good approximation also in the NRIA case.

It is not possible to prove mathematically which of the two approximations expressed in eqs. (4.26) and (4.28) is the better one. The first, which is based on an accurate equivalence relation, uses the rather poor Bell factor collision probability approximation. On the other hand eq. (4.28) is only correct in the NR approximation, but the applied collision probabilities are very precise. In chapter 6 the equivalence principles are investigated numerically.

If the considered resonance is extremely wide and the condition $\sigma_{T2} \gg S$ is not fulfilled, then eq. (4.25) is incorrect. The absorption in the low-energetic part of the resonance is affected by the drop in the neutron source due to the absorption in the part of the resonance situated at higher energies. If, however, the resonance integral, RI'_{R0}, is still calculated by the NR external moderator approximation, this effect may be taken into account by the formula

$$RI_{R0} = \langle \sigma_S \xi \rangle \cdot (1-p) \ .$$

$$p = \exp(-RI'_{R0}/\langle \sigma_S \xi \rangle) \ , \qquad (4.30)$$

$$(p = 1 - \frac{RI_{R0}}{\langle \sigma_S \xi \rangle}) \ .$$

$\langle \sigma_S \xi \rangle$ is the average slowing-down power of the cell per absorbing atom, and p is the resonance escape probability. This formula is identical to that generally used to allow for the interaction between resonances. In this latter case RI'_{R0} is the sum of the resonance integrals calculated for the resonances one by one neglecting the existence of all the other resonances. The formula expresses the total resonance escape probability as the product of the individual escape probabilities. It is here presumed that the considered reaction, R, is the dominating absorption process in the system. A great many numerical calculations support eq. (4.30) also when it is used on a single resonance. A few examples are listed in section 6.1. Whenever mistakes are possible, the symbols RI' and RI are used below in order to distinguish the two types of resonance integrals. It has been proposed [96] to name RI the absorption rate and reserve the designation "effective resonance integral" for RI', but in fact a lot of confusion exists regarding the resonance integral definition (cf. section 2.1).

A different way of treating a non-NR external moderator has been developed by Goldstein and Seghal [96]. By the Intermediate Resonance (IR) formalism they have obtained an expression, which relates the heterogeneous resonance integral to a well-known formula for the homogeneous integral. However, the lacking equivalence manifests itself through a relationship varying from resonance to resonance and depending on the lattice geometry in a complicated way. For this reason the resonance effects may not be represented by one function of only two parameters (S,T) per energy group per fuel material as is the case in the above treatment. It is one of the main purposes of the present work to establish by exact numerical calculation that all important quantities concerning resonance reaction may be determined with adequate accuracy by such a "two-parameter" description. Furthermore, it has as yet not been possible to solve the heterogeneous IR-equations if scattering interference is included, and for this reason the approximation is not very accurate. In the homogeneous calculation of $RI'_R(S,T)_{u1,u2}$ the IR approach is, however, frequently applied below.

4.4. Determination of Homogeneous Resonance Integrals by the IR Iterative Method

A summary of the IR method development together with the relevant references is presented in reference B. The deduction of the basic equations including scattering interference at zero temperature is presented below in a compact formulation.

The slowing-down equation is considered in the form

$$H\,\varphi(u) = S \tag{4.31}$$

$$H = \sigma_T(u) - K_0\sigma_{S0}(u) - \sum_j \sigma_{Sj}\,K_j \tag{4.32}$$

$$\sigma_T(u) = \sigma_A(u) + \sigma_{S0}(u) + \sum_j \sigma_{Sj} + S \ .$$

The region index has been skipped here.

$\sigma_A(u)$ = absorption cross section of the resonance absorber.

$\sum_j$ includes only terms with $j > 0$. Isotope number 0 is the absorber.

As a first-order solution of eq. (4.31) we choose

$$\varphi^{(1)}(\lambda, u) = \frac{S+\lambda_0\sigma_p + \sum_j \lambda_j\sigma_{Sj}}{S+\sigma_A+\lambda_0\sigma_{S0}+\sum_j \lambda_j\sigma_{Sj}} \ , \tag{4.33}$$

where λ is a symbol for the array $\lambda_0, \lambda_1, \ldots, \lambda_j, \ldots$, and σ_p is the potential scattering cross section of the absorber. This solution interpolates between the WR- and the NR-approximation when λ_k ranges from 0 to 1.

If H_0 is introduced as the nonsingular, self-adjoint, multiplicative operator in the equation

$$H_0\,\varphi^{(1)}(\lambda, u) = S \tag{4.34}$$

and H_1 as

$$H_1 = H - H_0 \ , \tag{4.35}$$

we see in analogy with the procedure of Goldstein and Brooks [97] that pro-

$$R(\lambda) = \int_{res} \sigma_A H_0^{-1} H_1 \varphi^{(1)} du = \frac{1}{S} \int_{res} \sigma_A \varphi^{(1)} H_1 \varphi^{(1)} du \qquad (4.36)$$

and

$$R(\lambda) = 0 \ , \qquad (4.37)$$

the first- and second-order resonance integrals are equal. The integrals are extended over one single resonance, and the second-order flux is defined by the iteration

$$H_0 \varphi^{(2)}(\lambda, u) = S - H_1 \varphi^{(1)}(\lambda, u) \quad \text{(cf. eqs. (4.31) and (4.35))}.$$

Now

$$H \varphi^{(1)} = S + \lambda_0 \sigma_p + \sum_j \lambda_j \sigma_{Sj} - [(\lambda_0 - 1 + K_0) \sigma_{S0} + \sum_j \sigma_{Sj}(\lambda_j - 1 + K_j)] \varphi^{(1)} \qquad (4.38)$$

and

$$H_1 \varphi^{(1)} = H \varphi^{(1)} - S \ . \qquad (4.39)$$

Eqs. (4.38) and (4.39) are substituted in (4.36):

$$R(\lambda) = \frac{1}{S} \int_{res} \sigma_A \varphi^{(1)} [\lambda_0 \sigma_p - (\lambda_0 - 1 + K_0) \sigma_{S0} \varphi^{(1)} + \sum_j \sigma_{Sj}(\lambda_j - (\lambda_j - 1 + K_j) \varphi^{(1)})] du \ . \qquad (4.40)$$

The following conditions are introduced:

$$\left.\begin{aligned} &\lambda_0 = 1 \text{ if } K_0 \sigma_{S0} \varphi^{(1)} = \sigma_p \\ &\lambda_j = 1 \text{ if } K_j \sigma_{Sj} \varphi^{(1)} = \sigma_{Sj}, \quad j > 0 \end{aligned}\right\} \text{(NR approximation)}$$

$$\lambda_k = 0 \text{ if } K_k \sigma_{Sk} \phi^{(1)} = \sigma_{Sk} \phi^{(1)} \qquad \text{(WR approximation)}$$

With these conditions eq. (4.40) may easily be broken down into M + 1 coupled transcendental equations where M is the number of non-NR moderators.

When the resonance cross sections are expressed by the single-level Breit-Wigner formulas and the integrals are solved the following equations are obtained [98, 99] (fission is neglected):

$$\lambda_0 - 1 + X_0 - \frac{\delta_0(\theta - \sigma_{is}/\sigma_p)}{2 \cdot C_0} Y_0 = 0 \tag{4.41}$$

$$\lambda_j - 1 + X_j - \frac{\delta_j \theta}{2 \cdot C_1} Y_j = 0 \ , \tag{4.42}$$

where

$$\delta_k = E_r(1 - a_k)/\Gamma, \ \sigma_{is} = (\sigma_0 \sigma_p g_j \Gamma_n / \Gamma)^{1/2}$$

$$C_0 = 1 + \frac{\sigma_0 \Gamma_n}{\sigma_p \Gamma} - \beta + 2\theta \ (\theta - \sigma_{is}/\sigma_p) \ , \ C_1 = 1 - \beta^2 + 2\theta^2$$

$$X_k = (\tan^{-1} z_k)/z_k \ , \ Y_k = [\log (1 - z_k^2)]/z_k^2$$

with

$$\beta^2 = 1 + \frac{\sigma_0}{\lambda_0 \sigma_p + \sum_j \lambda_j \sigma_{Sj} + S} \ \frac{\Gamma_\gamma + \lambda \Gamma_n}{\Gamma} \ , \quad \theta = \frac{\lambda_0 \sigma_{is}}{\lambda_0 \sigma_p + \sum_j \lambda_j \sigma_{Sj} + S}$$

$$z_k = \delta_k / (\beta^2 - \theta^2)^{1/2} \ .$$

The corresponding first-order resonance integral is given by

$$I^{(1)}(\lambda) = \int_{res} \sigma_A \phi^{(1)} \, du = \frac{\pi \sigma_0 \Gamma_\gamma}{2 E_r (\beta^2 - \theta^2)^{1/2}} \ . \tag{4.43}$$

The standard version of the method comprises a determination of λ without taking the scattering interference into account, i.e. $\sigma_{is} = 0$ in eqs. (4.41) and (4.42). This simplifies the equations very much, and the solutions can always be obtained by simple iteration. The λ-value is then used in conjunction with Doppler broadening and possibly scattering interference. This procedure is apparently acceptable as far as Doppler broadening is concerned [100, 101], but it is a rather unsatisfactory way to treat the scattering interference, which was in a previous article [A] shown to be very important for resonances with appreciable scattering. When the scattering interference is considered, the solution of eqs. (4.41) and (4.42) may quite often not be determined by simple iteration and is not confined to the interval $0 \leq \lambda_k \leq 1$. In fact the solution is not even unique. In reference B the ways of solving these difficulties are discussed. Furthermore, the accuracy of the method is proved by exact numerical calculation on a large number of resonances, and a way of treating the Doppler broadening by means of the function, $J(\theta, \beta, i)$, introduced by Dresner [24] is discussed in detail.

4.5. RESAB Programme System, Link ALFA

Homogeneous resonance integrals may be determined by use of this module of the programme system. It comprises a deck containing most of the equivalence principles in common use for infinite lattices. Also group cross sections may be calculated (cf. chapter 8).

In the statistical region the single-level resonance integrals are calculated by the NR approximation (method 1). Resolved resonances may be treated by the standard version of the IR method (method 2, cf. section 4.4) or by complete IR inclusion of the scattering interference (method 3, eqs. (4.41) and (4.42)). Furthermore, the link contains a routine, RESCOLDENS that solves eq. (4.31) by means of a step by step Simpson-rule integration (method 4). In all these methods one resonance is considered an indivisible whole belonging completely to the energy group in which the resonance peak is situated. For very wide resonances this may be objectionable if the groups are narrow. Such resonances may alternatively be treated by the SDP routine contained in a different link of the programme system (cf. fig. 2.1). This procedure, which is described in detail in the next chapter, considers in addition the heterogeneous effects exactly.

Accuracy, but also calculation time, increase rapidly with the method numbers above. In calculations of total resonance integrals the following

combination of the methods is generally used in order to optimize the accuracy achieved during a reasonable running time. All resolved s-wave resonances are treated by method 2. The resonances are sorted according to decreasing contribution to the total resonance integral, and the greatest resonances, constituting 90% of the total s-wave integral, are separated. For e. g. ^{238}U this corresponds to 20-40 out of 188 resolved resonances. The three or four largest resonance integrals are then recalculated by method 4, and the rest of the selected resonances are corrected by method 3. The statistical region resonance integrals and the p-wave contribution from the region of resolved s-wave resonances are estimated by method 1. Calculations following schemes like this are automatically controlled by the programme, and running times ranging between 0.2 and 1 minute are typical (IBM 7094). A few remarks concerning the different methods are quoted.

4.5.1. Statistic Calculation

In the unresolved region the resonance integrals are immediately obtained by substitution of the single-level resonance integrals, expressed by the $J(\theta,\beta,i)$ function [24, 102], for RS_R^{Jl} in eq. (3.23) and integration over energy. Gaussian integration in logarithmic scale is favourable here, and six Gauss points suffice in all energy intervals. The integration over x_n in cases with one degree of freedom ($\nu = 1$) for non-fissile nuclides is performed by half-range Hermite quadrature after a transformation of variable $2y^2 = x_n$ (Gaussian quadrature for the interval $(0,\infty)$ with weight function $\exp(-y^2)$). More weight functions have been examined, but that above requested the lowest number of Gauss points. 8 points are applied here. Recently Steen [103] has used the same method. If x_n is distributed with two degrees of freedom, then the single-level resonance integral, calculated at average parameters, is multiplied by the analytic expression for the so-called statistical modification factor, $S_\gamma^{(2)}$, determined at infinite dilution. This approximation is acceptable because the effect of the Γ_n distribution is considerably smaller than for $\nu = 1$, and $\nu = 2$ only occurs for the p-wave resonances, where the shielding effect is weak.

$$S_\gamma^{(2)} = (1+r)(1-re^r E_1(r)) = (1+r)\, e^r E_2(r) \quad , \quad \text{(ref. 104)} \qquad (4.44)$$

$$r = \Gamma_\gamma / \langle \Gamma_n \rangle$$

For fissile nuclides, where the whole theory is of a more approximative

nature, the simple method of integration over x_n and x_f introduced by Greebler and Hutchins [102, 105] is applied. Four and three points are used in the x_n and x_f integration respectively, by which the error due to averaging is about 5 per cent.

When more isotopes belonging to the same element are included in one problem (cf. section 3.3), the resonance integrals should be determined as

$$RI = \sum_i a_i R(a_i) , \qquad \sum_i a_i = 1 ,$$

where $a_i R(a_i)$ is the self-shielded resonance integral calculated for one isotope, when $a_i g_J$ is substituted for g_J. $R(a_i)$ is here assumed to be independent of i. Instead the formula

$$RI = R(\langle a_i \rangle) , \qquad \langle a_i \rangle = \sum_i a_i^2$$

is used in RESAB in order to reduce the running time. The two expressions are identical if all a_i's are equal. This is also true if $R(a_i)$ may be approximated by a linear function in a_i.

In order to provide some sort of a verification of the statistical model, a few calculations for the upper part of the resolved resonance region were performed by means of the statistical approach. The applied average parameters were deduced directly from the resolved resonance data in the intervals under consideration. Partial, self-shielded, s-wave resonance integrals were determined for a NR-moderated system with S = 20 b and a temperature equal to 300 K, and the results obtained are in table 4.1 compared with resolved resonance calculations based on the NR approximation. It appears that the statistical model provides self-shielded resonance integrals with an accuracy of about 5%.

4.5.2. Standard Version of the IR Method

The λ's are determined by the equations used by Sumner in the programme ERIC I [106]. They are almost equal to those obtainable from eqs. (4.41) and (4.42) by setting σ_{is} equal to 0. By means of these λ's the first order resonance integral with Doppler broadening and scattering interference included is determined.

4.5.3. IR Method Including Scattering Interference

All important details are found in reference B.

Table 4. 1.

Verification of the statistical model.
Self-shielded resonance integrals in an NR-moderated system.
S = 20 b, T = 300 K (barns).

Resonance nucleus		^{238}U		^{232}Th	
Energy interval, eV		1000-2000	2000-3900	1000-2000	2000-3900
Resolved resonance treatment, s-wave		0.408	0.331	0.484	0.386
Statistical approach	s-wave	0.416	0.327	0.461	0.357
	p-wave *)	0.250	0.308	0.234	0.300

*) Calculation performed by an old version of the RESAB library. $s_T^1 = 2.4 \times 10^{-4}$ and 2.2×10^{-4} for U and Th respectively.

4.5.4. Residual Terms Applicable in Connection with Numeric Calculation of the RESonance COLlision DENSity, RESCOLDENS

In order to obtain a well-defined, single-level resonance integral which is independent of the upper and lower cut-off energies for the numerical integration it has been necessary to introduce suitable residual terms. By subtraction of the "1/v-tail", a logarithmic integrable reaction cross section around E = 0 is obtained. Only regions where the Doppler broadening may be neglected are considered, i.e. [24]

$$x \gg 6/\theta^2$$

with the symbols introduced in section 3.1. Actually

$$x^2 > 100 \cdot 6/\theta^2 \ . \qquad (4.45)$$

The residual term is now defined as (no self-shielding)

$$I(E_1, E_2) = \int_{E_1}^{E_2} \left[\sigma_R(E) - \sqrt{\frac{E_r}{E}}\, \sigma_R^*(0) \right] \frac{dE}{E} \quad \text{(cf. eq.(3.1))} \qquad (4.46)$$

$$I(E_1, E_2) = \frac{\sigma_0 \Gamma_R \sqrt{E_r}}{\Gamma} \int_{E_1}^{E_2} \left(\frac{1}{1+x^2} - \frac{1}{1+x_0^2} \right) \frac{dE}{E^{3/2}} \ , \qquad (4.47)$$

$$x_0 = 2E_r/\Gamma \quad \text{and} \quad x = 2(E-E_r)/\Gamma \ . \quad \sigma_R^*(0) = \lim_{E' \to 0} \sqrt{\frac{E'}{E_r}}\, \sigma_R(E') \ .$$

By performing the integrations we obtain

$$I(E_1, E_2) = C \left[-\frac{f}{\sqrt{m}} \left(\tan^{-1} \frac{\sqrt{E}-n}{\sqrt{m}} + \tan^{-1} \frac{\sqrt{E}+n}{\sqrt{m}} \right) + \frac{f_1}{2} \log\left(\frac{(\sqrt{E}+n)^2+m}{(\sqrt{E}-n)^2+m} \right) \right]_{E=E_1}^{E_2} \qquad (4.48)$$

with

$$n = (E_r \left[1 + (1 + 1/x_0^2)^{1/2} \right]/2)^{1/2} \ ,$$

$$m = E_r \left[-1 + (1 + 1/x_0^2)^{1/2} \right] /2 ,$$

$$f_1 = E_r \left[-2 - (1 + 1/x_0^2)^{1/2} \right] ,$$

$$f = E_r n \left[2 - (1 + 1/x_0^2)^{1/2} \right] ,$$

and

$$C = - \frac{\sigma_0 \Gamma_R E_r^{1/2}}{\Gamma^2 (1+x_0^2)^{3/2} \cdot n}$$

(note $I(0,\infty) = -C f \pi / \sqrt{m}$. Consider a narrow resonance at a high energy: $I(0,\infty) \simeq \sigma_0 \Gamma_R \pi / (2 E_r)$).

In the upper residual term the 1/v contribution should be added again because the upper tail of the resonance decreases much faster than 1/v. The IR calculation of resonance integrals ignores the energy dependence of the factor $E^{-3/2}$ over the range of integration. It is simply evaluated at E_r for which reason no "1/v-tail" of the resonance absorption cross section is included. When the residual terms above are added in order to extend the integration in RESCOLDENS from 0 to ∞, the calculation corresponds very well with the IR resonance integral definition.

In group cross section calculations the 1/v contribution is added in the groups below the resonance peak. Such a correction is also made for resonances treated by methods 2 and 3.

4.5.5. The Doppler Broadening Function, J(θ, β, i)

This function, which has been discussed thoroughly by Dresner [24], is applied in methods 1, 2 and 3. Its relation to the IR resonance integral is explicitly described in reference B. Link ALFA in RESAB contains two methods of calculating this function. In the resolved resonance region a numerical approach developed by Neltrup [107] has been applied. In the unresolved region the extremely fast method developed by Steen [103] is generally used. The result obtained by the latter method has been compared with the numerical approach, and the differences are generally smaller than one per cent in the statistical region even though the scattering interference is neglected in Steen's approximation (i = 0).

4.5.6. The Negative Energy Resonances

For some isotopes it is necessary to introduce a resonance level for

the compound nucleus at an excitation energy a little lower than the binding energy of the last neutron in order to fit the reacti n cross sections at low energies. Some remarks concerning the treatment of such a resonance in RESAB are collected in reference D.

4.6. Examples of the Use of Link ALFA

4.6.1. Effective Resonance Integrals and Doppler Coefficients of ^{232}Th and ^{238}U

Two reports concerning the resonance capture in ^{232}Th and ^{238}U have previously been issued [C, D]. In these reports the total resonance integrals are expressed by polynomials in $\sqrt{T}$ and $\sqrt{S}$. The parameter intervals cover the regions of interest for heterogeneous thermal reactor calculations, and the results are intended to meet the two-group resonance absorption data requirement. The resonance integrals as well as the Doppler coefficients are compared with the available experimental results, and the agreement is generally quite good. A more detailed investigation of Hellstrand and Lundgren's experiment for ^{238}U with emphasis on specific geometrical effects follows in section 7.3 of the present report.

4.6.2. ^{240}Pu Resonance Integral

On account of the lack of accurate integral measurements it is difficult to test the data library for ^{240}Pu. The epicadmium resonance integral as determined by use of the Carlvik collision probability approximation is in fig. 4.3 compared with the measurement made by Nichols [108]. The results have been renormalized to the infinite dilution resonance integral underlying the measurement (8607 b). Owing to the large experimental errors the results of the investigation are in fact not very informative.

4.6.3. Yankee Reactor Control Rod

In the Yankee pressurized light-water reactor a considerable fraction of the control rod absorption occurs in the epithermal region, which here, according to the LASER calculational scheme [109], is defined as the energy region above 1.855 eV. The control rod consists of Ag, Cd and In with a composition by weight of 80%-5%-15% respectively, and the predominant sort of epithermal absorption is resonance capture. Neither the white nor the black boundary condition provide a good representation of the control rod surface in the resonance region. Contrary to traditional control rod treatment, the standard resonance absorption methods have

been used. A control rod of the geometrical appearance shown in fig. 4.4 was considered as equivalent to an isolated cylindrical rod with equal mean chord length. According to Dresner [24] this is not a serious approximation as the slab character of the rod is predominant. Group cross sections, defined as partial resonance integrals (including 1/v contribution), divided by the average group fluxes inside the rod (cf. chapter 8) have been constructed by means of Carlvik's collision probability approximation combined with methods 1 and 2 (cf. section 4.5). These cross sections are listed in table 4.2. For illustration of the influence of the self-shielding the infinite dilution cross sections were also determined. It appears that it is disastrous to neglect the self-shielding, especially in the case of Ag. Resonance interference was neglected even though the rather large number of uncorrelated resonance series may cause a considerable resonance overlapping effect. This is perhaps the most serious approximation in the whole procedure. The method now comprises a cross section condensation performed by a control cell, slab geometry, collision probability routine, which provides effective cross sections suitable for a two-dimensional difference equation treatment (diffusion theory). Using the TWODIM SYSTEM, Lindstrøm Jensen [7] has according to the sketched control rod approach investigated the variation in ^{239}Pu with fuel depletion in a Yankee reactor assembly. For non-control materials the LASER [109] cross sections have been applied. The result of the study is shown in fig. 4.5 by courtesy of Lindstrøm Jensen. Even in the corner at the control rod the accordance with the measurement is satisfactory. The large oscillations of the curve representing the corner cell are due to spectrum variations originating in control rod movements. They indicate that the variation in ^{239}Pu concentration is an appropriate measure of the control rod influence. In the actual case about 40% of the total control rod effect is due to the epithermal capture.

The value of the quantity λ_{ext}, defined by

$$\lambda_{ext} = \frac{-D\nabla\varphi}{\varphi}\Big|_{boundary} = -\frac{J}{\varphi}\Big|_{boundary},$$

provides a measure of the greyness of the rod. D is the diffusion coefficient and J the surface neutron current. For a black rod it is equal to 0.467, while a value equal to 0 applies to the limit of a white rod. The variation with the energy is indicated in table 4.3. It appears that the rod is rather black in the thermal group and white at high energies.

The reader interested in more details concerning the calculation is referred to the work of Lindstrøm Jensen [7].

Table 4.2.

Effective microscopic capture cross sections of the elements in a Yankee reactor control rod

Temperature T = 541 K. S/4V = 0.757 cm^{-1}

Group boundaries (eV)	^{nat}Ag, $4.433 \cdot 10^{22}$ nuclei/cm^3		^{nat}In, $0.781 \cdot 10^{22}$ nuclei/cm^3		^{nat}Cd, $0.266 \cdot 10^{22}$ nuclei/cm^3	
	Self-shielded (b)	Infinite dilution (b)	Self-shielded (b)	Infinite dilution (b)	Self-shielded (b)	Infinite dilution (b)
1.855-78.88	17.06	193.7	21.56 *)	38.43 *)	1.24	1.46
78.88-748.4	2.60	7.55	5.91	9.28	5.05	6.85
748.4-5530	1.92	2.35	2.47	2.63	1.28	1.35
5530-4.978·10	0.80	0.81	0.66	0.66	0.34	0.34
$4.978 \cdot 10^5$-$1.353 \cdot 10^6$	0.20	0.20	0.14	0.14	0.06	0.06

*) 11.30 b, representing the upper "tail" of the 1.456 eV ^{115}In resonance, has been added.

Table 4.3.

The value of $\lambda_{ext} = -J/\varphi$ at the surface of a Yankee reactor control rod. 4-group calculation

Group boundaries (eV)	λ_{ext}
0-1.855	0.4218
1.855-5530	0.1000
5530-$4.978 \cdot 10^5$	0.0137
$4.978 \cdot 10^5$-ca. 10^7	0.0035

5. DETERMINATION OF EPITHERMAL FLUX SPECTRUM BY INTEGRAL TRANSPORT THEORY

In this chapter the SDP module of the RESAB programme system will be described. The idea of solving eq. (4. 1) in the resonance region by direct numerical integration is not of recent date. In 1962 Nordheim[111] calculated resonance integrals in a two-region lattice by means of approximate collision probabilities and numerical treatment of the slowing-down kernel. A further development of the method is condensed in the STRIP code [112,113], where much computer time is saved by the introduction of variable energy meshes. The codes SDR[15,32], EPITHET[114], PETARD[115] and RICM[92,116] allow a subdivision of the material regions for obtainment of a better representation of the flux distribution. Lewis and Adler[117] have developed a sophisticated technique that permits the spatial dependence of the flux inside each region to be expressed by a polynomial, and a similar method has been proposed by Kier[118].

SDP is the result of an attempt to set up a code which may be used in fast routine calculations with only two or three regions and flat fluxes. However, the same code should comprise facilities for more involved investigations, where the different approximations underlying more ordinary resonance absorption theories are eliminated one by one. It has been concluded that the best way of meeting these requirements is to use the multi-region collision probability approach without any energy mesh restrictions. This last demand may have complicated the calculation of the neutron transfer from one energy mesh to another, but the radical reduction in the necessary number of meshes is more important for the running time. In this sense the SDP code is closely related to STRIP, while for instance the very extensively developed and frequently used British code SDR allows the mesh intervals to be halved but not quartered inside an energy interval equal to the maximum neutron energy change in one collision. Scatterings on hydrogen nuclides are exceptions to this rule. Deuterium scatterings cannot be treated by the SDR code at all.

Some of the effects to be examined are of the order of a few per cent. Therefore care was taken to avoid any uncontrollable approximations apart from the assumption of isotropic scattering in the laboratory system, an approximation which is partly eliminated later on. Most of the codes listed above that consider spatial distribution, contain approximations which are not eliminated, for instance, by simple increments in spatial mesh-point numbers. For example, the RIFF-RAFF code of Kier and the EPITHET

code imply that neutrons enter the fuel rod isotropically, and, furthermore, in the RIFF-RAFF code the source distribution is expressed by a three-term polynomial of even order. In the PETARD code the collision probabilities are calculated according to Bonalumi's approximate technique[119], while the exact method of Carlvik[80] is mostly applied in SDP, (cf. section 4.2

The effect of removing the flat flux assumption as calculated by means of SDP is somewhat smaller than the reported RIFF-RAFF and PETARD results, while the deviation from Lewis and Adler's calculation has opposite sign even though it is small. It is, however, difficult to compare the investigations of the different authors directly because these investigations are concerned with problems of limited as well as varied nature. This ambiguous situation stresses that a very careful code testing is necessary. For this reason among others a Monte Carlo programme, MCSUP, which may simulate exactly the same physical situation as SDP, has been worked out at Risø[82] by Kirkegaard. It uses the very fast method of Spanier and Gelbard[120]. Many of the above-mentioned programmes have also been tested against Monte Carlo calculations, but in all cases the accuracy has been so poor that effects of the order of magnitude considered here are difficult to investigate. The use of Spanier's method has reduced the standard deviation of the absorption rate by almost one order of magnitude and, for instance, it has been shown that PETARD overestimates the influence of the flat flux assumption, while the results of SDP are reproduced within less than two standard deviations.

The choice of the simple multi-regional method of representing the spatial flux distribution is also supported by the fact that it makes it very easy to introduce detailed material inhomogeneities produced by, for example, the temperature distribution and the plutonium build-up in the fuel rod surface.

Most slowing-down codes integrate in energy space, but SDP is based on lethargy. This has the advantage that relatively wide lethargy groups may be used in intervals where the departures from the "1/E-flux" are small. The shape of the internal weighting function in the groups is identical to this asymptotic flux because it is constant per lethargy unit. As a consequence the step-by-step integration may be initiated at the upper cut-off energy and with the 1/E boundary condition simply by placing a very wide group above this energy, where all total cross sections are put equal to the potential scattering cross sections, and where the flux per unit lethargy is normalized to one. Integration in energy, on the other hand, makes it necessary to use special expressions for the sources from energies above the upper cut-off energy.

5.1. Formulation of the Multi-Group Problem

The lethargy axis is divided into intervals or groups inside which the cross sections are considered constant. Instead of being functions of u, the cross sections, collision probabilities and group average collision densities are now provided with an upper index indicating the group number. u_n and Δu_n are the lower lethargy limit and group width respectively of group number n. u_1 is the lower cut-off lethargy corresponding to the upper cut-off energy, while u_0 symbolizes a lethargy very much smaller than u_1. With these abbreviations the integral of eq. (4.1) calculated from u_n to u_{n+1} may be expressed as

$$V_i F_i^n \Delta u_n = \sum_{j=1}^{NOR} V_j P_{ij}^n \sum_{k=1}^{M_j} \sum_{s=0}^{n} h_{jk}^{ns} \cdot F_j^s \quad , \tag{5.1}$$

where

$$h_{jk}^{ns} = \frac{\Sigma_{Sjk}^s}{\Sigma_{Tj}^s} \int_{u_n}^{u_{n+1}} \int_{u_s}^{u_{s+1}} \frac{e^{u'-u}}{1-\alpha_{jk}} e_{jk}(u'-u)\, du'du \quad . \tag{5.2}$$

and

$$e_{jk}(u) = \begin{cases} 1 & -\Delta_{jk} \leq u \leq 0 \\ 0 & \text{all other arguments.} \end{cases} \tag{5.3}$$

In eq. (5.1) the collision density $F_j(u)$ was put outside the integral signs as the average value F_j^s, and therefore the transition from eq. (4.1) to eq. (5.1) is only exact in energy regions with asymptotic flux, even when the cross sections are forced to be constant within the groups. This approximation is permissible if the neutron balance is still exactly maintained throughout the slowing-down process. Neutron balance here means that the sum of the neutrons which are scattered from a group and region back to itself and into other groups and regions must be equal to the total number of colliding neutrons minus absorbed neutrons in the group and region under consideration. That is

$$V_i F_i^n \Delta u_n \sum_{k=1}^{M_i} \frac{\Sigma_{Sik}^n}{\Sigma_{Ti}^n} = \sum_{q=n}^{\infty} \sum_{j=1}^{NOR} V_j P_{ji}^q \sum_{k=1}^{M_j} h_{jk}^{qn} \cdot F_j^n \, . \tag{5.4}$$

If the h_{ik}^{qn}'s are calculated from (5.2), the condition expressed in eq. (5.4) may easily be shown to be fulfilled. Here

$$\sum_{l=1}^{NOR} P_{li}^{q} = 1 \qquad (5.5)$$

must be used.

By solving of the integrals in eq. (5.2), rather complicated expressions containing exponential functions result. In the code SDR, mentioned above, simple approximations for the corresponding energy integrals are deduced[15] on the assumption that all groups are extremely narrow. If wider groups are used, the energy distribution of the neutrons after collisions is slightly wrong. In all cases, however, the neutron balance is strictly maintained. In the homogeneous slowing-down procedure, RESCOLDENS, mentioned in section 4.5, a Simpson's-rule integration of eq. (4.1) is used. Here neutron balance only exists in the limit of very small step length, and because of error accumulation it is necessary to use a relatively large number of mesh points in spite of the superiority of the parabolic approximation of the integrands compared with the step functions used in the SDP code.

As discussed above it should not be a condition for the running of SDP that the groups should be narrow even in intervals where the flux is approximately asymptotic, and therefore, in contradiction to SDR, SDP is constructed on the basis of the exact integrals in eq. (5.2).

5.2. Determination of the Multi-Group Flux Spectrum

Depending on the relative position of the boundaries of groups numbers n and s, one out of six fundamentally different situations may occur. In fig. 5.1 all six cases are illustrated. With the numbering shown in the figure the following expressions are calculated

$$H_{jk}^{s} = \frac{\Sigma_{Sjk}^{s}}{\Sigma_{Tj}^{s}(1-\alpha_{jk})} .$$

$0 \leq s < n$

1:

$$h_{jk}^{ns} = H_{jk}^{s} (e^{u_{s+1}} - e^{u_s}) (e^{-u_n} - e^{-u_{n+1}}) \quad . \tag{5.6}$$

2:

$$h_{jk}^{ns} = H_{jk}^{s} [(e^{u_{s+1}} - e^{u_s})(e^{-u_n} - e^{-u_s - \Delta_{jk}}) + e^{u_{s+1}}(e^{-u_s - \Delta_{jk}} - e^{-u_{n+1}}) - e^{-\Delta_{jk}}(u_{n+1} - u_s - \Delta_{jk})] . \tag{5.7}$$

3:

$$h_{jk}^{ns} = H_{jk}^{s} [e^{u_{s+1}}(e^{-u_n} - e^{-u_{n+1}}) - e^{-\Delta_{jk}} \cdot \Delta u_n] . \tag{5.8}$$

4:

$$h_{jk}^{ns} = H_{jk}^{s} [(e^{u_{s+1}} - e^{u_s}) (e^{-u_n} - e^{-u_s - \Delta_{jk}}) + e^{u_{s+1} - \Delta_{jk}}(e^{-u_s} - e^{-u_{s+1}}) - e^{-\Delta_{jk}} \Delta u_s] . \tag{5.9}$$

5:

$$h_{jk}^{ns} = H_{jk}^{s} [e^{u_{s+1}}(e^{-u_n} - e^{-u_{s+1} - \Delta_{jk}}) - e^{-\Delta_{jk}}(u_{s+1} + \Delta_{jk} - u_n)] . \tag{5.10}$$

6:

$$h_{jk}^{ns} \neq 0 . \tag{5.11}$$

$s = n$ Only cases 1 and 2 may arise.

1:

$$h_{jk}^{ns} = H_{jk}^{s} \left[\Delta u_n - e^{u_n} (e^{-u_n} - e^{-u_{n+1}}) \right] . \qquad (5.12)$$

2:

$$h_{jk}^{ns} = H_{jk}^{s} \left[\Delta u_n - 1 + e^{-\Delta_{jk}} - (\Delta u_n - \Delta_{jk}) e^{-\Delta_{jk}} \right] . \qquad (5.13)$$

These expressions as well as some of those stated below may be simplified by introduction of the energies corresponding to the lethargies. As the formulas must be thoroughly reorganized in any case before they take a form convenient for numerical computations, it was, however, decided to be consistent in the use of lethargy throughout this section. A discussion of some aspects of the computer programming follows later on.

Cases 1 ($s < n$) and possibly 6 are the cases most often occurring in eq. (5.1) if the groups are narrow. Expression (5.6) must be used whenev

$$N_{jk}^{n} \leq s \quad \text{and} \quad s < n .$$

N_{jk}^{n} is the smallest N fulfilling the condition

$$u_N + \Delta_{jk} \leq u_{n+1} .$$

Obviously

$$1 \leq N_{jk}^{n} \leq n + 1 \text{ (scattering on hydrogen demands special treatment).}$$

The simple structure of expression (5.6) is extremely important for the ap plicability of the method. We introduce

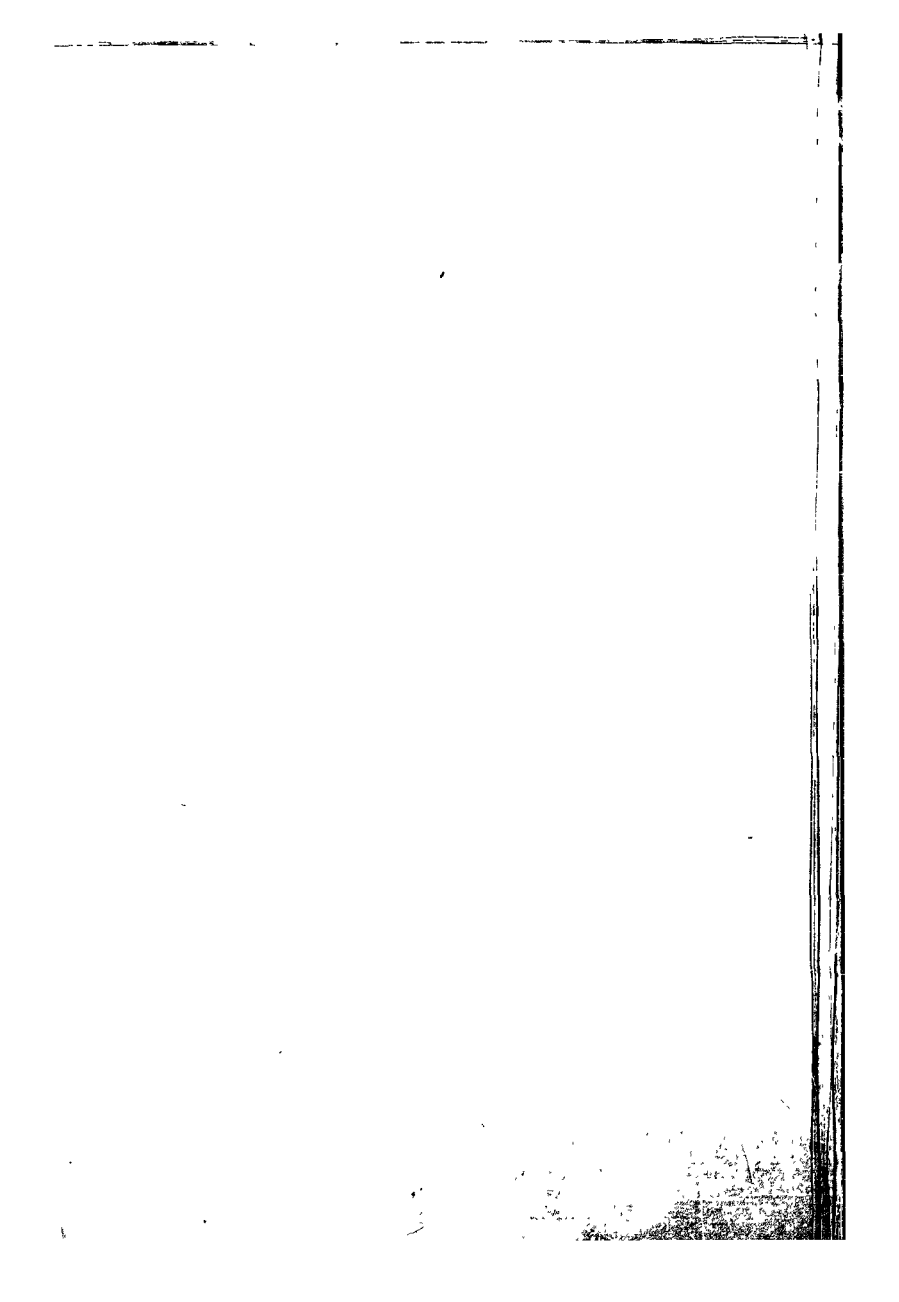

$$b_{jk}^{n} = \frac{1}{e^{-u_n} - e^{-u_{n+1}}} \sum_{s=N_{jk}^{n}}^{n-1} h_{jk}^{ns} F_j^s$$

$$= \sum_{s=N_{jk}^{n}}^{n-1} F_j^s \cdot H_{jk}^s (e^{u_{s+1}} - e^{u_s}) \quad , \tag{5.14}$$

$$b_{jk}^{n} = 0 \qquad \text{if} \quad N_{jk}^{n} > n-1 \quad . \tag{5.15}$$

Furthermore

$$b_j^n = \sum_{k=1}^{M_j} b_{jk}^{n} \quad . \tag{5.16}$$

From this it follows that

$$b_j^n = b_j^{n-1} - \sum_{k=1}^{M_j} \sum_{s=N_{jk}^{n-1}}^{N_{jk}^{n}-1} F_j^s \cdot H_{jk}^s (e^{u_{s+1}} - e^{u_s})$$

$$+ \sum_{k=1}^{M_j} F_j^{n-1} \cdot H_{jk}^{n-1} (e^{u_n} - e^{u_{n-1}}) \quad * \quad . \tag{5.17}$$

Because this simple recurrence relation is available, the determination of the right-hand side of eq. (5.1) is not so prohibitive as it appears at first sight, even when the group number runs up to several thousand. In this connection it is essential that generally

$$(N_{jk}^{n} - 1) - N_{jk}^{n-1} \ll n \quad .$$

* The summing through s should only be performed if $N_{jk}^{n-1} \neq N_{jk}^{n} - 1$, and special provisions must be taken against the occurrence of cases with $N_{jk}^{n} > n$ (cf. eq. (5.15)).

Now we define

$$A_j^n = \sum_{k=1}^{M_j} h_{jk}^{nn} \tag{5.18}$$

and

$$B_j^n = (e^{-u_n} - e^{-u_{n+1}})\, b_j^{'n} + \sum_{k=1}^{M_j} \sum_{s=N_{jk}^{n-1}}^{N_{jk}^n - 1} F_j^s\, h_{jk}^{ns} \quad * \tag{5.19}$$

Again the sum comprises only few terms.

It is noted that subdivision of a material region causes little additional work as the only quantity in eqs. (5.17), (5.18) and (5.19) that is different in two subregions with the same isotopic composition is F_j^s.

By use of eqs. (5.14), (5.16), (5.18), and (5.19) the multi-group equation (5.1) may be reduced to

$$V_i F_i^n \cdot \Delta u_n = \sum_{j=1}^{NOR} V_j P_{ij}^n (B_j^n + A_j^n \cdot F_i^n) \ . \tag{5.20}$$

B_j^n and A_j^n depend only on collision densities with group numbers smaller than n. If all these are known, formula (5.20) constitutes a system of NOR linear equations in the NOR collision densities, F_i^n, in group n. By assumption

$$\varphi_i^o = 1 \quad \text{or} \quad F_i^o = 1/\Sigma_{Ti}^o \ , \tag{5.21}$$

and now the whole slowing-down problem may be solved by stepping through the groups starting with group number one.

The inhomogeneous linear equations are solved by the "point Gauss-Seidel iterative method" with $F_i^n = F_i^{n-1}$ as a first estimate which is obviously

---

* The upper limit of the summation must be replaced by s = n-1 if $N_{jk}^n = n$.

a good estimate on a fine mesh. This is much faster than direct solution by, for instance, Crout's method on account of the strictly diagonal dominance.

The SDP code allows the inclusion of a NR moderator in, say, region m. This is achieved simply by adding a term

$$D_{im}^{n} = \Sigma_{NR,m} V_m P_{im}^{n} \Delta u_n$$

on the right-hand side, eq. (5.20). $\Sigma_{NR,m}$, which symbolizes the cross section of the NR moderator, is included in Σ_{Tm}^{n}.

5.3. The Consequences of the Numerical Noise (Truncation Error)

If the formulas (5.6)-(5.13) are used without modifications, only problems involving a few groups may be solved with reliable results because of the truncation error in the computer. As an example case 2 fig. 5.1 and the corresponding eq. (5.7) are considered at group widths in lethargy equal to 10^{-3}. In resonance problems the necessary group widths are usually even smaller than this. The two differences which occur in eq. (5.7)

$$e^{u_{s+1}} - e^{u_s} \quad \text{and} \quad e^{-u_n} - e^{-u_s - \Delta_{jk}}$$

are both of the order of 10^{-3}, while $\exp(u_s)$ is perhaps about 1, and therefore the relative accuracy of the differences is about three orders of magnitude poorer than the maximum obtainable relative accuracy, δ, in the computer. It was assumed here that the differences are calculated by subtraction without any modifications. The quantity δ may, for example, be defined as the smallest value of δ' for which the following inequality

$$A < 1 \quad \text{with} \quad A = 1 - \delta'$$

is true when A is calculated from δ' by the computer. Even worse results are obtained for the last part of eq. (5.7). In order to make the contents clearer, the expression is reorganized a bit. We have to calculate

$$e^{-\Delta_{jk}} \left[e^{u_{s+1} - u_s} (1 - e^{-x}) - x \right]$$

with

The result is of the order of

$$e^{-\Delta_{jk}} \left(\Delta u \cdot x - \frac{x^2}{2}\right),$$

and with the group widths used above approximately six orders of magnitude in accuracy are lost. Errors of this type are generally systematical because the computer truncates instead of rounding off. If δ is of the order of 10^{-8} (IBM 7094), the accumulated error may easily run up to about one per cent after, say, 10^3 groups, and this is completely unacceptable.

By careful programming the error per group was reduced to the machine accuracy. *This is perhaps more* than strictly necessary, but it has the advantage that the neutron balance is now an extremely sensitive tool for error identification. Furthermore, group numbers as large as 10^5 will not cause serious error accumulation when the code is run on IBM 7094. This is the number of energy points listed on GENEX[32] output tapes (SDR input tapes).

A few of the means by which this calculational accuracy has been achieved will be described briefly. Taking case 2 as example again we now replace eq. (5.7) by

$$h^{ns}_{jk} = H^{s}_{jk}\, a_{jk} \left(\frac{\Delta E_s}{E_s \cdot E_{s+1}} \left[\frac{E_n(1-a_{jk})}{a_{jk}} - \Delta E_s - SE^{n}_{jk} \right] + \frac{E_s}{E_{s+1}} \left[\frac{\Delta E_s}{E_s} + \left(-\frac{1}{2!} + \left(\frac{1}{3!} + \left(-\frac{1}{4!} + \frac{x}{5!} \right) x \right) x \right) x \right] x \right) \tag{5.7b}$$

when $x < 0.1$. The symbols for the energy quantities are derived from the corresponding lethargy nomenclature simply by substituting E for u.

$$SE^{n}_{jk} = \sum_{s=N^{n}_{jk}}^{n-1} \Delta E_s, \quad SE^{n}_{jk} = 0 \quad \text{if} \quad N^{n}_{jk} > n-1 . \tag{5.22}$$

SE^{n}_{jk} may rapidly be obtained by a simple recurrence relation corresponding to (5.17). Obviously, e^{-x} has been replaced by its power series. The inclusion of a fifth-order series to represent the exponential function is not

so luxurious as it may seem at first sight. It is in fact considerably faster in practical use than one call of the standard exponential function. We see that the group structure is now characterized by the group widths besides by the boundaries. The parenthesis containing SE^n_{jk} in eq. (5.7b) is another way of expressing

$$E_n/\alpha_{jk} - E_s.$$

The use of SE^n_{jk} implies in fact that the maximum neutron energy loss in one collision is compared with the exact energy interval which has actually been used in the step-by-step energy integration, while the much simpler expression above may introduce an error on the maximum slowing-down interval that is effective in the calculation. If $1-\alpha_{jk}$ is about 0.01 as is the case in for instance ^{238}U scatterings, this error becomes two orders of magnitude larger than δ. For the same reason x is not calculated directly from the definition above, but instead

$$x = Su^n_{jk} + \Delta u_n + \Delta u_s - \Delta_{jk}. \qquad (5.23)$$

where Su^n_{jk} is the lethargy interval corresponding to SE^n_{jk}. Also the material constants $(1-\alpha_{jk})$ and Δ_{jk} in eqs. (5.22) and (5.23) must be determined with a relative error of the order of δ, and this cannot be achieved here either by using the definitions without modifications.

Finally we return to the sums b^m_j and Su^n_{jk}. They are calculated from recurrence relations and not by repetition of the summation in each group, and it is therefore important that the numbers which are added to the sums are exactly the same as those which are subtracted later on. This is, however, prevented by the truncation, if the addenda are of another order of magnitude than the sums, and this is mostly the case. One way of overcoming this is to store the sums as double-precision numbers, but this is not possible in ILLINOIS ALGOL. Instead the Møller device [120, 121] was used by which the sums are stored in two words, and some sort of double-precision is, nevertheless, attained.

5.4. The Narrow Lethargy Groups and the Corresponding Group Cross Sections

A distinction is now introduced between narrow groups and wide groups. The designation "narrow groups" refers to a mesh structure which is so close that detailed cross sections and fluxes are represented accurately across

each resonance, while the wide groups are those used in more ordinary multi-group theory, where perhaps the main problem is to determine spatial effects in the macro-geometry. By averaging of the cross sections over the fluxes in the narrow groups, the wide group effective cross sections are obtained. In this section the construction of the narrow groups is discussed.

Instead of constant energy, lethargy or velocity intervals SDP uses a mesh structure dependent to some degree on the rate of change of the cross sections at each energy. In the lethargy region around a resonance very narrow groups are used, while between the resonances only a few mesh points are necessary. The extension of the intervals with very narrow groups is determined from the Doppler-broadened resonance widths, while the total number of narrow groups per resonance is a slowly varying function which depends on the resonance energy only. If more resonances overlap in an interval, the resulting group structure is determined by the narrowest of the resonances. As the total resonance reaction in thermal-reactors is dominated by the reactions which take place at low energies, the required accuracy decreases when the energy increases with a reduction of the necessary number of groups as a consequence. At low energies only a difference of about one per thousand is accepted when calculations performed with extremely narrow groups are compared with those based on the selected group structure. At energies above one thousand eV an accuracy of about one per cent is considered satisfactory. This rule applies for thick rods as well as in highly diluted cases. The flux-weighted cross sections vary most rapidly when infinite dilution is approached because of the lacking self-shielding.

Finally, the calculations in SDP are organized in such a way that the code profits from a constancy in the lethargy width of consecutive groups, and therefore the maximum efficiency of the code is achieved if the mesh length changes as rarely as possible.

The group structure requirements sketched here are almost the same as those on which the code STRIP[113] is based, and therefore the method used in this code for construction of the groups was applied. Some test calculations showed however, that the demanded accuracy is not achieved if the method is used without modifications. This is true at least if the resonances are considered one by one, but perhaps error cancellations may improve the overall results. This is not considered sufficient, however, for which reason the grouping method was modified somewhat. For example, the group widths between the resonances from cadmium cut-off up to approx. fifty eV were reduced. At 10 eV the width is 0.08 eV in SDP, while 0.25 eV is obtained by the STRIP method. In STRIP all cross sections are cal-

culated in the mid-point of each group, and it is shown that this approach is generally better than the assumption of linear variation within the group. This rule is utilized in SDP as far as the extremely narrow groups very near the resonance energies are concerned. However, some investigations have proved that much more accurate results are obtained for some resonances if group average reaction cross sections are employed in those of the relatively wide groups between the resonances which are next to the extremely narrow resonance groups. Alternatively, some rather narrow groups could be introduced in a transitional region, and in fact the code system contains facilities for this. In this transitional interval, however, the flux is not fast-varying because it approaches the asymptotic 1/E-flux, and the additional groups are only necessary because this interval contains too few mesh points for accurate integration of the reaction cross sections. Therefore the first method, which is the faster one, is recommended. The SDP method of constructing group structures from resonance parameters was tested on many different geometries by means of synthetic resonances with typical as well as marginal parameters, and in all cases the above-stated accuracy requirements were achieved.

Another way of setting up group structures which is included in the programme system is based on the United Kingdom Nuclear Data Library (UKNDL)[123,124]. Here the distance between tabulated energy points also depends on the rate of change of the cross sections. The library is said to contain so many energy points that the cross sections may everywhere be calculated with adequate accuracy by linear interpolation in a double logarithmic scale between tabulated points. At least for the best tabulated neutron cross sections this ideal situation has been reached. A procedure in the RESAB programme system builds up group structures with group widths that are approximately proportional to the distance between tabulated points in the UKNDL. However, the lethargy widths of the groups are changed in steps of at least thirty per cent for them to comply with the mentioned wish for constant lethargy widths of as many consecutive groups as possible. Some test calculations proved that for fissile nuclides it is generally adequate to use a number of groups about equal to the number of tabulated points in UKNDL.

In table 5.1 the number of groups in specified intervals generated by the SDP method is compared with available information concerning the group numbers used in other multi-group resonance-region slowing-down codes.

The group structures may be supplied with group editions calculated by the multi-level routine, DOREN, described in section 3.4. DOREN deter-

Table 5. 1

Number of groups used in different slowing-down codes at 300 K

Energy interval (eV)	0.5-3940		0.5-1200	0.5-150 *)			References
Isotopes / Code	^{238}U	^{232}Th	^{238}U	^{238}U	^{235}U-^{238}U	^{235}U-^{238}U-^{239}Pu-^{240}Pu	
STRIP flat flux in two regions	2210	2355					113)
SDP multi-region code	2789	2765	1714	798	1415	1633	
SDR multi-region code, particularly for fast reactors	78000		43000	11400	11400	11400	15)
LEWIS AND ADLER flux represented by polynomials			6100				117)
SDP tape numbers cf.table 5.2	21093	21094	21093	21093	21078	20527	

*) The main resolved region for fissile nuclides.

mines the group mid-point cross sections, while the mentioned group averaging is performed afterwards by adding to the DORES results the differences between mid-point and average cross sections in the actual groups. These differences are calculated by single-level formalism in order to speed up the cross section generation.

Naturally narrow group cross sections may also be obtained from the UKNDL. In this case the cross sections in any group are average cross sections calculated according to the described linearity in double logarithmic scale.

One may ask why two methods have been developed for solving of the same problem. Several reasons may be emphasized. First of all the UKNDL comprises today only tabulations at a temperature of 300 K even though the Doppler broadening is very important for some nuclides. Not only the cross sections, but also the group structures are changed at elevated temperature. Next, one of the main objectives of setting up SDP has been to investigate the accuracy of current resonance absorption approximations,and therefore it is considered important to know the exact parameters on which the cross section tabulations used in SDP are based. These test calculations concern the mathematical slowing-down formalism, and comparison of different cross section evaluations is not of interest in this connection. It is supposed that the best way of meeting this requirement is to perform the cross section calculation instead of using known tabulations. Furthermore, the UKNDL shows some minor inconsistencies in the upper part of the resolved resonance region for fertile nuclides as discussed in section 3.3. On the other hand the UKNDL tabulation for the fissile nuclides is considered the best available, at least when it is desired to avoid a large evaluational effort.

If more resonance isotopes are included in one slowing-down calculation, it is important that the used group structure is at all energies as close as the group structure belonging to any one of the isotopes. In order to build up such common group structures a special mixing procedure has been developed.

The procedures described in this section are collected in the programme introduced in section 2.5 as REBAB system FILE 2. The resulting group structure together with scattering-, absorption- and fission-microscopic, narrow-group cross sections of the corresponding isotopes are read out on magnetic tape with fifty groups per record. Afterwards SDP may be run with this tape as input tape. It is clear that a tape should not be used in calculations comprising fewer isotopes than listed on the tape because the tabulation contains more groups than necessary for such calculations.

Even though all input tapes may be reproduced at any time with the RESAB resonance parameter library and/or the UKNDL, input tapes for some frequently occurring configurations were preserved as library tapes. In table 5.2 these are listed together with the data from which they originate.

Alternatively, SDP itself contains facilities that allow the resonance integral of an isolated resonance to be determined directly with single-level parameters as the only input. In this case the code constructs the interval inside which numerical slowing-down calculations must be performed and provides analytic rest terms of the form described in section 4.5.4. Also wide group cross sections in specified subintervals may be determined if the code is run in this way. On this point it differs from the equivalent homogeneous RESCOLDENS code, which always considers one resonance as an indivisible whole.

5.5. Storage Organization

It appears from section 5.2 that the calculation of collision densities in a group, n, presumes knowledge of the collision densities and cross sections in the groups round the energy E/α_{jk}. If α^M is the smallest of all α_{jk}'s it is obvious that group structures, collision densities and energy-dependent cross sections in the interval from E_{n-1} to roughly E_n/α^M must be stored, but it is also clear that the values belonging to the groups above this interval may be deleted. Hydrogen, for which storage is never necessary ($\alpha_{jk} = 0$), constitutes an exception to this rule. If the fast memory of the computer at a certain n is filled up with previously stored numbers, and if those that were stored first are now unnecessary for the above reason, then the quantities from group n and further on may be transferred to the beginning of the list before they are stored. By this "cycling" an unlimited number of narrow groups may be treated. If, however, the sketched condition for the applicability of the cycling is not fulfilled, the necessary quantities for the lightest isotopes may by SDP be stored on magnetic tape, which is the only type of disposable external storage on the computer actually used (IBM 7094, NEUCC). It has been possible to organize the use of tapes in such a way that its influence on the running time is only small. Two tapes are used per isotope. On one tape the results from group number n are read out, while the quantities belonging to the groups round E_n/α_{jk} are read from the other. When all data on the latter tape have been used, the tapes are rewound, and the modes of operation of the two tapes are interchanged. In this way any backspacing is avoided. In practice it was in all calculations performed until now necessary to use external storage only for deuterium.

Table 5.2

SDP input tapes of general character

Tape number (IBM 7094 NEACC, binary)	DFN	Temp. (K)	Energy interval (eV)	Number of groups	Materials and kind of data (the symbolism is explained in table 5.3 below)
20527	358940	300	$0.24\text{-}10^4$	4090	^{235}U (11) ^{238}U (01) ^{239}Pu (11) ^{240}Pu (11)
20631 *)	238	1200	0.24-4000	2497	^{238}U (00) s-wave resonances
21072	235238	300	$0.24\text{-}10^4$	3497	^{235}U (11) ^{238}U (01)
21093 *)	238	300	0.24-4000	2828	^{238}U (00) s-wave resonances
21094 *)	232	300	0.24-4000	2804	^{232}Th (00) s-wave resonances

*) Suitable for comparisons with link ALFA calculations because the cross sections are based on the RESAB resonance parameter library.

Table 5.3

Explanation of the symbols used in the last column of table 5.2

Source of cross section \ Source of group structure	RESAB resonance parameter library	UKNDL
RESAB resonance parameter library	(00)	(10)
UKNDL	(01)	(11)

although the programme was run on a machine with only 32 K memory locations, and 15 spatial regions have often been used. The extensive use of dynamic overlay storage allocation[125] in the RESAB programme system form the basis of this result.

In STRIP[113] and RIFF RAFF[118] the storage problem was solved by setting the flux equal to the asymptotic flux whenever the necessary fast memory for treating of the light nuclides happens not to be available. It is obvious that the neutron balance is destroyed by the use of the asymptotic flux in the groups round E_n / α_{jk}.

The number of spatial regions and the number of isotopes are unlimited in SDP, but of course the number of available tapes and the demand for a reasonable running time imply restrictions in practice.

5.6. Numerical Checks of SDP

As discussed in section 5.3 an investigation of the neutron balance may be considered as a highly sensitive test of SDP. Out of 10^8 neutrons about one is lost or gained per group if the computer in use is an IBM 7094. An earlier version of the code was written for the very small computer GIER, and here the corresponding numbers were about one neutron out of $2 \cdot 10^9$. Both results are about equal to the maximum obtainable accuracy on the respective machines. It indicates how accurately the asymptotic 1/E-flux may be reproduced in non-absorbing cases with energy-independent cross sections. It is of course a condition that the accuracy of the iteration mentioned in section 5.2 is of the same order.

The homogeneous problem with constant absorption in a pure moderator, which may be solved analytically[24], was also investigated with ^{12}C as moderator. The SDP result is equal to the analytic solution.

The most important test is, however, the comparison with the Monte Carlo programme, MCSUP[82], mentioned in the introduction to this chapter. The ^{238}U resonance at 6.7 eV was examined with 14 and 3 eV as upper and lower cut-off energies. The parameters, which are the same as those used by J. Megier in PETARD[115], but different from those contained in the RESAB library, are listed in reference 82. In the Monte Carlo calculations the isotropic laboratory scattering used in SDP is simulated. The SDP calculations comprise eight spatial regions in the absorber and seven in the moderator. This is perhaps more than strictly necessary, but it makes the choice of region thicknesses less critical. The determination of spatial mesh structure is discussed in greater details in chapter 7. In the calculations the cell radius is a hundred times as large as the radius of the ab-

sorbing rod, and thus the rod may be considered as isolated. No differences exist between the physical assumptions underlying the two methods, while the mathematical techniques are completely unrelated. The results are listed in table 5.4. Included in the table are also the results based on the assumption of flat flux in two regions. The effect of subdivision of spatial regions will be analysed in detail later on, and the results are only listed here to supply a better background for the comparison between the Monte Carlo calculations and the multi-group multi-region approach. It is pointed out that differences of up to two standard deviations are acceptable from a statistical viewpoint, and it must be recalled that the SDP results may contain errors of up to one per thousand. Also the Monte Carlo technique used in MCSUP includes systematical errors of this order of magnitude. The SDP results are obtained ten times as fast as the Monte Carlo results. However, in most practical cases it is enough to use two or three spatial regions instead of fifteen, and the SDP running time is roughly proportional to the square on the number of regions. On the other hand a more reasonable accuracy requirement will also speed up the Monte Carlo calculation very much.

For non-isolated rods the MCSUP and SDP calculations may not be compared directly because the flux in MCSUP obeys the reflecting boundary condition in a square cell, while the SDP cell is circular and the isotropic return boundary condition is used. This latter case is, however, simulated by an older Monte Carlo code also developed by Kirkegaard [126]. This code is based on a much more direct simulation than MCSUP. The statistical quality of the code is inferior to that of MCSUP, for which reason accurate results demand much more computer time. The results appear from table 5.5. The latter case, which concerns a rod with a diameter of 20 cm, is without any practical importance. On the other hand this marginal problem constitutes a thorough check of the codes. Actually, 15 spatial regions in SDP were not enough, and 26 were used.

Apart from this numerical check the reliability of SDP was confirmed by several experimental results. This sort of verification forms a minor part of the objective of the rest of this report.

Table 5.4.

Comparison of Monte Carlo and SDP resonance integrals, RI, for the ^{238}U resonance at 6.7 eV in an isolated metal rod

Rod radius (cm)	Moderator	MCSUP		SDP	
		RI (b)	Standard deviation (b)	RI subdivision (b)	RI, only two spatial regions (b)
1.0	H	3.032	0.006	3.037	3.121
1.0	H_2O	3.017	0.007	3.022	3.121
1.0	D	3.061	0.012	3.059	3.121
1.0	D_2O	3.005	0.006	3.010	3.121
1.0	C	2.933	0.016	2.941	3.121
1.7	H	2.249	0.007	2.247	2.337

D and H moderations mean light- and heavy-water moderation respectively where the influence of oxygen is neglected.

Table 5.5

Resonance integrals, RI, for the ^{238}U resonance at 6.7 eV in non-isolated metals rods. The outer cell boundaries are circular and white, and the moderator is hydrogen with density as in light water

Rod radius (cm)	Cell radius (cm)	Monte Carlo		SDP	
		RI (b)	Standard deviation (b)	RI subdivision (b)	RI, only two spatial regions (b)
0.2	0.3	4.279	0.015	4.293	4.305
1.0	1.1	1.578	0.007	1.577	1.585
1.0	1.5	2.794	0.008	2.790	2.823
10.0	15.0	0.689	0.003	0.691	0.802

6. RESONANCE INTEGRAL CALCULATIONS BASED ON THE FLAT FLUX ASSUMPTION

The accuracy of the approximate methods developed and described in chapter 4 is now investigated by means of numerical slowing-down calculations performed by SDP. As subdivision of the material regions is left out in SDP, the numerical approach as well as the methods of analytic character (the "link ALFA" methods) originate in the flat flux assumption. The use of link ALFA always comprises one or more homogeneous resonance integral calculations, and in such calculations the different available approximations are combined according to the scheme described in section 4.5 unless it is explicitly mentioned that the approach is different.

6.1. The Effect of a Non-NR External Moderator

In section 4.3 a method of allowing for the finite slowing-down power of an actual reactor cell was discussed. It is obvious and well known that the approximation expressed in eq. (4.30) is accurate in so far as resonance interference is concerned owing to the flux recovery between the resonances. That eq. (4.30) applies to a single, very wide resonance too, must be established by numerical calculation.

The 6.68 eV ^{238}U resonance with the parameters Γ_n = 1.52 meV, Γ_γ = 23.43 meV and σ_p = 10.64 b (RESAB library) is considered with the "1/v-tail" subtracted below the resonance peak (cf. section 4.5.4). The applied densities appear in table 6.1, and the temperature is 300 K. The moderator cross sections are listed in table 6.2. The validity of eq. (4.30)

Table 6.1.

Material densities

Material	U-metal	UO_2	C	D *)	$H_{(1)}$ **)	$H_{(2)}$ ***)
ρ (g/cm^3)	18.57	10.6	1.6	0.2	0.1107	0.05535

*) Deuterium density in heavy-water.
**) Hydrogen density in light-water.
***) Hydrogen density in light-water with 50% void.

was investigated in homogeneous as well as in heterogeneous cases. From the tables 6.3 and 6.4 it is concluded that the approximation is most accu-

Table 6.2.

Microscopic cross sections

Isotope	O	C	D	H
σ (barns)	3.8	4.65	3.4	20.4

Table 6.3.

Homogeneous, exact calculation for the 6.68 eV ^{238}U resonance

Moderator	N_{mod}/N_{238_U}	$\langle \sigma_S \xi \rangle$ (barns)	Resonance integral (barns)		
			RI	RI'_1 calculated from RI *)	RI' NR moderator
H	1:1	20.49	3.824	4.233	4.222
H	1:2	40.89	5.565	5.981	5.973
D	1:4	9.95	2.998	3.567	3.458
D	1:10	24.75	4.976	5.556	5.448
D	1:40	98.74	10.67	11.29	11.18
C	1:10	7.43	4.672	7.368	6.384
C	1:50	36.77	13.08	16.17	14.96
C	1:400	293.5	44.79	48.60	47.02

*) $RI'_1 = -\langle \sigma_S \xi \rangle \log(1 - RI/\langle \sigma_S \xi \rangle)$. Cf. eq. (4.30).

rate when the system is hydrogen moderated. This is due to the simple structure of the Placzek function [24] for this isotope. The difference between RI and RI' for a single resonance is unimportant unless the lattice is highly undermoderated (i.e. $\langle \sigma_S \xi \rangle$ small), a situation which in practice only occurs in light-water reactors, where the dominating moderator is hydrogen. Generally the use of eq. (4.30) introduces a smaller error in the calculation than most of the other approximations involved in link ALFA.

Table 6.4.

Two-region, heterogeneous SDP calculation for the ^{238}U resonance at 6.68 eV. The resonance integrals include analytic residual terms (cf. section 4.5.4). The cell is cylindrical

Fuel	Mod.	Radius		$\langle \sigma_S \xi \rangle$	Resonance integral, barns		
		Rod	Cell		RI	RI'_1 calculated from RI *)	RI', NR external moderator
U	$H_{(1)}$	1.0	1.5	36.29	2.993	3.124	3.119
U	$H_{(1)}$	0.2	0.3	36.29	4.447	4.744	4.737
U	$H_{(2)}$	0.2	0.3	18.19	3.312	3.656	3.645
U	D	0.5	1.0	9.576	2.557	2.975	2.898
U	D	0.5	2.0	47.53	4.042	4.224	4.193
U	C	0.5	2.0	18.90	4.076	4.591	4.472
U	C	0.5	4.0	79.11	4.550	4.686	4.656
UO_2	$H_{(1)}$	1.0	1.5	72.94	4.604	4.756	4.721
UO_2	$H_{(2)}$	0.2	0.3	36.47	5.136	5.529	5.451

*) $RI'_1 = -\langle \sigma_S \xi \rangle \log(1 - RI/\langle \sigma_S \xi \rangle)$. Cf. eq. (4.30).

6.2. The Isolated Rod

According to the discussion in section 4.3 the external moderator may be exactly represented by a NR moderator in the case of an isolated rod. One of the main purposes of the present section is to compare the equivalence principles expressed in eqs. (4.26) and (4.28) and derived from the Bell factor and the Carlvik collision probability approximation respectively (eqs. (4.4) and (4.5)).

6.2.1. Single Resonance Investigation

Four ^{238}U resonances of greatly differing characters were selected. The parameters as taken from the RESAB library are listed in table 6.5, and the densities 18.8 and 10.6 g/cm^3 are used for U-metal and UO_2 respectively. The configurations applied are described in table 6.6. The correlating parameter, S_c, contained in the table is defined as

$$S_c = \begin{cases} S & \text{U-metal} \\ S + 1 \times 2 \times v_{O_2} = S + 4.7 \times 2 \times 5.29 & UO_2 \end{cases} \qquad (6.1)$$

S is introduced in eq. (4.18) and the factor f was discussed in reference C.

Table 6.5.

The parameters of four representative resonances (RESAB library, ^{238}U, σ_p = 10.64 b)

E_r, eV	6.68	66.30	80.77	190.34
Γ_n, meV	1.52	25.16	2.07	150.4
Γ_γ, meV	23.43	26.07	21.17	23.21

Table 6.6.

The rods considered in section 6.2

Number	Material	Radius (cm)	Surface to mass ratio S/M (cm^2/g)	σ_{ex} (eq. (4.6)) (barns)	S (eq. (4.18)) (barns)	S_c (eq. (6.1)) (barns)
1	U-metal	1.4	0.076	7.51	8.45	8.45
2	U-metal	0.5	0.212	21.03	24.19	24.19
3	U-metal	0.2	0.531	52.57	60.99	60.99
4	UO_2	2.0	0.094	10.58	11.64	17.15
5	UO_2	0.85	0.222	24.89	28.22	33.73
6	UO_2	0.625	0.301	33.85	38.65	44.16
7	UO_2	0.3	0.627	70.52	81.40	86.91

Resonance integrals determined by means of RESCOLDENS (exact, homogeneous. Cf. section 4.5) combined with an equivalence principle are in figs. 8.1-6.4 compared with SDP calculations based on exact collision probabilities. It appears that the accuracies obtained by the two investigated equivalence principles are about equal, and the error is largest when the resonance is dominated by scattering ($\Gamma_n > \Gamma_\gamma$. Cf. the 190 eV resonance). The optimum character of the chosen Bell factor manifests itself in the fluctuating sign of the error involved in this approximation, while the deviation is more systematic in those cases where the Carlvik approximation is applied. Heterogeneous SDP calculations were also per-

formed by direct use of Carlvik's probability approximation. Here the errors were considerably smaller than 1%, proving that the lack of an exact equivalence principle is the main source of the error connected with the two-term equivalence relation (eq. (4.28)). When the Bell factor is applied (eq. (4.26)), the deviation is entirely due to the collision probability approximation as emphasized in section 4.3.

It is seen that the correlation of the metal and oxide resonance integrals expressed in eq. (6.1) may only qualitatively be extended to the fractional error of the equivalence principles.

The detailed fluxes around 190 eV, by which the absorption cross section was multiplied before the integration, are in fig. 6.5 illustrated for configuration number 2. The flux corresponding to the two-term equivalence principle is determined by combination of two homogeneous calculations. For explanation of the appearance of the curves representing the fractional errors of the approximations fig. 4.1 should be consulted. Especially the so-called "flux-bump" [127, 128] just below the resonance peak, which is characteristic for a strongly scattering resonance, is badly reproduced by means of the equivalence principles.

One may think that the efforts spent on the inclusion of the scattering interference in the IR method were spent in vain owing to the rather poor accuracy of the equivalence principles when used on resonances with predominant scattering (and therefore large scattering interference). That this conclusion is wrong appears from table 6.7, where two resonances with considerable scattering are investigated. The scattering interference is represented fairly well by the combination of the equivalence principles and the complete IR treatment (cf. eqs. (4.41) and (4.42)).

Table 6.7.

The influence of scattering interference on heterogeneous resonance integrals (barns). T = 300 K ("1/v-tail" subtracted)

E_r (eV)	Rod number cf. table 6.6	Scat. int. neglected		Scat. int. included	
		SDP exact	IR*)	SDP exact	Complete IR*)
66.30	1	0.371	0.378	0.451	0.447
	6	0.803	0.823	0.965	0.943
190.34	1	0.120	0.128	0.174	0.167
	6	0.221	0.230	0.267	0.275

*) Carlvik's collision probability approx.

6.2.2. Total Resolved s-wave Resonance Integrals

Some of the different methods of treating the two-region problem available in the RESAB programme system are compared in table 6.8. The configurations with the numbers 1 and 6 above are considered. In the table methods 3, 4, 5, and 6 include resonance overlap effects. Methods 2 and 4 are based on two homogeneous resonance integral calculations each, while one slowing-down calculation suffices in the other methods.

The investigations in section 6.2.1 combined with an analysis of table 6.8 show that the Carlvik collision probability approximation does not provide a more accurate equivalence principle than the Bell factor formalism, for which reason the latter method must be preferred because it is the simplest one. When other resonance nuclides than ^{238}U are considered, it should, however, be borne in mind that the Bell factor has been fitted to the case of ^{238}U.

It is concluded that the accuracy of the method of calculating homogeneous resonance integrals in link ALFA suits the accuracy of the Bell factor formalism very well. The fractional error in both approximations is about 2%.

Table 6.8.

Total s-wave resonance integrals below 3500 eV
1/v cross section is included above 0.5 eV. T = 300 K (barns)

Rod number, cf. table 6.6			1	6
1	Link ALFA approx.	Bell factor, eq. principle	9.21	18.13
2	Link ALFA approx.	Carlvik, eq. principle	9.45	18.42
3	SDP *), hom.	Bell factor, eq. principle	8.91	17.94
4	SDP *), hom.	Carlvik, eq. principle	9.17	18.26
5	SDP *), het.	Carlvik's collision prob. approx.	9.03	18.07
6	SDP *), het.	Exact collision prob.	9.01	18.05
		Exact		

*) Tape No. 21093 was applied, cf. table 5.2.

6.2.3. The Influence of an Internal Moderator in the Absorbing Rod

If the absorbing lump contains a moderator besides the resonance absorber, then the exact slowing-down kernel corresponding to this internal moderator is included in the equations on which the equivalence principles are based (eqs. (4.25) and (4.31)). Formerly such a moderator has often been treated as an NR moderator in analogy with the external moderator [24, 88]. This is a rather poor approximation, but the result may be improved somewhat by reduction of the cross section of the internal moderator by a factor, f, which, contrary to the interpolation parameter, λ, in the IR formalism, only depends on isotopic composition (cf. eq. (6.1) [84]. The value of f is 0.70 in UO_2, 0.72 in UC and 0.90 in ThO_2 [C, D].

Here it is the intention to investigate how accurately the influence of the internal moderator may be calculated by the equivalence principles when the correct slowing-down kernel is included. The resonance integral for rod number 1 was compared with that obtained if the metal rod is replaced by a fictive UO_2 rod with equal uranium concentration and radius. Correspondingly the UO_2 in rod number 6 was replaced by U-metal with a fixed concentration of the absorber. Now the reduction of the self-shielding due to oxygen may be determined by direct subtraction. The first highly academic example provides a very sensitive test, while the second one is more realistic. The results are collected in table 6.9. Especially in the second example the representation of oxygen in the equivalence principle is accurate.

6.2.4. The Accuracy of the Doppler Coefficient Determined by Link ALFA

In section 4.6.1 a comparison between measured Doppler coefficient and calculations based on link ALFA was mentioned. However, the calculations contain several approximations which may be eliminated by heterogeneous SDP treatment with the DORES cross section tabulations (section 3.1). If the temperature-dependent resonance integral is expressed as

$$RI(T) = RI(300\ K) \times (1 + \beta(\sqrt{T} - \sqrt{300\ K})), \qquad (6.2)$$

then the coefficient β varies only a little with the temperature. By means of tapes Nos. 21093 and 20831 (cf. table 5.2) β may be calculated for T = 1200 K if the temperature distribution is assumed to be flat. The results for some of the rods described in table 6.8 are compiled in table 6.10.

Table 6.9.

The reduction of self-shielding due to oxygen in a uranium fuel rod
Resolved s-wave resonances are considered in the energy interval
0.5-3500 eV. 1/v absorption included

Rod No.		1 $\rho = \begin{cases} 18.80\ g/cm^3, & U \\ 21.32\ - , & UO_2 \end{cases}$		6 $\rho = \begin{cases} 9.34\ g/cm^3, & U \\ 10.60\ - , & UO_2 \end{cases}$	
Method	Material	Res. int. (barns)	Influence of oxygen (barns)	Res. int. (barns)	Influence of oxygen (barns)
SDP, het., two regions, tape No. 21093	U	9.01		17.11	
	UO_2	10.36	1.35	18.05	0.94
Link ALFA, hom., eq. princ., Carlvik coll. prob. approx.	U	9.45		17.45	
	UO_2 *)	11.05	1.60	18.42	0.97
		(11.88)	(2.43)	(18.72)	(1.27)
Link ALFA, hom., eq. princ., Bell factor	U	9.21		17.19	
	UO_2 *)	10.89	1.68	18.13	0.94
		(11.75)	(2.54)	(18.49)	(1.30)

*) The numbers in the parentheses are based on NR treatment of O_2, while the other UO_2 calculations include the non-NR effects for all fuel material isotopes.

Table 6.10.

s-wave Doppler effect below 3500 eV. 1/v absorption above 0.5 eV is included in the resonance integrals from which β is determined

Rod No., table 6.6		1	2	4	5	6
β (cf. eq. (6.2))	SDP	0.44	0.54	0.52	0.62	0.67
	Link ALFA, eq. princ. *)	0.47	0.57	0.55	0.64	0.69

*) Bell factor coll. prob. approx.

The accuracy of the temperature coefficients determined by the link ALFA is better than could be expected considering the rather heuristic arguments on which the calculations are based. It should be borne in mind that only a very small part of the Doppler effect originates in the wide low-energetic resonances which according to the calculational scheme of link ALFA are treated by the accurate routine, RESCOLDENS.

6.3. Geometrical Effects Originating in Non-Absorbing Regions

The methods of handling the outer limitation of a cell in an infinite lattice will now be examined. In accordance with section 6.1 the cell is here considered as NR-moderated in the outer region. Also the influence of a cladding zone is investigated below.

6.3.1. Cylindricalized Cell

Even though the Dancoff factor may be calculated for a realistic square or hexagonal lattice, the cylindrical cell is still important because here the calculation of the Dancoff factor is extremely fast. From fig. 4.2 it appears that Nordheim's approximation is more accurate in the cylindrical geometry than in the square cell, and the error is so small that a very accurate representation of the influence of the Dancoff effect on the resonance integral must be contained in the equivalence principles based on Nordheim's formula. This is verified by a single example in table 6.11.

6.3.2. The Effect of Cylindricalization

A few single-resonance cases were investigated by means of the Monte Carlo programmes mentioned in section 5.6 in order to disclose whether there should be a coupling of any importance between the detailed spatial flux distribution and the square cell effects. In the collision probability approach it is only possible to consider the detailed flux by subdivision in a cylindrical cell (cf. chapter 7), while the square cell treatment is confined to two-region cases based on the flat flux assumption. For this reason it is important that a coupling does not exist. From table 6.12 it is concluded that the SDP two-region treatment in fact provides a good estimate of the effect of the cylindricalization. The last example, in which the lattice pitch is equal to the rod diameter, represents the closest possible square lattice, and even in this marginal situation the two-region approach gives the correct result.

In table 6.13 total resolved s-wave resonance integrals are analysed.

Table 6.11.

The reduction of the resonance integral due to the Dancoff effect (0.5-3500 eV, tape No. 21093). Rod radius = 0.625 cm and V_2/V_1 = 1.25. H_2O-NR-moderation, ρ = 0.497 g/cm^3 (50% void). The cell is cylindrical with C_o = 0.3954, and the fuel material is UO_2 (ρ = 10.6 g/cm^3)

Method		Res. int. (barns)	Reduction (barns)
SDP, exact coll. prob., het.	Isolated rod	18.05	3.45
	Lattice	14.60	
Link ALFA, eq. principle, Carlvik	Isolated rod	18.42	3.48
	Lattice	14.94	
Link ALFA, eq. principle, Bell f.	Isolated rod	18.13	3.38
	Lattice	14.75	

Table 6.12.

Comparison of cylindrical and square cells with H moderation (non-NR), $\rho = 0.1107$ g/cm^3 (~ H_2O). The ^{238}U resonance at 6.68 eV is considered in the energy interval 3-14 eV with 1/v contribution included. The resonance parameters applied are those used in section 5.6 (different from RESAB library). The rod material is U-metal with $\rho = 18.57$ g/cm^3

Rod radius (cm)	Eq. cell radius (cm)	Sq. cell Dancoff factor	Monte Carlo						SDP two-region		
			Res. int. (barns)				Difference (barns)		Res. int. (barns)		Difference (barns)
			cyl.	s.d.	sq.	s.d.		s.d.	cyl.	sq. **)	
1.6	1.5	0.1315	2.794	0.008	2.733	0.004	0.061	0.009	2.817	2.767	0.050
0.3	0.3	0.5760	4.28	0.02	4.22	0.01	0.06	0.02	4.30	4.23	0.07
1	1.129 *)	0.6014	1.780	0.009	1.626	0.007	0.154	0.012	1.794	1.641	0.153

cyl. = cylindrical cell, sq. = square cell, s.d. = standard deviation, Eq. = equivalent

*) sq. lattice pitch = 2 cm

**) collision probabilities obtained from the corrected Nordheim's approximation combined with exact P_0. Cf. section 4.2.4.

Table 6.13.

The influence of cylindricalization and the accuracy of Nordheim's formula. $V_2/V_1 = 1.25$. The Dancoff factors are listed in table 6.14 (0.5-3500 eV, tape No. 21093)

Rod radius			1 0.625 cm		2 0.2 cm	
Moderator			H_2O (NR) $\rho = 0.497$ g/cm^3		H (NR)*) $\rho = 0.05535$ g/cm^3	
Fuel			UO_2, $\rho = 10.6$ -		U, $\rho = 18.8$ -	
Method	Collision prob.	Cell geometry	Res. int. (barns)	Cyl. cell - sq. cell (barns)	Res. int. (barns)	Cyl. cell - sq. cell (barns)
SDP, het.	Exact	Cyl.	14.60		11.26	
	Nordheim, p_o exact	Sq.	14.36	0.24	11.07	0.19
	Corrected do.	Sq.	14.38	0.22	11.12	0.14
Link ALFA,	Nordheim, Bell f.	Cyl.	14.75		11.40	
eq. princ.	do.	Sq.	14.52	0.23	11.22	0.18

*) Hydrogen in water, 50% void.

Table 6.14.

Dancoff factors (C_o) applied in table 6.13

Rod number	1	2
Cyl. cell	0.3954	0.7326
Sq. cell	0.4198	0.7423

The first example corresponds with the case examined in section 6.3.1, while the geometry in the second example is that described in fig. 4.2. In the latter case a difference between Nordheim's uncorrected and corrected formula (cf. section 4.2.4) may be detected according to fig. 4.2, while the two formulas provide almost equal results in the first case, in which the moderator-region optical mean chord-length is larger. A more extensive analysis of the errors introduced by Nordheim's approximation has been performed by Mizuta and Fukai [92] for the hexagonal lattice. The error is always far below 1% on the resonance integral.

From the calculations above it is concluded that in most cases the cylindricalization only implies a small error.

6.3.3. Comparison of Cell Geometries

In table 6.15 the resonance integrals determined by SDP for a series of different geometries are compared. The mean chord-length of the fuel region and moderator to fuel volume ratio are equal in all the cases. It appears that the resonance integral may only be varied by a few per cent when these parameters are fixed.

6.3.4. The Influence of Cladding

Two types of cladding material were investigated.

1. Al, A = 26.98, σ_S = 1.418 b, ρ = 2.699 g/cm^3 .
(research reactor)

2. SS348 + "air gap", A_{eff} = 55.02, σ_S = 11.97 b, ρ = 7.93 g/cm^3
(stainless steel, Yankee reactor)

On account of the low macroscopic cross section of Al a region containing this material resembles an air gap very much. The cell considered is again equal to that described in section 6.3.1 with the exception that part of the water has been replaced by a thin cladding [illegible]

(0.075 cm). If the cladding material is treated as an NR moderator, the Dancoff factor may be calculated as

$$C_o = 1 - \frac{\sum_{j=2}^{3} V_j \Sigma_{Tj} P_{1j}^b}{S/4}, \qquad S = \text{fuel surface} \qquad (6.3)$$

where regions 2 and 3 are cladding zone and external moderator region respectively. The P_{1j}^b's are collision probabilities determined in the black absorber limit. In table 6.16 the resonance integrals obtained by different approximations are listed. As far as Al cladding is concerned, the link ALFA approximation works perfectly. The approximation is also satisfactory for SS348 in the academic NR case, but it is not sufficient to use eq. (4.30) to allow for the non-NR cladding effect. Owing to the relatively large atomic weight of the cladding it is in fact better to replace the cladding material by an air gap than to include an NR neutron source originating in the cladding zone. This conclusion is based on a comparison of cases numbers 6, 8 and 10 in table 6.16.

A long time ago Rothenstein proposed that the cladding should be treated as an air gap [129]. Rothenstein and Helholtz [130] have proved that the introduction of an air gap between the fuel and the moderator increases the resonance self-shielding a little, even though the moderator to fuel volume ratio is fixed. However, this effect is very small and unimportant in practice. If the cladding is removed, and the V_{mod}/V_{fuel} is fixed in the example of table 6.16, an SDP non-NR resonance integral equal to 11.15 b is obtained (cf. case No. 4).

Irrespective of the approach applied, the error introduced by the cladding treatment represents perhaps the most serious shortcoming of the link ALFA method. The influence of the cladding has also been investigated by Fukai and Mizuta [116], but an accurate equivalence principle has not been obtained here neither.

6.4. Effective Resonance Integrals of the Fissile Nuclides

The complexity of the detailed cross sections of the fissile nuclides necessitates a special testing of the approximations applied. The calculational methods have in fact a more approximate character here than in the case of fertile nuclides, but when the considerations are restricted to the epithermal region, the influence of the fissile nuclides is in thermal reactors generally correspondingly smaller than the effects related to the fertile isotopes.

Table 6.15.

^{238}U-oxide s-wave resonance integrals calculated by SDP in different cell geometries (two regions) (0.5-3500 eV, tape No. 21093). The absorber mean chord-length is fixed and moderator to fuel volume ratio is either 1.25 or ∞. Equivalent rod radius = 0.625 cm, ρ_{UO_2} = 10.6 g/cm^3, H_2O-NR-moderation, ρ = 0.497 g/cm^3

Geometry		Res. int. (barns)	Reduction due to Dancoff effect (barns)
Absorber	Cell		
Slab	Is.	17.84	
Cyl.	Is.	18.05	
Slab	Slab	14.79	3.05
Cyl.	Cyl.	14.60	3.45
Cyl.	Hex.*)	14.44	3.61
Cyl.	Sq.*)	14.36	3.69

Is. = isolated, Cyl. = cylindrical, Hex. = hexagonal, Sq. = square.

*) Collision probabilities obtained from Nordheim's approximation combined with exact p_o.

Table 6.16.

The influence of cladding on the ^{238}U-oxide resonance integral (0.5-3500 eV, tape No. 21093). The cell is described in the text

		Res. int., barns		
Clad. material		"H_2O"	Al	SS348
SDP, het., exact coll. prob., three regions	NR	(1) 14.60	(3) 13.89	(7) 14.76
	Non-NR		(4) 11.14	(8) 11.33
Link ALFA, eq. pr., Bell f.	NR	(2) 14.75	(5) 14.07	(9) 14.90
	Non-NR*)		(6) 11.22	(10) 11.78

eq. pr. = equivalence principle, NR = NR moderation in external regions.

*) cf. eq. (4.30).

6.4.1. Comparison with an Integral Measurement

The accuracy and mutual consistency of the available experimental data for the fissile nuclides are not too good. This is in particular true as regards integral data. Therefore the different calculations may not be directly compared with reference results, and instead an accordance between two results has to be considered as some sort of support for both methods.

In a 1/E-spectrum the shielded ^{235}U fission - and absorption resonance integrals have been measured by Schoenig et al. [131] for a cadmium-covered UO_2 rod enriched to 95.2% in ^{235}U (ρ = 10.35 g/cm^3, radius = 0.432 cm). In table 6.17 this measurement is compared with RESAB calculations. Here the terminology "no ^{238}U res." means that ^{238}U is included in the calculation as a purely potential scatterer, while "^{238}U res. incl." implies that the overlap effect due to the ^{238}U resonances is taken into account. The "smooth" cross section in this highly enriched rod is so large just above the cadmium cut-off that it is necessary in link ALFA to include a shielding factor, L_{sm}, accounting for the flux depression due to this non-resonance absorption. The WR approximation is applied here for all isotopes in the rod.

$$L_{sm}(E) = \frac{S}{S+\sigma_{T,\,smooth}(E)} \quad , \quad \sigma_{T,\,smooth}(E): \text{non-res. abs.} \qquad (6.4)$$

The link ALFA single-level treatment is based on Wigner's simple rational approximation (cf. section 4.2.3), and in the determination of the homogeneous resonance integrals only methods 1 and 2 (section 4.5) are used.

Table 6.17 comprises the Norwegian calculations based on the Adler and Adler multi-level method (RESU235 [33]), and also the calculational results of Schoenig et al. [131] are listed. This latter calculation, which resembles the link ALFA resolved-region treatment, includes only 87 resonances, while all lacking contributions are considered as "smooth" cross sections.

The difference between measured and calculated resonance integrals is in all cases smaller than the quoted experimental uncertainty. In table 6.18 the shielding factors below 100 eV are listed. The accordance between the SDP-UKNDL calculations and RESU235 is excellent. In the link ALFA treatment the shielding in the case of fission is a little too large. This is probably due to the neglected mutual shielding of consecutive resonances. The link ALFA capture calculations are a little controversial, which

is probably due to the large ^{235}U α-value inherent in the RESAB library (cf. table 3.2). The difference between the UKNDL ($\alpha = 0.50$) and the RESAB library α-value corresponds apparently to an unexplained inconsistency which generally occurs between cross section measurements ($\langle \alpha \rangle \sim 0.6$) and integral measurements ($\alpha \sim 0.5$).

Schoenig et al. have also measured Doppler coefficients. Here the status of calculational methods is more ambiguous as it appears from table 6.19. The discrepancy between RESAB calculations and the calculations of Schoenig et al. is presumably related to the low number of resolved resonances combined with the lacking statistical treatment in the analysis of Schoenig et al., while the difference between multi-level and single-level treatment is perhaps of a more fundamental character. Calculations of Doppler reactivity coefficients for fissile nuclides usually deviate very much from measurements, often by a factor of 2-3, and the theoretical explanation is in fact still lacking. This matter is, however, without practical importance in thermal-reactor calculations.

6.4.2. Self-Shielding and Resonance Overlap between ^{235}U and ^{238}U in the Region of Low Enrichment

An accurate analysis of the self-shielding and overlap effects was performed in the energy region 1.855-300 eV for isolated U-metal- and UO_2-rods by means of SDP and tape No. 21078 (UKNDL ^{238}U-^{235}U data, cf. table 5.2). With fixed ^{238}U number density, the enrichment in ^{235}U was varied between 0 and 5%, and the results obtained are illustrated in figs. 6.6-6.11. It appears that the ^{238}U capture decreases by about one per cent, when the enrichment increases by one per cent. Furthermore it is noted that the reduction in ^{235}U capture and fission due to the presence of ^{238}U resonances depends only slightly on enrichment, and when the fuel is less than 1.5-2% enriched this overlap effect is larger than the ^{235}U self-shielding. The total ^{235}U shielding is 20-25% at 2% enrichment for which reason this effect should not be neglected in for instance light-water reactor calculations.

In spite of the extreme complexity of the resonance overlap effect its order of magnitude may be estimated by very simple means. The ^{235}U resonance integral, I_R^5, is written down by use of a single term equivalence principle ($S^5 = S$ for ^{235}U) and the WR approximation for all rod isotopes.

$$I_R^5 = \int \frac{\Sigma_R^5 S^5}{\Sigma_f^5 + \Sigma_\gamma^5 + N_o^5 S^5 + \Sigma_\gamma^8} \frac{dE}{E}$$

$$\simeq \frac{S^5 N_o^5}{N_o^5 S^5 + \langle \Sigma_\gamma^8 \rangle} \; RI_R^5(S^5 + \langle \Sigma_\gamma^8 \rangle / N_o^5, T) \; . \qquad (6.5)$$

Σ_R^5 and Σ_γ^8 are ^{235}U reaction cross section and ^{238}U capture cross section respectively. N_o^5 is the ^{235}U number density, and $RI_R^5(S^5, T)$ the usual ^{235}U resonance integral for reaction R in the two-parameter homogeneous description with the ^{238}U resonances neglected. The permissibility of the substitution of $\langle \Sigma_\gamma^8 \rangle$ for Σ_γ^8 may only be established by numerical calculation. The average cross section is estimated as

$$\langle \Sigma_\gamma^8 \rangle = \frac{RI_\gamma^8(S^8, T)}{\Delta u} N_o^8 \; , \qquad (6.6)$$

in which the influence of ^{235}U is neglected. Δu is the lethargy width of the group considered. An expression analogous to (6.5) may be deduced for the ^{238}U resonance integral, I_γ^8. By means of the approximations

$$\frac{dRI_R^5}{dS^5} \simeq 0 \quad \text{and} \quad \frac{dRI_\gamma^8}{dS^8} \simeq \frac{RI_\gamma^8}{2S^8}$$

(cf. the approximate linear relationship between $RI_\gamma^6(S^8, T)$ and $\sqrt{S^8}$) the final expressions are deduced.

$$I_R^5 \simeq \frac{N_o^5 S^5}{N_o^5 S^5 + \langle \Sigma_\gamma^8 \rangle} \; RI_R^5(S^5, T) \qquad (6.7)$$

and

$$I_\gamma^8 \simeq \left(1 - \frac{\langle \Sigma_\gamma^5 \rangle + \langle \Sigma_f^5 \rangle}{2 N_o^8 S^8}\right) RI_\gamma^8(S^8, T) \qquad (6.8)$$

$(N_o^5 S^5 \simeq N_o^8 S^8)$.

The formalism has in a slightly different way been deduced by Askew [87] and is contained in the British WIMS code.

How this intuitive theory works in practice is illustrated in figs. 6.6-6.11. The resonance integral at the right-hand side of eq. (6.7) is determined by the SDP calculation with "no ^{238}U res.", while $RI_\gamma^8(S^8, T)$ equals

11.74 b for U-metal and 15.56 b for UO_2. The approximations are in fact more accurate than could be expected considering the statistical nature of the problem. It shows that a good estimate of the overlap effect may be obtained inside the framework of the two-parameter resonance reaction description (cf. section 4.3).

Included in the figures is also the single-level link ALFA treatment of the ^{235}U self-shielding based on Wigner's rational approximation. The resonance integrals are at infinite dilution normalized to the values of tape No. 21078. The accordance with the SDP self-shielding is satisfactory.

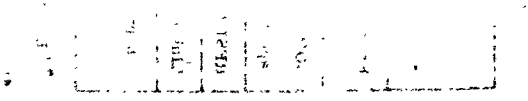

Table 6.17.

Comparison of ^{235}U resonance integral calculations with the experiment of Schoenig et al. (1969)

		Fission						Capture					
		Shielded res. int. (barns)			Inf. dilution res. int. (barns)			Shielded res. int. (barns)			Inf. dilution res. int. (barns)		
Energy region, eV		E_c*)-100	100-10 k	**) total	E_c*)-100	100-10 k	**) total	E_c*)-100	100-10 k	**) total	E_c*)-100	100-10 k	**) total
SDP tape No. 21078	no ^{238}U res.	86.8	38.0	135.5	204.9	49.1	264.7	41.9	17.0	61.6	114.0	22.5	138.2
	^{238}U res. incl.	86.3	37.9	134.9				41.4	16.9	61.0			
RESR235, ^{238}U res. incl.		89.6			205.7			40.0			110.5		
Link ALFA, no ^{238}U res.		96.9	41.7	149.3	203.6	50.4	264.7	49.3	20.7	72.1	140.6	26.3	169.7
Schoenig et al.	Calculated			144						60			
	Measured			151±18						67±8			

*) E_c, fission = 0.56 eV. E_c, capture = 0.57 eV. (Note: Inf. dilution res. int.'s are normally based on E_c = 0.5 eV).

**) Resonance integrals above 10 keV: fission 10.74 b, absorption 2.68 b [38].

Table 6.18.

Shielding factors below 100 eV calculated from table 6.17

	Fission	Capture
SDP, tape No. 21078, UKNDL	0.421	0.363
RESU235, multi-level	0.436	0.362
Link ALFA, single-level	0.476	0.351

Table 6.19.

Calculated and measured Doppler effect (ΔRI/RI)

	Fission 300-1800 K (%)	Capture 514-1550 K (%)
RESU235, multi-level	3.1 (0.58-100 eV)	6 (0.57-100 eV)
Link ALFA, single-level	6 (total)	9 (total)
Schoenig et al. calculated	4 (-)	5.7 (-)
Schoenig et al. measured	2.8 ± 1 (-)	15.5 ± 1.8 (-)

7. THE LIMITATIONS OF THE FLAT FLUX ASSUMPTION

The most serious shortcoming of ordinary resonance absorption theory is perhaps the flat flux assumption. As already discussed in section 4.1 this approximation only causes small errors in many cases, but the point is that it is very difficult to estimate the magnitude of the errors. An analytic approach was presented by Goldstein and Brooks in 1964 [95], but really reliable results may apparently only be obtained by numerical means, and as mentioned in the introduction to chapter 5 it is even in this case necessary to proceed with extraordinary care. This kind of treatment has not been performed successfully until during the last years, and an examination of systematic character has so far not been made.

Below a general analysis of the influence of the flux distribution inside homogeneous material regions is presented. From this investigation it is concluded that an accurate testing of resonance integral calculations as against isolated rod measurements should not be restricted to an analysis of the absorbing rod. Also the external region geometry and the combination of moderation and transport properties of the materials here occurring affect the results. This is in practice exampled by a detailed analysis of the experiment of Hellstrand and Lundgren.

Finally, the investigations comprise the consequences of some material inhomogeneities occurring in power reactors.

7.1. Detailed Flux Distribution within Homogeneous Regions

7.1.1. Isotropic Scattering in the Laboratory System

The influence of the lacking flat flux was investigated by means of SDP with exact collision probabilities and material region subdivision. The rods consist of either ^{238}U-metal or $^{238}UO_2$. In most cases seven moderator regions and eight absorber regions were used. The introduction of so many regions implies that the results obtained are not critically dependent on the chosen spatial mesh structure. The regions are narrowest near the interface between moderator and fuel, where the flux gradients become largest. In the absorbing rod a thickness of 0.004 cm ensures that even at resonance energies the thickness is smaller than one mean free path. Some test calculations indicated that the minimum thickness may be increased to 0.01 cm without affecting the results seriously. However, the smaller value above was chosen here. The thickness of the smallest moderator region surrounding the rod is about equal to one tenth of the

moderator mean free path. For "isolated" rods six of the moderator regions are situated inside a distance of two-three mean free paths from the rod, while the radius of the outermost region is one hundred times the rod radius.

The SDP integration covers the interval between 1200 and 0.5 eV, and the resonance integrals include the 1/v absorption. In the calculations the interval 600-1200 eV was investigated separately, and it was established that the influence of the lacking flat flux is very small here. For this reason it is concluded that the flat flux approximation supplies very accurate results above 1200 eV.

The rod radii are confined to the interval 1.7-0.5 cm in order to limit the investigation to the realistic rods that show an effect when subdivision is performed. The applied material densities are listed in table 7.1, and the resonance cross sections used are those tabulated on tape No. 21093 (temperature: 300 K).

The results obtained for isolated rods are in figs. 7.1 and 7.2 compared with two-region calculations also based on exact collision probabilities. The quantity in the figures called the "fractional error" is defined as

$$fr = \frac{-RI_{15\ regions} + RI_{2\ regions}}{RI_{2\ regions}} \quad . \qquad (7.1)$$

According to this a positive error means that the flat flux approximation over-estimates the resonance integral. It appears from the figures that for thick rods the error is in fact quite large. In practice such rather thick rods occur mainly in graphite and heavy-water moderated reactors of an earlier date. For instance in the Magnox-reactors the pin diameters are about 2.8 cm, and the fuel consists of U-metal.

Some calculations were performed with flat moderator flux and spatial-dependent absorber flux in order to distinguish the absorber and the moderator effect. Both effects reduce the resonance integral, which may easily be understood by investigation of the collision probabilities. A flux maximum in the rod at the surface increases the rod escape probability, while the moderator flux depression at the surface diminishes the moderator to absorber collision probability.

The position of the curves representing light-water moderation is greatly surprising. It was expected that the great average neutron energy

change per collision in this moderator would prevent large source gradients from occurring in the outer region. It seems obvious that such gradients require more moderator collisions to take place inside an energy interval comparable with the practical resonance width. The paradox was shown to originate in the resonance overlap effect. The neutron slowing-down in light-water is so fast that it prevents the moderator flux recovery between the resonances. This explanation was established by determination of the flat flux error when the resonance integrals considered only cover the interval from 13.84 to 0.5 eV and therefore only comprise the large ^{238}U resonance at 6.68 eV apart from the "1/v-tails" of the remaining resonances. The partial resonance integrals calculated with asymptotic source above this interval are compared with those obtained when the SDP calculation is initiated at 1200 eV, and the flux perturbations due to the resonances above 13.84 eV are taken into account. The results, which are listed in table 7.2, show that the resonance overlap effect is very large for light-water moderation provided the detailed flux distribution is considered.

In a lattice where the extension of the moderator zone is comparable with the mean free path, no large flux gradients may be created for which reason the error introduced by the flat flux assumption is about equal to the pure and quite small absorber effect. This is illustrated for UO_2 lattices in fig. 7.3. It is now evident that in the close lattices, which are common in light-water reactors, the error connected with the flat flux approximation is negligible in spite of the large isolated rod effect.

The magnitude of the error introduced by the flat flux assumption varies very much with the resonance characteristics as indicated in figs. 7.4 and 7.5. Here the partial resonance integrals in consecutive intervals were determined. For the total resonance overlap effect to be included in the analysis the results are obtained by treating the whole interval from 1200 to 0.5 eV in one continuous slowing-down calculation. It appears from the figures that the largest error occurs in the group surrounding the 36.7 eV resonance (group 3), and it is evident that here a large error exceptionally originates in the absorbing region. Also Mizuta (ref. 99, p. 81) has concluded that for this wide and predominantly scattering resonance the flat flux approximation is unusually poor.

Fig. 7.6 shows that a case considered by Lewis and Adler [117] in their analysis of graphite-moderated systems is in fact quite far from representing an isolated rod. This is not due to the Dancoff effect, which is very small. The explanation is derived from the accumulated flux gradient occurring around an isolated rod. However, the consistency between

the two calculations is rather good in spite of a large difference in applied resonance parameters. (Note that the resonance integrals reported in ref. 117 do not include the 1/v absorption). A comparison with the calculation of Megier [115] was less favourable. Megier only considers the resonance at 6.68 eV, and from the discussion of the resonance overlap above it follows that such a calculation probably is not very informative. It is, however, well suited for testing purposes. The results obtained in the case of a typical metal rod are compared in table 7.3. The resonance parameters are equal to those applied by Megier, and differences in the cross section calculation cannot cause the large difference in the flat flux fractional errors which appear from the table. In fact an analysis showed that the total difference is connected with the flux distribution inside the rod. In the table is also listed the Monte Carlo result obtained with the MCSUP [82] code and that indicates that the SDP calculation is correct. Also Megier reports Monte Carlo results, but they are presumably not accurate enough for disclosing deviations of this order of magnitude.

In fig. 7.7 the detailed flux distribution in an energy region around 200 eV is shown. In this calculation the flux is normalized to unity above the 208.7 eV resonance, and the spatial mesh structure was chosen for the sake of the illustration. It is completely different from the structure applied in the calculations above. The "flux-bumps" (cf. section 6.2.1) and the lacking flux recovery between the resonances appear from the figure.

7.1.2. Isotropic Scattering in the Centre of Mass System

Throughout the resonance region most scattering processes are isotropic in the centre of mass system, and therefore the scattering on the lightest nuclei is highly anisotropic in the laboratory system. However, the relatively flat fluxes and the small resonance widths imply, according to the discussion in section 4.1, that the influence of the anisotropic scattering on the resonance integral is usually negligible. The investigation above of the effect of the lacking flat flux indicates, however, that in case of light-water moderation this effect is probably influenced by the preferential scattering in the forward direction. It is to be expected that the reduced average change in the direction of neutron motion per hydrogen collision will restrain the accumulation of moderator flux gradients during the slowing-down process. Therefore the inclusion of anisotropic laboratory scattering results in a resonance integral still somewhat smaller than the flat flux result, but a little larger than the resonance integral based on

Table 7.1.

Material densities applied in section 7.1

Material	U-metal	UO_2	H_2O	D_2O	C	"D" (cf. D_2O)
Density, g/cm^3	18.8	10.6	1.0	1.1	1.6	0.22

Table 7.2.

The ^{238}U resonance integral in the energy region 13.84-0.5 eV (incl. 1/v abs.). Rod material: U-metal. Rod radius: 1.7 cm

Moderator	Res. overlap included			Asymp. source above 13.84 eV		
	Res. int., barns		Flat flux fr. error (eq.(7.1)) %	Res. int., barns		Flat flux fr. error (eq.(7.1)) %
	15 regs.	2 regs.		15 regs.	2 regs.	
C	3.038	3.367	9.8	3.110	3.371	7.7
D_2O	3.085	3.367	8.4	3.203	3.371	5.0
H_2O	3.008	3.367	10.7	3.212	3.371	4.7

regs. = regions.

Table 7.3.

The ^{238}U resonance at 6.7 eV considered by Megier [115] (14-3 eV)
Rod radius = 1 cm. Moderator: D_2O. Rod material: U-metal

Method	PETARD, Megier		SDP		MCSUP	
	15 regs.	2 regs.	15 regs.	2 regs.		S.d.
Res. int., barns	2.960	3.134	3.010	3.121	3.005	0.006

S.d. = standard deviation, regs. = regions.

subdivision and isotropic scattering. These considerations are illustrated in fig. 7.8.

The effect may easily be included in Monte Carlo calculations, but has never attracted any attention. Its practical importance is limited because, as proved above, the total influence of the lacking flat flux is very small in realistic light-water lattices where no accumulated flux gradients occur.

7.1.2.1. The SDP Intuitive Approach. The transport correction available by option in SDP is strictly limited to the case of an isolated rod. If the Dancoff effect is recognizable, then moderator cross section manipulations as those performed below are inadmissible owing to the change in the moderator transparency involved.

Two sorts of transport corrections that are closely related to normal diffusion theory are in common use: the "large" and the "small" correction. The former is often applied in few-group collision probability theory, and it forms the basis of the THERMOS code. Here its reliability has been confirmed by comparison between calculated and measured thermal spectra. The scattering cross sections are reduced by the fraction of neutrons that are scattered forward.

$$\sigma_{S,\text{corrected}} = \sigma_S(1 - \langle \mu_0 \rangle) \qquad (7.2)$$

where

$$\langle \mu_0 \rangle = \langle \cos \phi \rangle \ .$$

ϕ is the scattering angle. In the epithermal region

$$\langle \mu_0 \rangle = \frac{2}{3A}$$

if the scattering is isotropic in the centre of mass system. By inclusion of the total correction in the group self-scattering cross section affecting of the slowing-down picture is to a certain extent avoided. If the groups are narrow, as in THERMOS (and SDP in particular), this artifice results in negative formal self-scattering cross sections.

In the "small" correction mentioned above only the values of ϕ that are connected with scatterings inside the group itself are considered. This prevents the occurrence of negative cross sections, but the correction is group-structure-dependent and vanishes if the groups are narrow.

By introduction of the "large" correction in SDP a reasonable weakening of the accumulated flux gradients is obtained, but the sharp flux depression that occurs in the few groups round a resonance peak disturbs the neutron slowing-down because the total correction is attached to only one of the very narrow groups. This brings about the next artifice. It is assumed that the spatial flux distribution inside the homogeneous moderator region is improved by the correction, while the transfer across the abrupt boundary between the moderator and the absorber should be based on the correct slowing-down distribution. Therefore the absorber fluxes are recalculated with the moderator fluxes fixed at the values determined by the use of the "large" transport correction. However, the energy distribution of the transport-corrected moderator source is changed by reduction of the original physical group transfer and self-scattering cross sections by an equal fraction. The formal total scattering cross sections are still calculated by means of eq. (7.2), but the equal distribution of the correction between all groups eliminates the negative self-scattering. The point is that the collision probabilities are still calculated from the transport-corrected total cross sections.

The theoretical foundation of the transport corrections in the multigroup scheme is very poor, but this has not prevented their frequent use. The SDP approach described here is solely supported by its relationship to well-established transport corrections, the accordance with Monte Carlo calculations and the fact that the approximation interpolates between the result determined by the flat flux assumption and the multi-region approach based on isotropic scattering.

7.1.2.2. Monte Carlo Single Resonance Investigation. The aim of the analysis in the present section is to provide some exact Monte Carlo results concerning the effect of anisotropic scattering and in particular to test the SDP approach. The Monte Carlo code applied is again MCSUP (cf. section 5.6), which only considers one isolated resonance at a time. In such a case the total effect of the detailed spatial flux distribution is rather small as previously pointed out but the influence of the anisotropic scattering is, nevertheless, still large enough to be recognized in the MC calculation. The Monte Carlo method is not really suitable for investigation of small differential effects. Introduction of correlated sampling was attempted, but in vain. Instead the statistical difficulties have now been overcome simply by using a very large amount of computer time. In the SDP calculations 15 spatial regions are still applied, but the changed

moderator mean free path was taken into account in choice of mesh structure.

The results obtained with the parameters applied in ref. 82 are listed in table 7.4. In the cases where the influence of the anisotropic scattering is of any importance (E_r = 6.68 eV, mod.: H-H_2O) the SDP approach gives the correct answer. For the 36.7 eV resonance the effect as determined by both methods is very small even though the importance of the lacking flat flux is great. The effect is also small in the case with D_2O moderation, because the deuterium cross section is of the same order of magnitude as that of oxygen contrary to what is the case with hydrogen in H_2O. Furthermore, $1 - \langle \mu_0 \rangle$ is of course considerably larger for deuterium than for hydrogen.

7.1.2.3. SDP Estimate of the Influence of Anisotropic Scattering between 1200 and 0.5 eV. Some of the resonance integrals determined in section 7.1.1 were recalculated with the SDP transport correction included. The results are shown in figs. 7.9-7.11. It appears that the influence of the lacking flat flux is now reduced considerably if the moderator is light-water, but of course it is still larger than the pure absorber effect. In heavy-water the anisotropic scattering may be neglected.

7.1.3. A Summary of the Total Effect of the Lacking Flat Flux

When the anisotropic scattering is taken into account in light-water, the influence of the detailed flux distribution on the resonance integral shows in fact a simplified dependence on moderator type as compared with the results illustrated in figs. 7.1 and 7.2. An increment in slowing-down power now reduces the effect of the lacking flat flux as it appears from figs. 7.12 and 7.13. Fig. 7.14 gives an impression of the variation of the isolated rod resonance integral when the moderator is changed, a variation which is always neglected when theories and experiments are compared.

7.1.4. The Spatial Distribution of the Resonance Absorption in a Fuel Rod

Two approximate methods of calculating the variation of the resonance absorption with depth in a fuel rod have previously been proposed by Wagner [132] and Bogart [133]. Investigators have also tried to use the Monte Carlo method, but on account of large standard deviations this method is not suitable for the problem.

By means of SDP the average resonance integral in different subregions

Table 7.4.

The influence of anisotropic moderator scattering (in D_2O and H_2O the scattering on oxygen is considered isotropic). The quoted quantities are isolated rod resonance integrals in barns. Rod material: U-metal

Res. energy	Energy interval	External mod.	Rod radius	Isotropic scattering				Anisotropic scattering		
				SDP		MCSUP		SDP	MCSUP	
(eV)	(eV)		(cm)	2 regs.	15 regs.		S.d.	15 regs.		S.d.
6.7	14-3	H	1.0	3.121	3.037	3.032	0.006	3.072	3.075	0.005
36.7	42-32	H	1.0	1.117	1.052	1.047	0.005	1.057	1.056	0.004
6.7	14-3	H	1.7	2.337	2.247	2.249	0.007	2.282	2.289	0.006
6.7	14-3	H_2O	1.0	3.121	3.022	3.017	0.007	3.061	3.058	0.006
6.7	14-3	D_2O	1.0	3.121	3.010	3.005	0.006	3.027	3.015	0.009

H means hydrogen with density as in water

S.d. = standard deviation

regs. = regions

Res. = resonance

in the absorbing rod may be determined accurately. Some test calculations have shown that the spatial distribution of the flux in the external moderator region affects the resonance absorption almost equally in all subregions, and therefore subdivision in the moderator region is not necessary. The use of only one moderator region speeds up the calculation very much.

Hellstrand has long ago measured the spatial distribution of the resonance absorption in various isolated metal rods [134]. For comparison of the SDP calculation with these measurements the s-wave resonance integral below 3920 eV was calculated by means of tape No. 21093 for two of the rods considered by Hellstrand. The "resolved region" p-wave contribution and the capture above 3920 eV are considered constant throughout the rods and calculated by means of link ALFA, and 1.1 b are, according to Hellstrand's method, subtracted in order to correct for epicadmium 1/v capture. Finally the SDP resonance integrals are renormalized forcing the total integrals for the rods to comply with the old Hellstrand measurement (1957). The results obtained are in figs. 7.15 and 7.16 shown together with the experimental distributions. In so far as it is at all possible to compare smooth curves with step curves, the accordance is excellent.

7.2. Material Inhomogeneities within the Fuel Rod

7.2.1. The Influence of the Spatial Distribution of Plutonium on the ^{240}Pu Resonance Capture

Owing to the spatial distribution of the ^{238}U capture the concentration of plutonium in an irradiated uranium fuel rod is much larger at the rod surface than in the centre. Even though the content of plutonium never becomes large, the flux near the extremely high ^{240}Pu resonance at 1.06 eV is often far from being flat for which reason one might imagine that it is important to take the plutonium inhomogeneity into account when the ^{240}Pu resonance capture is calculated.

This matter was in a few cases investigated by means of SDP. The ^{240}Pu distribution is obtained by the following approximate method. The main part of the ^{238}U capture in a light-water reactor takes place in the epithermal region. The thermal contribution, which is about 25%, is neglected below. A portion of the ^{239}Pu created in the process after the beta decay, is by neutron capture transformed into ^{240}Pu. However, the neutron absorption in plutonium is flat compared with the ^{238}U resonance

absorption (cf. ref. 109 p. 108; the ratios between the concentrations of the different Pu isotopes vary by only a few per cent across the rod). Therefore the ^{240}Pu distribution may be approximated by the distribution of ^{238}U resonance capture.

An isolated UO_2 rod with a radius of 0.5 cm and surrounded by light-water is considered. This rod was also investigated in section 7.1. To the s-wave ^{238}U resonance integral below 1200 eV, 3.5 b are added accounting for all other ^{238}U resonances. This latter contribution is considered constant throughout the rod, which of course is incorrect, but it compensates to a certain extent for the neglected thermal capture. The ^{240}Pu distribution used is indicated in table 7.5. The ^{240}Pu cross section data are taken from the UKNDL, and the SDP calculation for ^{240}Pu covers the interval 0.5-10 eV. ^{238}U is here included as a pure scatter with a cross section of 9 b (1.0 eV). The average ^{240}Pu resonance integral for the whole rod is compared with the integral calculated with unchanged spatial mesh structure (eight fuel regions), but with constant ^{240}Pu concentration throughout the rod. By varying of the total ^{240}Pu contents in the rod the curves shown in fig. 7.17 are obtained. Fig. 7.18 illustrates the variation across the rod of the effective ^{240}Pu resonance cross section per absorbing atom. Here it is noticed that the spatial distribution of the absorption is influenced very much by the ^{240}Pu inhomogeneity. Nevertheless, the effect on the total ^{240}Pu capture is negligible as shown in fig. 7.17. This means that the increment in self-shielding due to the increased ^{240}Pu density in the outer regions is balanced by the fact that the ^{240}Pu is transferred to regions with high fluxes. On the other hand it is, however, not certain that such a cancellation occurs for other rods than the typical light-water reactor rod considered here.

In the treatment above up-scattering was neglected. It is not likely, however, that an inclusion of thermalization effects would modify the conclusions very much.

7.2.2. Evaluation of the Effective Resonance Temperature in Power Reactors

So far it has been assumed that the temperature distribution in the fuel is uniform, which is of course incorrect if the reactor power does not approach zero. Provided the power distribution is flat within the fuel rod and the thermal conductivity, k_f, is independent of the temperature, the temperature distribution is parabolic.

Table 7.5.

The ^{240}Pu distribution applied in section 7.2.1

Subregion outer radius (cm)	^{240}Pu number density divided by the average ^{240}Pu number density for the whole rod
0.15	0.734
0.27	0.758
0.36	0.807
0.43	0.897
0.47	1.072
0.488	1.449
0.496	2.359
0.5	4.453

$$T = T_C - \frac{q'''}{4k_f} r^2 = T_C - \frac{T_C - T_S}{R^2} r^2 . \qquad (7.3)$$

q''', T_C, T_S, r, and R are volumetric thermal source strength, centre temperature, rod surface temperature, distance from centre of rod, and rod radius respectively.

A few examples are investigated by means of SDP with three subregions in the fuel. For each region a cross section tabulation at the average temperature of the region is performed by use of the RESAB SYSTEM FILE 2 in the energy interval: 0.5-3920 eV. Only s-wave resonances are considered. The energy mesh structure is generated at a temperature deviating equally from the average temperature in the outermost and in the innermost region. The spatial mesh structure is determined by the condition that the temperature variation must be negligible in the outer region where the flux gradients are very large, while the innermost region should cover the extensive part of the fuel where the flux is almost flat (cf. section 7.1.4). Finally, the third region forms a transitional zone. Binnebeck [135] has analysed two typical ^{238}U resonances, using two spatial regions. He concludes that the thickness of the outer region should be about ten times the mean free path at the resonance energy. In practice this rule agrees in fact with the above method of choosing the

size of the thinnest region. Only three regions are used because the cross section calculation consumes quite a lot of computer time.

An isolated UO_2 rod with a radius of 0.5 cm is investigated. Apart from calculation of the resonance integral at the actual temperature distribution, three calculations at constant fuel temperature are performed, each based on one of the three cross section tabulations used in the non-uniform case. The spatial mesh structure is the same in the four slowing-down calculations. By means of the three last computations the relation between the temperature and the resonance integral determined at uniform temperature distribution is established. The function is almost linear in $\sqrt{T}$. Now the uniform temperature T_{eff} that would produce the same capture rate as that calculated at non-uniform temperature may be determined. The resonance integral variations are very small, but by use of the method described here most of the systematical errors due to, for instance, group structure and cross section evaluation are eliminated in the determination of the effective temperature.

By varying of the temperature in the centre of the fuel the curve shown in fig. 7.19 is obtained. When the temperature gradients are not extremely large, the result agrees with the old formula proposed by Rowlands[136], while the relation of Arnold and Dannels[137] underestimates the effective temperature. The result is in good agreement with the recent Monte Carlo calculations performed by Olhoeft[138] below 1200 eV. At the largest temperature gradients the SDP result deviates a little from the MC calculation perhaps because three spatial regions are not an adequate representation of the temperature profile, when the temperature variation is very great. On the other hand the SDP integration covers a much larger energy interval than that considered by Olhoeft, and, furthermore, the probable error of the capture rate in the MC calculation is about 0.8%, which is in fact quite a lot compared with the magnitude of the resonance integral variations under consideration. According to Olhoeft the result may approximately be expressed as

$$T_{eff} = 0.86 \langle T \rangle + (1 - 0.86) T_S \ , \qquad (7.4)$$

which also applies to the more realistic case with non-parabolic temperature shape. $\langle T \rangle$ is the volume-average temperature. If the distribution is parabolic eq. (7.4) is equivalent to

$$T_{eff} = 0.43 \ T_C + 0.57 \ T_S \ . \qquad (7.5)$$

In any case the difference between the effective resonance temperature and the average fuel temperature is small, which is in agreement with the interpretation of measured reactor power coefficients presented by Hellens et al. [139]. This rule has also been established by a Doppler effect measurement on ^{232}Th performed by Pettus and Baldwin [140].

7.3. Hellstrand and Lundgren's Resonance Integral Measurements

For illustration of how the use of more and more accurate methods of computation affects the comparison between measured and calculated resonance integrals, the Swedish measurements [141] on ^{238}U-metal and $^{238}UO_2$ cadmium-covered rods surrounded by heavy-water were analysed in detail. The resonance integrals for the four rods applied in the experiment were determined by use of three different methods. In all methods the external moderator is treated as being infinite as the experimental results have been corrected for the non-1/E dependence of the external distant neutron flux. The capture above 10^4 eV contributes 1.2 barns to the resonance integrals in accordance with the result of a Monte Carlo simulation of high-energetic neutron capture in the cadmium-covered rods [85]. In the energy region between 3920 and 10^4 eV the resonance integrals are calculated by means of the statistical method included in link ALFA, and the p-wave contribution from the resolved s-wave resonance region is determined in the same way. The treatment of the s-wave resonances below 3920 eV differs in the three methods. In method A this resonance capture is determined by means of the Bell factor formalism and link ALFA, while method B uses the SDP two-region approach. Finally the actual geometry is in method A simulated as accurately as possible when SDP is applied and the detailed flux distribution together with the anisotropic deuterium scattering are taken into account. Th material regions applied are shown in fig. 7.20. Eight subregions are used in the rod and six in the D_2O moderator. Above 1200 eV, where the effect of the lacking flat flux within the material regions is negligible, this detailed calculation is, however, replaced by the two-region approach. The Cd cross section data are taken from the UKNDL, and the epicadmium 1/v contribution is in method C calculated by continuous SDP integration down to 0.1 eV. The effect of the up-scattering was neglected. In methods A and B a cadmium cut-off energy of 0.5 eV was used in agreement with the estimate of Hellstrand and Lundgren. By the use of method C above 0.5 eV with the modification that the cadmium cover was neglected and by comparison with the original method C calculation above the effect of the im-

proved Cd treatment was determined. The effect is designated the capture in the interval 0.5 - $Cd_{cut-off}$. Some investigations have shown that the ^{238}U capture is only affected by the cadmium cover at low energies. The ^{238}U data applied in SDP are those tabulated on tape No. 21093.

The results are listed in tables 7.6 and 7.7. The experimentally determined resonance integrals were corrected in accordance with our improved knowledge of the Au resonance integral, which constitutes the standard for the measurement.

RI_{Au} (Hellstrand and Lundgren) = 1525 b [141].

Now RI_{Au} = 1566 b [142].

Considering the experimental uncertainty, which is estimated to ±4%, the differences between the results obtained by the three calculational methods are not large. This is partly due to the large amount of air in the experimental arrangement that reduces the influence of the spatial flux distribution within the moderator region. However, systematical calculation errors even of the same order as the experimental uncertainty are undesirable, when the methods are tested against each other.

Many reactor physical computations are based on a very simple treatment of the resonance absorption, but reliable results are nevertheless obtained by use of a renormalization, which brings about an agreement with resonance integral measurements. In calculations concerning the close lattices occurring for instance in light-water reactors the accordance between the simple approximations and the accurate methods (e. g. Monte Carlo or SDP multi-region approach) is often much better than that found when isolated rods are considered. This fact justifies the use of a simple approach in lattice calculations. However, undesirable systematical errors may be introduced, if the simple methods (two-region approaches, link ALFA, tabulations combined with equivalence principles etc.) are applied without precaution, not only in the pure lattice calculation but also in the determination of the renormalization factors that relate the lattice treatment to measurements on isolated rods or other experimental arrangements complicated from a computational point of view.

Table 7.6.

Comparison between resonance integral calculations and measurements. The reported numbers are epicadmium resonance integrals (barns) including 1/v capture.

Method A: semi-analytic. Method B: two-region SDP treatment. Method C: accurate SDP simulation

Rod	U-metal, 2.80 cm$^{\varnothing}$			U-metal, 1.00 cm$^{\varnothing}$			UO_2, 1.70 cm$^{\varnothing}$			UO_2, 1.25 cm$^{\varnothing}$		
Method	A	B	C	A	B	C	A	B	C	A	B	C
Cd cut-off - 0.5 eV	0.00	0.00	-0.06	0.00	0.00	-0.06	0.00	0.00	-0.05	0.00	0.00	-0.05
0.5-1200 eV, s-wave, 1/v	8.84*	8.58	8.32	13.39*	13.32	13.11	15.49*	15.36	15.10	17.48*	17.38	17.13
1200-3920 eV, s-wave	0.44	0.46	0.46	0.56	0.60	0.60	0.62	0.66	0.66	0.66	0.71	0.71
Below 3920 eV, p-wave	0.89	0.89	0.89	0.95	0.95	0.95	0.97	0.97	0.97	0.98	0.98	0.98
3920-10^4 eV, all	0.80	0.80	0.80	0.86	0.86	0.86	0.89	0.89	0.89	0.71	0.71	0.71
10^4 - ∞, all	1.20	1.20	1.20	1.20	1.20	1.20	1.20	1.20	1.20	1.20	1.20	1.20
Calculated total res. int.	11.97*	11.73	11.41	16.76*	16.73	16.46	18.97*	18.88	18.57	21.03*	20.98	20.68
Measured res. int.	11.57			16.53			18.39			20.46		

*) Method A includes a 1/v contribution of 0.99 b (cf. the discussion of the low-energetic capture in section 4.5.4 in the present report and in references C and D). If the estimate of Hellstrand and Lundgren is applied (1.20 b) the method A calculated resonance integrals for the four rods become 12.18, 16.97, 19.18 and 21.24 b respectively.

Table 7.7.

Comparison of experimental resonance integrals with the best estimate of the RESAB programme system

Rod	Measurement (barns)	Calculation (barns)	Deviation (%)
U-metal, 2.80 cm$^{\Phi}$	11.57	11.41	-1.4
U-metal, 1.00 cm$^{\Phi}$	16.53	16.46	-0.4
UO_2, 1.70 cm$^{\Phi}$	18.39	18.57	1.0
UO_2, 1.25 cm$^{\Phi}$	20.48	20.68	1.0

8. EFFECTIVE REACTION CROSS SECTIONS IN THE RESONANCE REGION

The most important effects in the resonance region are the self-shielding and heterogeneity, leakage being of only marginal interest. The investigation in the greater part of the present report concerns the reaction rates (or resonance integrals) in very simple geometries that allow the first mentioned two effects to be determined very accurately. However, in a whole-reactor code it is better to use effective (wide) group cross sections than reaction rates determined by cell calculations. The over-all reactor spectrum, which is slowly varying in space and energy, has a large effect on the latter quantities, while the related effective cross sections, if calculated in a proper way, are almost independent of such spatial source disturbances [87]. The objective of the present chapter is to show how the cell reaction rates may be converted into group constants for use in transport and diffusion codes that do not include more groups than necessary for describing the slow variations of the over-all spectrum adequately. Apart from the exact SDP treatment the approach applied is closely related to the method incorporated in the Winfrith Improved Multigroup Scheme (WIMS) [87, 143].

8.1. Group Fluxes and Effective Reaction Cross Sections

8.1.1. Group Cross Section Definitions

Two sorts of effective group cross sections may be calculated by the RESAB programme system. If cross sections are prepared for a calculation that does not homogenize the absorber material with the surrounding materials, but instead preserves the actual geometrical configuration (e.g. a collision probability few-group treatment), then the following effective cross section per absorber atom should be applied

$$\sigma_{R,u_1u_2} = \frac{\frac{1}{N_0}\int_{V_1}\int_{u_1}^{u_2} \Sigma_R \varphi \, du \, dV}{\int_{V_1}\int_{u_1}^{u_2} \varphi \, du \, dV} \qquad (8.1)$$

Σ_R is the macroscopic cross section for the reaction under consideration

and φ the flux per unit lethargy. The resonance absorber occurs in region number one. If on the other hand the cell is to be homogenized (in e. g. a diffusion-theory over-all calculation), then the cross section per absorbing atom is expressed as

$$\sigma'_{R,u_1u_2} = \frac{\frac{1}{N_0 V_1}\int_{V_1}\int_{u_1}^{u_2} \Sigma_R \,\varphi \,du\,dV}{\frac{1}{V_{cell}}\int_{V_{cell}}\int_{u_1}^{u_2} \varphi \,du\,dV} , \qquad (8.2)$$

where N_0 still is the absorber number density within the rod. The cross section determined by use of eq. (8. 1) is described below as the effective "rod cross section", while eq. (8. 2) provides the "cell cross section". Generally the external flux is approximately asymptotic for which reason the denominators in the two expressions are closely related. The numerators are the partial resonance integrals in the group. The flux integrals are much easier to calculate than the resonance integrals because they are approximately equal to the lethargy width of the group (1/E-flux), while the resonance effects are only corrections for which rough estimates suffice. In SDP the flux integrals are solved exactly, while approximations usable in the two-parameter description (cf. section 4. 3) and in link ALFA are discussed below.

In order to show what the detailed spectrum within a rod looks like, a Swedish experiment [144] was simulated. Here the flux in a lead scatterer surrounded by a natural uranium-metal tube was measured with a fast chopper. The experimental arrangement was in SDP reproduced in the way indicated in fig. 8. 1. By means of tape No. 21078 the average flux in the lead scatterer was determined, and the result appears from fig. 8. 2. The agreement between calculation and experiment is excellent. The measured points reproduce not only the flux round the ^{238}U resonances, but also indicate some of the ^{235}U resonances.

8. 1. 2. Infinite Slowing-Down Power

The group flux approximations are discussed on the basis of rods containing only one non-fissile resonance absorber. When an isolated rod is considered any effect originating in resonance escape probability (p(u)) variations during the neutron slowing-down is avoided (p(u) = 1). After the

flux integral is determined in this limited case, modifications are discussed to take into account the finite number of neutrons slowed down in an actual reactor cell ($p(u) < 1$).

The spatial integrations in eqs. (8.1) and (8.2) are easily performed when the flat flux approximation is applied. For an isolated rod the flux integral in eq. (8.2) is of course equal to the lethargy width of the group, Δu, while the denominator in eq. (8.1) may be estimated by use of the first-order IR flux (cf. section 4.4, eq. (4.33)). The group is supposed to contain only one resonance.

$$\int_{u_1}^{u_2} \varphi \, du = \int_{u_1}^{u_2} \frac{\sigma_m}{\sigma_A + \lambda_0 \sigma_{Sr} + \sigma_m} \, du \qquad (8.3)$$

with

$$\sigma_m = \lambda_0 \sigma_p + \sum_i \lambda_i \sigma_{Si} + S \ . \qquad (8.4)$$

σ_{Sr} symbolizes the pure resonance scattering cross section per absorber atom. If scattering interference is neglected, we have

$$\int_{u_1}^{u_2} \varphi \, du \simeq \Delta u - \frac{\Gamma_\gamma + \lambda_0 \Gamma_n}{\sigma_m \Gamma_\gamma} \int_{u_1}^{u_2} \sigma_A \, \varphi \, du \ , \qquad (8.5)$$

where the integral on the right-hand side is simply the resonance integral. Eq. (8.5) may be used directly if the Bell factor approximation is applied, while the equivalence principle based on the collision probability approximation of Carlvik results in a flux expression where two terms corresponding to the two homogeneous calculations are subtracted from Δu. If the lethargy group contains more resonances, the second term in eq. (8.5) must be replaced by a sum comprising all the resonances.

How this approximation works in practice is illustrated in figs. 8.3 and 8.4. The figures show the internal average flux in the interval 1.855-3500 eV calculated for a series of U-metal and UO_2 rods by means of link ALFA, which among other flux approximations contains this one ("preliminary estimate"). Only s-wave resonances are considered. The results are compared with the flux determined by means of MUFT multigroup flux

21093 (two-region approach).

An effective moderation cross section, S_{eff}, for the flux calculation is now introduced by writing of the flux integral in the following form:

$$\int_{u_1}^{u_2} \varphi \, du = \Delta u - \frac{RI_{u_1 u_2}}{S_{eff}} , \qquad (8.6)$$

where $RI_{u_1 u_2}$ is the resonance integral in the group. According to the discussion above S_{eff} depends in a complicated way on the rod geometry. If the rod material consists of the pure resonance absorber and the Bell factor formalism is used, then $S_{eff} \simeq S$ at low energies because $\Gamma_n \ll \Gamma_\gamma$ for the resonances occurring here and $\lambda_0 \ll 1$. S_{eff} is considerably larger than S at higher energies where generally $\Gamma_n > \Gamma_\gamma$, unless the rod is very thick (i.e. $\lambda_0 \simeq 0$). A flux expression of the same form as (8.6) has been proposed by several authors who all use different arguments [6, 87, 145]. In practical use a constant value of S_{eff} is usually applied throughout the resonance region. In figs. 8.3 and 8.4 the curves calculated with $S_{eff} = S$ (Bell factor formalism) are shown, and surprisingly this estimate provides a better approximation than the method above. The explanation is the following. A resonance scattering may remove a neutron from the energy interval with large resonance capture, and therefore the scattering is important in the calculation of the resonance integral. Owing to the large absorber mass such a scattering does on the other hand not diminish the time very much that the neutron spends in the epithermal region, and therefore the flux integral is almost unaffected. An increment in the flux below the resonance counterbalances the reduction in neutron flux at the resonance energy produced by the resonance scattering (cf. the "flux-bump", sections 6.2.1 and 7.1.1). Therefore it is reasonable to neglect this scattering in the calculation of the average flux, i.e. to use the WR approximation ($\lambda_0 = 0$ in eq. (8.5)). Now $S_{eff} \simeq \sigma_m$, and the dominating term in σ_m is S. Fig. 8.2 shows that in practice it is a good approximation to neglect the second term in the definition of σ_m (eq.(8.4)) and replace σ_m by S.

The average fluxes shown in figs. 8.3 and 8.4 are dominated by the low-energetic resonances. In order to illustrate that the approximation also applies in the lower keV-region, average fluxes were determined in relatively narrow groups for a $^{238}UO_2$ rod. The results appear from fig. 8.5.

The possibility of constructing one function of only two parameters

$(RI_R(S,T)_{u_1u_2})$ that for a certain fuel material and lethargy interval is capable of describing the resonance reaction was investigated and described in section 4.3 by consideration of the heterogeneous resonance integrals. The fact that eq. (8.6) with $S_{eff} = S$ provides a good flux estimate implies that the formalism may also be extended to the effective cross sections if p(u) is approximately equal to one. On the other hand the flux approximation proposed at first was not compatible with the two-parameter description because the relation between S and S_{eff} depends in a complicated way on the resonance structure in the group under consideration.

If the correction in eq. (8.6) is about equal to Δu, as it may be for a thick rod in a narrow group round a very large resonance, then the approximation is of course poor. The important information is here that almost every neutron within the group striking the rod is absorbed (black rod limit), while the effective rod cross section is in fact not very well defined.

8.1.3. Finite Slowing-Down Power

The approximate method for calculation of the average flux within the absorbing rod is now extended to cover limited cells. The problem is analogous to that discussed in section 4.3, where two types of resonance integrals were introduced. In the following discussion φ' symbolizes the flux determined in the NR-moderated case. In accordance with the discussion in section 4.3 and the verification in section 6.1 the real flux per unit lethargy in the rod may be approximated by

$$\varphi = \varphi' \, p(u) \quad . \tag{8.7}$$

We introduce

$$RI_{u_1u} = \int_{u_1}^{u} \sigma_A \, \varphi \, du'' \tag{8.8}$$

and

$$RI'_{u_1u} = \int_{u_1}^{u} \sigma_A \, \varphi' \, du'' \quad . \tag{8.9}$$

With [illegible] eq. (8.7) may be [illegible]

$$p(u) = \exp(-RI'_{u_1 u} / \langle \sigma_S \xi \rangle) \tag{8.10}$$

($p(u_1) = 1$ here) we have

$$RI_{u_1 u} = - \int_1^{p(u)} \langle \sigma_S \xi \rangle \, dp = \langle \sigma_S \xi \rangle \, (1 - p(u)) \ , \tag{8.11}$$

which shows that eq. (8.7) is correct (cf. eq. (4.30)). By analogy with eq. (8.6) it is deduced that

$$\int_{u_1}^{u_2} \varphi \, du = \Delta u \, \langle p \rangle = \frac{RI_{u_1 u_2}}{S_{eff}} \tag{8.12}$$

($S_{eff} \simeq S$). Here

$$\langle p \rangle = \int_{u_1}^{u_2} p(u) \, du / \Delta u \ , \tag{8.13}$$

which may easily be calculated if p(u) is described by a step function. This implies the approximation that all resonance absorption takes place at the resonance energies. The group flux approximation expressed in eq. (8.12) is included in link ALFA.

The effective rod cross section may now be determined.

$$\sigma_{R, u_1 u_2} \simeq \frac{RI_{u_1 u_2} / \langle p \rangle}{\Delta u - \dfrac{RI_{u_1 u_2} / \langle p \rangle}{S_{eff}}} \ . \tag{8.14}$$

From eqs. (8.10) and (8.11) it follows that

$$RI_{u_1 u_2} = \left[\frac{\displaystyle\int_0^{RI'_{u_1 u_2}} p(u) \, d(RI'_{u_1 u}) }{\displaystyle\int_0^{RI'_{u_1 u_2}} d(RI'_{u_1 u}) } \right] \times RI'_{u_1 u_2} \tag{8.15}$$

and in the particular case where the group contains many resonances uniformly distributed in lethargy, this equation indicates that

$$RI_{u_1u_2} \simeq \langle p \rangle \times RI'_{u_1u_2} \quad . \tag{8.16}$$

If the group contains only one large resonance situated at the lethargy midpoint of the group, then

$$\langle p \rangle = (1 + p(u_2))/2 \quad ,$$

and therefore (eqs. (8.10) and (8.11))

$$RI_{u_1u_2} = RI'_{u_1u_2} \cdot (\langle p \rangle - \frac{1}{12} [\, 1-p(u_2) \,]^2 + O([1-p(u_2)]^3)) \quad . \tag{8.17}$$

Also in this case the approximation (8.16) is rather accurate. On the other hand we have for a different group structure where the large resonance occurs in the top or the bottom of the group

$$RI_{u_1u_2} = RI'_{u_1u_2} \cdot (\langle p \rangle \pm \frac{1}{2} [\, 1-p(u_2) \,] + O([\, 1-p(u_2) \,]^2)) \quad , \tag{8.18}$$

and here the approximation (8.16) is poor if $p(u_2)$ deviates considerably from one. In the cases where the relation (8.16) applies, eq. (8.14) is reduced to

$$\sigma_{R,u_1u_2} = \frac{RI'_{u_1u_2}}{\Delta u - \frac{RI'_{u_1u_2}}{S_{eff}}} \quad . \tag{8.19}$$

In these and only these situations the effective group cross sections in a lattice may be calculated accurately by means of the previously introduced function $RI_R(\beta,T)_{u_1u_2}$

$$RI'_{u_1u_2} \simeq RI_R(\beta,T)_{u_1u_2} \quad .$$

(8.20) of the [illegible] code. The treatment of the [illegible] The group structures applied in the two large [illegible] are shown in such that [illegible]

8.6 illustrates a situation where this precaution in selecting of groups is not taken. The group extends from 1.855 eV to 3500 eV, and it is evident that eq. (8.19) overestimates the cross section in this case.

If it is assumed that the flux per unit lethargy outside the rod is equal to p(u) throughout the resonance region, the flux integral in eq. (8.2) may now easily be determined

$$\frac{1}{V_{cell}} \int_{V_{cell}} \int_{u_1}^{u_2} \varphi \, du \, dV \simeq \Delta u \, \langle p \rangle - \frac{V_1}{V_{cell}} \frac{RI_{u_1 u_2}}{S_{eff}} , \qquad (8.20)$$

and again the calculation of the effective cross section is simplified very much if the relation (8.16) applies. Fig. 8.7 illustrates the difference between the average flux in the cell and in the rod. A comparison with the SDP calculations indicates that eq. (8.20) slightly overestimates the flux in the cell which is due to the neglected resonance shielding in the moderator region.

8.2. Effective Scattering Cross Sections

Apart from the few remarks in the present section this work only considers the resonance scattering in connection with its influence on the resonance reaction. An accurate calculation of the effective epithermal scattering cross sections of the heavy nuclides is not very important, because these cross sections enter into the neutron balance (k_{eff}) in a much more indirect manner than does the neutron capture. Epithermal elastic scatterings on the heavy nuclides have an extremely small effect on the slowing-down power of the cell, but they influence the neutron diffusion and thereby the neutron leakage.

By substitution of the resonance absorber scattering cross section for Σ_R in eqs. (8.1) and (8.2), the effective scattering cross section results. If the interference between resonance and potential scattering is neglected, we obtain by use of eq. (8.1) that

$$\sigma_{s,u_1u_2} \simeq \sigma_p + \frac{\frac{\Gamma_n}{\Gamma_\gamma} RI_{u_1u_2}}{\int_{u_1}^{u_2} \varphi \, du}$$

(8.21)

if the group contains only one resonance. The numerator in the second term is replaced by a sum if the group comprises more resonances. σ_{S,u_1u_2} calculated in this way may be obtained by means of link ALFA (also in the statistical region). The neglecting of the scattering interference is problematic because the "tails" of this part of the resonance cross section are not integrable to infinity. However, the two "tails" of a resonance counterbalance each other if the extensions of the intervals of integration above and below the resonance are about equal. At high energies, where a group generally contains a large number of resonances, the "tails" more or less cancel each other, but at lower energies (E < 100 eV) the correct effective scattering cross section is even smaller than σ_p for some relative positions of group boundaries and resonances. This is illustrated in fig. 8.9, where effective scattering cross sections estimated by the approximation above are compared with exact values calculated by means of SDP (two-region approach, tape No. 21093). It appears from the figure that the approximation (8.21) is satisfactory above 100 eV.

For most purposes it is presumably sufficiently accurate to use the potential scattering cross section as effective cross section throughout the resonance region, and this approximation is definitely much better than the use of the large unshielded scattering cross section (SIGMA approach, cf. section 3.3).

Finally, it should be borne in mind that the effective removal (slowing-down) group cross section for the total cell is also affected by the flux perturbations produced by the resonances of the heavy nuclides. The p(u) variation through the group, which is the most important resonance effect in this connection, may according to Askew [87] easily be included in the simple approximate formalism by consideration of the neutron balance in the group.

8.3. Comparison with Calculations Performed by Means of the LASER Code, OYSTER CREEK Unit 2

For demonstration of the use of the RESAB programme system in a more practical situation, a cell in the pressurized light-water reactor OYSTER CREEK unit 2 [146] was examined. The calculations were compared with results obtained with MUFT IV, which constitutes the epithermal part of the LASER code [100]. The treatment of the resonance absorption in this code is of a rather simple and approximate character, but in practice the LASER code has proved capable of producing a fairly reliable

of experimental information. The LASER code has been modified a little by Lindstrøm Jensen [7] because the original version allows the epithermal microscopic cross sections to be printed out in two wide groups only. Now microscopic cross sections may be obtained in any group structure with group boundaries coinciding with the LASER narrow-group boundaries (LASER uses 85 groups between 10 and 0 MeV).

8.3.1. Reactor Cell Description

In the reactor cell the cladding zone was neglected, while the moderator to absorber volume ratio was preserved. A fuel rod radius of 0.5 cm and a cell equivalent radius of 0.82 cm was used. The cell is a square cell, and a moderator density of 0.7041 was applied. A fuel rod initially enriched to 2.94% in ^{235}U was considered at a burn-up of 5098 MWD/TU, and the isotopic composition was obtained by means of LASER. The fuel material is described in table 8.1, where the composition at maximum depletion (34000 MWD/TU) is also indicated. Material inhomogeneities in the fuel were neglected in agreement with the investigation in section 7.2.1. Most of the calculations were performed at an average fuel temperature of 300 K, which is not very realistic (cold reactor), but allows calculations to be accomplished by means of the UKNDL. A few investigations were made for the reactor in hot condition at full power (average fuel temperature 978 K).

According to the discussion in section 7.1.1 the flat flux assumption introduces only a very small error in the present case.

8.3.2. Group Structure

The effective group cross sections were calculated in the groups listed in table 8.2. This group structure was chosen partly in order to distinguish resonance regions of different characters. However, the group structure is also related to that applied in the practical control rod calculations described in section 4.6.3.

8.3.3. Effective Group Cross Sections Calculated for OYSTER CREEK Unit 2 at a Depletion of 5098 MWD/TU

The results obtained by different calculation methods are collected in tables 8.3-8.7. The cross sections are all call cross sections (eq. (4.2)). In the calculations performed with "no res. overlap" only the potential scattering has been included for isotopes other than the one considered at the moment. The results supposed to be the most accurate are under-

Table 8.1.

Composition (number densities, atoms/cm^3 x 10^{-24})
of an OYSTER CREEK unit 2 fuel rod (initial enrichment: 2.94%)

Burn-up, MWD/TU	5098	34000
^{235}U	5.451×10^{-4}	1.585×10^{-4}
^{238}U	2.169×10^{-2}	2.116×10^{-2}
^{239}Pu	5.119×10^{-5}	1.237×10^{-4}
^{240}Pu	5.354×10^{-6}	5.075×10^{-5}
O	4.487×10^{-2}	4.487×10^{-2}
ρ , g/cm^3	10.00	9.69

Table 8.2.

Group structure

Group boundaries (eV)	Group No.
1.855	
	1
78.877	
	2
748.36	
	3
3353.9	
	4
9116.9	
	5
111070	

lined in the tables. In the case of ^{238}U capture at 300 K for instance, the SDP calculation based on tape No. 20527 is recommended in the first two groups because this treatment includes resonance overlap between the different isotopes. This tape is, however, generated by use of the UKNDL cross section tabulation for all isotopes, and as shown in section 3.3 this evaluation underestimates the ^{238}U capture in the upper part of the resolved s-wave resonance region for which reason the SDP calculation with tape No. 21093 combined with the link ALFA p-wave treatment is preferred in group number 3. Finally, the link ALFA calculation is recommended in the statistical (smooth) region because only this method takes the resonance self-shielding into account in the groups occurring here.

The LASER calculation for ^{238}U at 300 K is quite accurate in the low-energetic groups, but very poor in groups 3 and 4, which is probably due to the renormalization technique applied in MUFT. The determination of the renormalization factor is completely dominated by the large absorption in the low-energetic groups. When the cross sections multiplied by the group lethargy widths are added up, a quantity of a character like that of a resonance integral results (RI', related to the epithermal capture in an infinite lattice - i.e. zero buckling). As indicated in table 8.4 the agreement between the RESAB and the LASER treatment is at this stage satisfactory.

When MUFT is applied in power reactor computations, an "effective resonance temperature" somewhat larger than the physical average fuel temperature should be used (see e.g. references 110 (pp. 30 and 61) and 147). However, the investigation in section 7.2.2 of the present report showed that the volume-average rod temperature represents a good estimate of the pointwise effective temperature, and Hellens et al. [139] have recently indicated that this rule also applies to the three-dimensional whole-reactor weighting effect. Now the ^{238}U capture for the reactor in hot condition was determined in the following way. The RESAB treatment was based on the physical average temperature (978 K), while the recommended "effective resonance temperature" (1144 K) [147] was applied in LASER (MUFT). As the Doppler effect in LASER is taken into account only through the renormalization factor, the effect is distributed incorrectly among the groups, as it appears from the calculation results listed in table 8.3. Table 8.4 shows that the total capture is almost the same in the LASER and the RESAB treatment.

For ^{235}U and ^{239}Pu the agreement between the RESAB and the LASER calculation is better than for ^{238}U, which is probably due to the reduced

importance of the self-shielding. According to section 6.4.1 σ_γ for ^{235}U determined by means of link ALFA is presumably too large (a too large). For ^{240}Pu the only method providing reliable epithermal cross sections is the link ALFA treatment, which is based on recent and accurate cross section measurements (cf. section 3.3). The epithermal ^{240}Pu capture (E > 1.855 eV) is, however, not very important in reactor calculations because of the low ^{240}Pu number density.

8.3.4. Multi-Group Spectrum

The epithermal spectrum in the OYSTER CREEK cell (at zero buckling) determined by means of LASER was compared with average group fluxes (for the whole cell) calculated by means of SDP in the LASER groups. The SDP spectrum is based on a calculation performed in 4000 narrow groups. The results appear from fig. 8.9. The agreement between the two calculations is better than could be expected considering the large differences that occur in the underlying cross sections. The high ^{238}U resonance at 6.68 eV is situated at the bottom of one of the LASER groups, and a rather large part of the resonance belongs to the next group. LASER includes, however, the whole resonance in the group in which the resonance energy occurs, while SDP treats the resonance correctly. This is the reason why the two codes give quite different results in the two groups considered here.

Below 1.855 eV it is common practice to determine the flux by means of a thermalization code, and the number of groups is here large enough to describe the detailed flux variation with energy. In fig. 8.9 the SDP slowing-down calculation was compared with a thermal calculation [148] in the upper part of the thermal region. The two methods give almost equal fluxes round the ^{240}Pu resonance (1.06 eV), but at the ^{239}Pu resonance (0.296 eV) the up-scattering neglected in SDP is important.

8.3.5. Detailed Spectrum

As an illustration of the complexity of a detailed reactor spectrum the SDP narrow group spectrum was plotted for the OYSTER CREEK cell below 82 eV (the resolved resonance region for ^{238}U extends to 3920 eV). Fig. 8.10 shows the total cross section within the rod per ^{238}U atom at a depletion of 8000 MWD/TU, while the corresponding moderator and absorber fluxes appear from figs. 8.11 and 8.12 respectively. At 34000 MWD/TU the composition of the fuel material has changed radically as indicated in table 8.1. How this change affects the absorber flux is shown

in fig. 8.13. In fig. 8.12 the flux between the large ^{238}U resonances is dominated by the ^{235}U resonances, while the influence of ^{239}Pu is appreciable in fig. 8.13. Furthermore the large ^{240}Pu self-shielding (1.06 eV) at maximum irradiation is noticed in fig. 8.13. The figures 8.10-8.13 were obtained by means of the RESAB programme system FILE 3, which controls a digital plotter. The plotting is off-line in the sense that an output magnetic tape from SDP is applied as input to FILE 3.

Table 8.3.

Effective group cross sections for ^{238}U

Temp. (K)	Group No.	σ_γ (barns) 1	2	3	4	5	σ_s (barns) 1	2	3	4	5
Cold 300	Link ALFA, Bell factor, no res. overlap	3.55	1.64	0.97	0.78	0.42	10.6 [1]	13.1	13.2	13.3	13.2
	SDP [4], tape No. 21093, no res. overlap [3]	3.58	1.66	1.00			9.0	12.6	12.8		
	SDP [4], tape No. 20527 (UKNDL)	3.59	1.58	0.85	0.90	0.47 [2]	9.7	12.5	12.9	14.5	13.1 [2]
	LASER, no res. overlap	3.76	1.28	0.44	0.38	0.41	10.7	10.7	10.7	11.4	12.0
Hot 978	Link ALFA, Bell factor, no res. overlap	3.76	1.99	1.10	0.83	0.43					
1144	LASER, no res. overlap	4.30	1.45	0.51	0.39	0.41					

1) $\sigma_s = \sigma_p$. 2) Unshielded UKNDL average cross section. 3) p-wave contribution from link ALFA.
4) Two-region sq. cell approach.

Table 8.4.

$\sum_{i=1}^{5} \sigma_{\gamma,i} \Delta u_i$, barns ($^{238}U$ "res. int." from table 8.3)

	Cold	Hot
Link ALFA	20.3	22.1
LASER	19.1	21.6

Table 8.5.

Effective group cross sections for ^{235}U at 300 K

	σ_γ (barns)					σ_f (barns)				
Group No.	1	2	3	4	5	1	2	3	4	5
Link ALFA, Wigner, no res. overlap	29.8	10.9	3.1	1.5	0.8 *)	34.0	17.6	7.6	4.4	2.3 *)
SDP **), tape No. 20527 (UKNDL)	22.4	8.7	2.4	1.5	0.8 *)	33.0	17.5	6.8	4.0	2.3 *)
LASER, no res. overlap	24.6	7.6	2.9	1.6	0.7	37.7	16.3	6.7	4.0	2.1

Table 8.6.

Effective group cross sections for ^{239}Pu at 300 K

	σ_γ (barns)					σ_f (barns)				
Group No.	1	2	3	4	5	1	2	3	4	5
Link ALFA, Wigner, no res. overlap	33.9	14.0	3.3	1.5	0.5 *)	45.5	15.7	5.0	2.8	1.6 *)
SDP **), tape No. 20527 (UKNDL)	30.4	12.0	4.2	2.1	0.5 *)	44.2	17.1	3.9	2.2	1.6 *)
LASER, no res. overlap	39.6	14.5	3.2	2.0	0.8	52.7	20.1	4.4	2.8	2.1

*) Unshielded UKNDL average cross section. **) Two-region sq. cell approach.

Table 8.7.

Effective group cross sections for ^{240}Pu at 300 K

	σ_γ (barns)				
Group No.	1	2	3	4	5
Link ALFA, Bell factor	27.0	12.9	2.7	1.2	0.6
SDP, tape No. 20527 (UKNDL)	7.5	1.6	2.7	1.3	0.8
LASER	17.2	69.9	13.7	5.6	3.1

9. SUMMARY AND MAIN CONCLUSIONS

For several years great efforts have been made to develop semi-analytic methods (e. g. the IR method) for determination of resonance reactions. Besides these studies accurate numerical integration of the slowing-down equation has in the last few years been given increasing attention. The methods were further developed and thoroughly tested against each other in the present work. For configurations that are not too complicated the deviation of the semi-analytic results from those obtained by the numerical treatment is a few per cent. However, the refinement of the numerical approach has caused a reduction in calculation time, and the method now only requires a computer time about three times as long as the semi-analytic calculations, which on the other hand have gradually become quite complicated. Therefore it is natural to prefer the numerical integration in accurate calculations even though rather good results may be obtained by means of the approximate methods.

For many purposes the determination of effective group cross sections directly from a detailed resonance cross section description (resonance parameters or detailed cross section tabulations) is, however, much too slow. In these cases the generation of group sections must be based on tabulations of suitable functions. It was shown above that for each group the homogeneous resonance integrals, if suitably defined, are capable of providing the demanded cross sections with adequate accuracy (a few per cent). Even complicated effects such as the overlap between the resonances of different nuclides may be taken into account with reasonable accuracy. The homogeneous resonance integrals are functions of only two parameters and therefore easy to tabulate for instance by use of numerical slowing-down calculation.

When resonance integral calculations are tested against measurements, it may be important to remember that the effect of the lacking flat flux inside each material region is quite large for more or less isolated, thick rods, while it is often negligible when a cell in a close reactor lattice is considered. The measured resonance integral is not completely described by rod geometry only, but depends also a little on the moderating material. Furthermore the occurrence of an extensive region with air or other materials between the absorber and moderator in the experimental arrangement may also affect the experimental results.

ACKNOWLEDGEMENTS

The author wishes to express his appreciation to the members of the Reactor Physics Department of Risø for their valuable assistance. Particularly P. Kirkegaard, who developed the Monte Carlo codes applied, is thanked. Thanks are likewise due to A. M. Hvidtfeldt Larsen, H. Neltrup and K. E. Lindström Jensen for their support and criticism.

E. Hansen of the computer group at Risø is thanked for his continuous aid, and finally the author is much indebted to the staff of the NEUCC for the large amount of computer time that was placed at his disposal.

REFERENCES

(The first four references form part of the present work)

A) H. Neltrup and J. Mikkelsen, "The Influence of Scattering Interference on Resonance Absorption in ^{238}U and ^{232}Th", J. Nucl. Energy 22, 601-610 (1968).

B) J. Mikkelsen, "Extrapolation and Interpolation in Calculation of the Resonance Absorption of Neutrons of Intermediate Energy", Nucl. Sci. Eng. 39, 403-407 (1970).

C) J. Mikkelsen, "The Effective Resonance Integral of ^{238}U", Risö-M-865 (1969). 17 pp.

D) J. Mikkelsen, "Calculation of the Resonance Integral of ^{232}Th and Summary of Experimental Results", Risö-M-966 (1969). 22 pp.

1) E. Hansen, "ILLINOIS ALGOL for IBM 7090/94, Users Manual" (Danish Atomic Energy Commission, Risö, 1968). 23 pp.

2) O. Kalnæs, H. Neltrup and P. L. Ølgaard, "A Recipe for Heavy-Water Lattice Calculations", Risö Report No. 81 (1964). 41 pp.

3) D. C. Leslie and A. Jonsson, Nucl. Sci. Eng. 23, 82-89 (1965).

4) D. Bollacasa and R. Bonalumi, Trans. Am. Nucl. Soc. 12, 627-628 (1969).

5) H. Neltrup, "Integral Transport Theory in Various Geometries", Risø-M-1289 (1970). 16 pp.

6) J. Carlvik, "Methods and Computer Codes Developed in Sweden for Reactor Physics Calculations", Tekniska Högskolan, Avd. för Teknisk Fysik, Finland, Rapport Nr. 506/1969 (In Swedish, 1969). 106 pp.

7) K. E. Lindstrøm Jensen, "Development and Verification of Nuclear Calculation Methods for Light-Water Reactors", Risö Report No. 235 (1970). 180pp.

8) E. Vogt, Phys. Rev. 112, 203-214 (1958).

9) J. E. Lynn, "Quasi-Resonance and the Channel Theory of Neutron-induced Fission". Nuclear Structure Study with Neutrons. Proceedings of an International Conference, Antwerp. 19-23 July 1965. Editors: M. Neve de Mevergnies, P. Van Assche and J. Vervier

(North Holland Publishing Co., Amsterdam, 1966) 125-155.

10) J. E. Lynn, The Theory of Neutron Resonance Reactions (Clarendon Press, Oxford 1968). 504 pp.

11) E. P. Wigner and L. Eisenbud, Phys. Rev. 72, 29-41 (1947).

12) A. M. Lane and R. G. Thomas, Rev. Mod. Phys. 30, 257-353 (1958).

13) E. Vogt, Phys. Rev. 118, 724-733 (1960).

14) C. W. Reich and M. S. Moore, Phys. Rev. 111, 929-933 (1958).

15) R. J. Brissenden and C. Durston, "The Calculation of Neutron Spectra in the Doppler Region". Proceedings of the Conference on the Application of Computing Methods to Reactor Problems, Argonne, Ill., 17-19 May 1965, (Argonne National Laboratory, Argonne, Ill., 1965) 51-76. (ANL-7050).

16) J. A. Farrell, Phys. Rev. 165, 1371-1374 (1968).

17) J. D. Cramer, "A Multilevel Analysis of the U^{235} Fission Cross Section". Los Alamos Scientific Laboratory, LA-3917-MS (1968). 9 pp.

18) F. T. Adler and D. B. Adler, "Calculation of Resonance Integrals for Fissile Materials". Reactor Physics in the Resonance and Thermal Regions. Proceedings of the National Topical Meeting of the American Nuclear Society, San Diego, 7-9 February 1966. Edited by A. J. Goodjohn and G. C. Pomraning, 2, (M.I.T. Press, Cambridge, Mass., 1966) 47-95.

19) H. Derrien and G. de Saussure, "Neutron Physics Division Annual Progress Report for Period Ending May 31, 1968, ORNL-4280 (1968). 194 pp.

20) P. L. Kapur and R. Peierls, Proc. Roy. Soc. A166, 277-295 (1938).

21) J. Humblet and L. Rosenfeld, Nucl. Phys. 26, 529-578 (1961).

22) R. A. Freeman and J. D. Garrison, "Resonance Parameter Distributions for Interfering Resonances". Proceedings of the Special Session on Resonance Cross Sections in Unresolved Resonance Region and Application of Monte Carlo Techniques to Reactor Physics, Toronto, 10-12 June, 1968, AMS-RPD-1, 195 pp.

23) P. A. C. Buckler and I. C. Pull, "Doppler Broadening of Cross Sections", AEEW-R 226 (1962). 48 pp.

24) L. Dresner, Resonance Absorption in Nuclear Reactors, (Pergamon Press, Oxford, 1960). 131 pp.

25) N. Lamb, Phys. Rev. 55, 190-197 (1939).

26) M. S. Nelkin and D. E. Parks, Phys. Rev. 119, 1060-1068 (1960).

27) W. M. Jones, J. Gordon and E. A. Long, J. Chem. Phys. 20, 695-699 (1952).

28) S. Christensen, BIT 5, 287-293 (1965).

29) H. Neltrup, "Error Integral with complex argument erfcpl(x,y,u,v,)", Danish Atomic Energy Commission, Risö, SA-84/1 (1965). 4 pp.

30) W. Gautschi, Comm. ACM 12, 635-636 (1969).

31) A. M. Hvidtfeldt Larsen, "Resonance Cross Sections", Master Thesis, Danish Atomic Energy Commission, Risö, (in Danish 1969). 125 pp.

32) R. J. Brissenden and C. Durston, "A User's Guide to Genex, SDR and Related Computer Codes", AEEW-R 622 (1968). 177 pp.

33) B. Frogner, "Resonance Absorption in ^{235}U", Thesis for the cand. real. Degree, Institutt for Atomenergi, Kjeller, Norway (1969). 102 pp.

34) E. P. Wigner, "Results and Theory of Resonance Absorption", Conference on Neutron Physics by Time-of-Flight, Gatlinburg, 1-2 November 1956, 59-70, ORNL-2309 (1956).

35) C. E. Porter and R. G. Thomas, Phys. Rev. 104, 483-491 (1956).

36) J. A. Harvey, "General Survey on Time-of-Flight Measurements Applied to Nuclear Physics". Neutron Time-of-Flight Methods. Proceedings of a Symposium, Saclay, 24-27 July 1961. Edited by J. Spaepeen (Euratom, Brussels, 1961) 23-56.

37) T. D. Newton, Can. J. Phys. 34, 804-829 (1956).

38) H. H. Hennies, "Cross-Sections and Resonance Parameters for ^{235}U, ^{233}U, ^{239}Pu, and ^{241}Pu Between Cadmium Cutoff and 10 keV". Nuclear Data for Reactors. Proceedings of a Conference, Paris, 17-21 October 1966, 2 (IAEA, Vienna, 1967), 333-358.

39) C. R. Adkins, T. E. Murley and M. W. Dyos, Nucl. Sci. Eng. 36, 336-350 (1969).

40) Y. Ishiguro et al., Nucl. Sci. Eng. 40, 25-37 (1970).

41) C.R. Adkins, M.W. Dyos, Nucl. Sci. Eng. 40, 159-172 (1970).

42) W.G. Davey, Nucl. Sci. Eng. 39, 337-360 (1970).

43) J.R. Stehn et al., "Neutron Cross Sections", BNL 325, Second Edition, suppl. 2, 2B (1966).

44) Ibid., 3 (1965).

45) Ibid., suppl. 1 (1961).

46) J.B. Garg et al., Phys. Rev. 134B, 985-1009 (1964).

47) A.G.W. Cameron and R.M. Elkin, Can. J. Phys. 43, 1288-1311 (1965).

48) C.A. Uttley, C.M. Newstead and K.M. Diment, "Neutron Strength Function Measurements in the Medium and Heavy Nuclei". Nuclear Data for Reactors. Proceedings of a Conference, Paris, 17-21 October 1966, 1, (IAEA, Vienna, 1967) 165-174.

49) M. Asghar, C.M. Chaffey and M.C. Moxon, Nucl. Phys. 85, 305-316 (1966).

50) N.W. Glass et al., "^{238}U Neutron Capture Results from Bomb Source Neutron". Neutron Cross Sections and Technology, Proceedings of the 2. Conference, D.C., 4-7 March 1968. Edited by T. Goldman, 1, (U.S. Department of Commerce/National Bureau of Standards, Washington, D.C., 1968) 573-587.

51) L.M. Bollinger and G.E. Thomas, Phys. Rev. 171, 1293-1297 (1968).

52) M. Asghar et al., Nucl. Phys. 76, 196-222 (1966).

53) G.J. Schmidt, "Neutron Cross-Sections for Fast Reactor Materials". Part I Evaluation, KFK 120 (1966).

54) J.C.D. Milton, "Summary of the Symposium". Physics and Chemistry of Fission. Proceedings of the 2. IAEA Symposium, Vienna, 28 July - 1 August 1969 (IAEA, Vienna, 1969) 879-884.

55) M. Asghar, A. Michaudon and D. Paya, Phys. Lett. 26B, 664-665 (1968).

56) M. Asghar, "Spin Assignment of Low-Energy Resonances in ^{238}U". Nuclear Data for Reactors. Proceedings of a Conference, Paris, 17-21 October 1966, 2, (IAEA, Vienna, 1967) 187-198.

57) H. Derrien et al., "Total and Fission cross-sections of ^{239}Pu". Nuclear Data for Reactors. Proceedings of a Conference, Paris, 17-21 October 1966, 2, (IAEA, Vienna, 1967) 195-210.

58) M. Wallin, AB Atomenergi, Private Communication, (1970).

59) B. Buck and F. Perey, Phys. Rev. Letters 8, 444-450 (1962).

60) W. Kolar and K.H. Böckhoff, J. Nucl. Energy 22, 299-315 (1968).

61) H. Weigmann and H. Schmid, J. Nucl. Energy 22, 317-320 (1968).

62) J.B. Garg et al., Phys. Rev. 137B, 547-575 (1965).

63) J.H. Gibbons et al., Phys. Rev. 122, 182-201 (1961).

64) D. Kompe, Nucl. Phys. 133, 513-536 (1969).

65) O. Kofoed-Hansen, Phys. Rev. 99, 154-158 (1955).

66) C. Sheer and J. Moore, Phys. Rev. 98, 565-578 (1955).

67) Yu. G. Shchepkin et al., "Neutron Spectro-scopic Study of Separated Cadmium Isotopes", Nuclear Data for Reactors. Proceedings of a Conference, Paris, 17-21 October 1966, 1, (IAEA, Vienna, 1967) 93-99.

68) J.A. Harvey, R.C. Block, G.G. Slaughter, "Fast Chopper Time-of-Flight Spectrometer", WASH 745, (1957) 24-25.

69) J.W. Codding, R.L. Tromp, F.B. Simpson, "The Total Neutron Cross Section of Pm-147", WASH 1124, (1968) 49-63.

70) C.J. Kirouac et al., "Total Neutron Cross Section and Resonance Parameters for ^{147}Pm". Neutron Cross Sections and Technology. Proceedings of the 2. Conference, Washington, D.C., 4-7 March 1968. Edited by T. Goldman, 2, (US. Department of Commerce, National Bureau of Standards, Washington, D.C., 1968) 687-694.

71) N.P. Baumann and D.J. Pellarin, Trans. Am. Nucl. Soc. 7, 27-28 (1964).

72) W.K. Foell and T.J. Connolly, Nucl. Sci. Eng. 21, 406-407 (1965).

73) F. Feiner and L.J. Esch, "Survey of Capture and Fission Integrals of Fissile Materials". Reactor Physics in the Resonance and Thermal Regions. Proceedings of the National Topical Meeting of the American Nuclear Society, San Diego, 7-9 February 1966. Edited by A.J. Goodjohn and G.C. Pomraning, 2 (M.I.T. Press, Cambridge, Mass., 1966) 299-318.

74) R.B. Tattersall, "Thermal Cross Section and Resonance Absorption Integral of Pu^{240}", AEEW-R 115 (1962).14 pp.

75) L. Le Sage and R. Sher, "Measurement of Infinite Dilution Capture Resonance Integrals with a Moxon-Rae Detector". Reactor Physics in the Resonance and Thermal Regions. Proceedings of the National Topical Meeting of the American Nuclear Society, San Diego, 7-9 February 1966. Edited by A.J. Goodjohn and G.C. Pomraning. 2 (M.I.T. Press, Cambridge, Mass., 1966) 175-192.

76) R.P. Schuman and J.R. Berreth, Nucl. Sci. Eng. 12, 519-522 (1962).

77) R.W. Sloughton et al., "Measurements of Thermal Cross-Sections and Resonance Integrals using Pile Neutrons and Activation Techniques". Pile Neutron Research in Physics. Proceedings of a Symposium, Vienna, 17-21 October 1960 (IAEA, Vienna, 1962) 239-246.

78) M.C. Moxon, "The Neutron Capture Cross-Section of ^{238}U in the energy region 0.5 to 100 keV", AERE-R 6074 (1969).22 pp.

79) V.J. Bell et al., "A User's Guide to Galaxy 3", AEEW-R 379 (1964).58 pp.

80) I. Carlvik, "A Method for Calculating Collision Probabilities in General Cylindrical Geometry and Applications to Flux Distributions and Dancoff Factors". Proceedings of the 3rd United Nations International Conference on the Peaceful Uses of Atomic Energy, Geneva, 31 August - 4 September 1964, 2, (United Nations, New York, 1965) 225-233.

81) H. Neltrup, Risö, Denmark, unpublished work, 1966.

82) Peter Kirkegaard, "Monte Carlo Superposition Calculations of Resonance Integrals in a Reactor Cell". Risö-M-1257 (1970).52 pp.

83) I. Carlvik, "Dancoff Correction in Square and Hexagonal Lattices", AE-257 (1966).23 pp.

84) M.M. Levine, Nucl. Sci. Eng. 16, 271-279 (1963).

85) D.C. Leslie, J.G. Hill and A. Jonsson, Nucl. Sci. Eng. 22, 78-88 (1965).

86) J. Codd et al., "Studies of Resonance Absorption and the Doppler Phenomenon for Fast and Thermal Reactors". Proceedings of the 3rd United Nations International Conference on the Peaceful Uses

of Atomic Energy, Geneva, 31 August - 9 September 1964, 2, (United Nations, New York, 1965) 5-13.

87) J.R. Askew, "The Calculation of Resonance Captures in a Few-Group Approximation", AEEW-R 489 (1966). 22 pp.

88) H. Neltrup, J. Nucl. Energy 18, Parts A/B, 704-708 (1964).

89) Y. Ishiguro and H. Takano, Nucl. Sci. Eng. 31, 388-395 (1968).

90) L.W. Nordheim, Proc. Symp. Appl. Math. vol. XI, 58-88 (1961).

91) R.S. Carlsmith and D. Steiner, Nucl. Sci. Eng. 37, 166-167 (1969).

92) H. Mizuta and Y. Fukai, J. Nucl. Energy, 23, 589-616 (1969).

93) Y. Fukai, Reactor Sci. Tech. 17, 115-120 (1963).

94) R.J. Brissenden, "A Formula for the Escape Probability of a Rod in a Uniform Lattice", AEEW-R 282 (1963). 9 pp.

95) R. Goldstein and H. Brooks, Nucl. Sci. Eng. 20, 331-337 (1964).

96) B.R. Sehgal and R. Goldstein, Nucl. Sci. Eng. 25, 174-182 (1966).

97) R. Goldstein and H. Brooks, Nucl. Sci. Eng. 17, 534-536 (1963).

98) Y. Ishiguro, Nucl. Sci. Eng. 32, 422-425 (1968).

99) Y. Ishiguro, "Improvements to the Intermediate Treatment of Resonance Absorption in Nuclear Reactor Theory". JAERI-memo 3700 (1969). 108 pp.

100) B.R. Sehgal, J. Nucl. Energy, Parts A/B, 19, 921-934 (1965).

101) M.H. McKay and J.P. Pollard, Nucl. Sci. Eng. 16, 243-245 (1963).

102) H.M. Sumner, "Eric 2, A FORTRAN Program to Calculate Resonance Integrals and from them Effective Capture and Fission Cross-Sections", AEEW-R 323 (1964). 26 pp.

103) N.M. Steen, Nucl. Sci. Eng. 38, 244-252 (1969).

104) A.M. Lane and J.E. Lynn, Proc. Phys. Soc. A70, 557-570 (1957).

105) P. Greebler and B.A. Hutchins, "The Doppler Effect in a Large Fast Oxide Reactor", Physics of Fast and Intermediate Reactors. Proceedings of the Seminar, Vienna, 3-11 August 1961, 3, (IAEA, Vienna, 1962) 121-138.

106) H.M. Sumner, "Eric 1, A FORTRAN Program for Calculating Resonance Integrals and Some Examples of its Use", AEEW-R 304 (1963). 59 pp.

107) H. Neltrup, Risö, Denmark, personal communication, 1968.

108) P.F. Nichols, Nucl. Sci. Eng. 17, 144-148 (1963).

109) C.G. Poncelet, "LASER - A Depletion Program for Lattice Calculations Based on Muft and Thermos", WCAP-6073 (1966). 104 pp.

110) P.G. Lacey and R.E. Radcliffe, "Diffusion-Theory Depletion Analysis of the Yankee Core", WCAP-6077 (1966). 124 pp.

111) L.W. Nordheim, Nucl. Sci. Eng. 12, 457-463 (1962).

112) J. Helholtz and D.H. Roy, Nucl. Sci. Eng. 32, 150 (1968).

113) J. Helholtz and D.H. Roy, "STRIP-Resonance Absorption Program Treating Overlap and Interference", TP-332 (Babcock and Wilcox Co., 1967).

114) F.E. Driggers, "A Method of Calculating Neutron Absorptions and Flux Spectra at Epithermal Energies", AECL 1996 (1964). 37 pp.

115) J. Megier, J. Nucl. Energy 22, 417-431 (1968).

116) Y. Fukai and H. Mizuta, J. Nucl. Energy 22, 355-370 (1968).

117) E.E. Lewis and F.T. Adler, Nucl. Sci. Eng. 31, 117-126 (1968).

118) P.H. Kier, Nucl. Sci. Eng. 26, 230-236 (1966).

119) R. Bonalumi, Energ. Nucl. (Milano), 8, 326-336 (1961).

120) J. Spanier and E.M. Gelbard, Monte Carlo Principles and Neutron Transport Problems (Addison-Wesley, Reading, Mass., 1969). 234 pp.

121) O. Møller, BIT 5, 37-50 (1965).

122) O. Møller, BIT 5, 251-255 (1965).

123) K. Parker, "The Aldermaston Nuclear Data Library as at May 1963", AWREO-70/63 (1963). 64 pp.

124) D.S. Norton, "The U.K.A.E.A. Nuclear Data Library February, 1968", AEEW-M 824 (1968). 23 pp.

125) E. Hansen, "ILLINOIS-ALGOL Dynamic Overlay Storage Allocation under IBJOB", Danish Atomic Energy Commission, Risö, SM-15 (1969). 9 pp.

126) P. Kirkegaard, Risö, Denmark, personal communication, 1969.

127) M. W. Dyos and A. Keane, Nucl. Sci. Eng. 26, 288 (1966).

128) G. C. Pomraning and M. W. Dyos, Nucl. Sci. Eng. 27, 137-139 (1967).

129) W. Rothenstein, Nucl. Sci. Eng. 7, 162-171 (1960).

130) W. Rothenstein and J. Helholtz, Nucl. Sci. Eng. 14, 239-243 (1962).

131) F. C. Schoenig, F. A. White and F. Feiner, Nucl. Sci. Eng. 37, 66-84 (1969).

132) M. Wagner, Nucl. Sci. Eng. 8, 278-281 (1960).

133) D. Bogart, Nucl. Sci. Eng. 41, 37-46 (1970).

134) E. Hellstrand, J. Appl. Phys., 28, 1493-1502 (1957).

135) J. J. Van Binnebeek, Nucl. Sci. Eng. 36, 47-58 (1969).

136) G. Rowlands, J. Nucl. Energy 16, 235 (1962).

137) W. H. Arnold and R. A. Dannels, Trans. Am. Nucl. Soc. 3, 229-230 (1960).

138) J. E. Olhoeft, Trans. Am. Nucl. Soc. 13, 306-307 (1970).

139) R. L. Hellens, C. O. Dechand and M. E. Congdon, Trans. Am. Nucl. Soc. 12, 914 (1969).

140) W. G. Pettus and M. N. Baldwin, Nucl. Sci. Eng. 26, 34-46 (1966).

141) E. Hellstrand and G. Lundgren, "The Resonance Absorption of Uranium Metal and Oxide". AE-77 (1962). 17 pp.

142) M. Brose, Nukleonik 6, 134-141 (1964).

143) J. R. Askew, F. J. Fayers, P. B. Kemshell, JBNES 5, 564-585 (1969).

144) E. Johansson et al., "The Neutron Spectrum in a Uranium Tube", AE-123 (1963). 36 pp.

145) O. Kalnes, "Spektrum, an ALGOL-code for GIER", Danish Atomic Energy Commission, RF-memo No. 93 (1963). 45 pp.

146) "Oyster Creek Nuclear Station, Unit 2. Preliminary Safety Analysis Report", 1, DOCKET-50328-1 (1968). 387 pp.

147) W. T. Sha, "An Experimental Evaluation of the Power Coefficient in Slightly Enriched PWR Cores", WCAP-3269-46 (1966). 46 pp.

148) C.F. Højerup, Risø, Denmark, personal communication, 1970.

APPENDIX A

Comments on the RESAB Programme System

The composition of the programme system was described in section 2.5. This appendix contains a few comments concerning calculation time, tape requirements and deck set-up.

A. 1. Running Time

The running times are greatly dependent on the resonance structure of the materials considered and the chosen combination of approximations. Typical running times for link ALFA extend from 0.2-1 min per nuclide and configuration (ILLINOIS ALGOL on IBM 7094). For SDP the times are reported per narrow group. If the collision probabilities are obtained by means of the corrected Nordheim's approximation, the time per group is about 0.0005 min, while the corresponding time when exact collision probabilities in two regions (5 Gauss points) are used is about 0.001 min. In a 15-region problem the time per group is 0.017 min (2 Gauss points). It is seen that a heterogeneous slowing-down calculation for ^{238}U in the interval 3500-0.5 eV may be performed in a little over 1 min (188 resonances). Production of SDP input tapes usually takes 1-5 min if multi-level formalism is not applied. Generation of tape No. 21093 took 30 min.

A. 2. Tape Requirements

The programme system, which comprises almost 10 000 binary cards, is generally read into the machine from a magnetic programme tape. During the calculation it uses 2 overlay tapes, and the programmes are organized in such a way on these tapes that the computer time spent on loading of programme segments is minimal. Resonance parameters are supplied from tape or punch cards. If external storage is necessitated by SDP, 2 scratch tapes are used per externally stored nuclide (generally only deuterium). A generation of an SDP input tape by means of FILE 2 uses up to 8 tapes apart from standard input, output and overlay tapes. The rather small size of the computer applied (32 K) causes this extensive use of external storage.

A. 3. Input Data

A separate report describing the use of the programme system is in

preparation.

A. 4. List of Decks

Fig. 2.1 shows the link structure of the programme system, while the physical deck set-up appears from tables A. 1 and A. 2. The decks with names beginning with LN or TP control the dynamic overlay storage allocation [125]. Those with the number one (e. g. LNKX1.)are FORTRAN subroutines, and those with the number two (e. g. LNKD2.)are MAP programmes. These decks are not further commented on here.

Below the main contents of the other decks are listed. Some decks appear more than once in the deck set-up with slightly changed deck names. Some of these repetitions are necessitated by the limited flexibility in the overlay administration of the computer actually used (e. g. PROCG. and PROAG., both containing the SDP heart). In other cases the deck repetitions are not strictly necessary, but they speed up the loading and computing time.

FILE 1

RESAB2	Control of FILE 1 calculations.
PROCY.	Control of SDP
PROX1.	Mixing of SDP and link ALFA results (pp. 37 and 119)
PROX2.	Group cross section output
PROCZ.	Link ALFA main block (chapter 4)
PROD1.	SDP input
PROD2.	do.
PROD3.	do.
PROD4.	Input to SDP single resonance treatment (p. 62)
PROD5.	Conversion of link ALFA data to SDP input data (p. 37)
PROCU.	Control of SDP single resonance treatment (p. 62)
PROE2.	Single resonance group structure generation (p. 62)
PROE3.	SDP residual terms (pp. 41 and 62)
PROE4.	Determination of fundamental constants for single-level treatment
PROCG.	SDP heart (chapter 5)
PROCH.	Output from SDP single resonance treatment
PROJ1.	Initial adjustment of SDP parameters
PROJ2.	do.
PROCK.	do.

PROL1.	Complex error function (p. 12)
PROL2.	Calculation of collision probability (p. 25)
PROCN.	SDP output
PROCV.	Control of SDP calculation based on cross section tabulations (p. 61)
PROCF.	Initial cross section, group-structure input tape administration
PROAG.	SDP heart (= PROCG)
PROAH.	= PROCH
PRAJ1.	= PROJ1
PRAJ2.	= PROJ2
PROAK.	= PROCK
PROAL.	= PROL2
PROAN.	= PROCN
PROI1.	Transformation of SDP results
PROI2.	SDP group cross section output
PROCA1	Transmission of RESAB resonance parameter library from punch cards to magnetic tape (pp. 18 and 134)
PROCA2	Administration of library tape with resonance parameters (p. 18)
PROCA3	do.
PROCC.	Equivalence principles, Dancoff factor determination (pp. 27, 28 and 37)
PROCS1	J-function (p. 42)
PROCS2	E_2-function (p. 38)
PROCS5	Statistic calculation (pp. 13 and 38)
PROCS6	Link ALFA output, administration of statistic calculation
PROCB.	RESCOLDENS (pp. 37 and 50)
PROCS3	HYP-determination of zero of real function
PROCS4	Determination of λ in the IR method with scatt. int. incl. (pp. 36 and 37, ref. B)
A. LGUN	MAP programme administrating tape stations

FILE 2

TRESA.	Control of FILE 2 calculation
PTPER.	Administration of UKNDL (pp. 10 and 59)
PTPEK.	Control of SDP input cross section, group-structure generation (p. 57)

PTPEA1 = PROCA1
PTPEA2 = PROCA2
PTPEA3 = PROCA3
PTPEC. SDP group structure from UKNDL (p. 59)
PTPED. SDP group structure from RESAB resonance parameter library (p. 57)
PTPEE. Mixing of group structures (p. 61)
PTPEF. Conversion of SDP input tapes to DORES input tapes (groups → points)
PTPEG. DORES (pp. 12 and 59)
PTPEH. Combination of group structure and cross sections
PTPEI. Midpoint - group average cross section conversion (p. 59)
PTPEJ1 Print-out of cross section tapes
PTPEJ2 Print-out of SDP cross section, group-structure tapes

FILE 3

PLOT1. Plotter programme (pp. 9 and 118)

If a certain calculation does not use all the decks in a file, it is not necessary to load the complete file. For instance "loaders" which only comprises SDP or link ALFA have been produced.

Table A.1
The RESAB PROGRAMME SYSTEM, FILE 1
Slowing-down calculation

```
          $*TAPE 21102    A9R       RESAR SYSTEM
          $PAUSE
          $ATTACH         A9
          $AS             SYSL82
          $REWIND         SYSL82
          $EXECUTE        IBJOB
$IBJOB         ALTIO
$IEDIT         SYSL82,SCHF1
$IBLCR RESAB2
$IBLDR LNKX1.
$IBLDR LNKY1.
$IBLDR LNKZ1.
$IBLDR A.LGUN
$ORIGIN        ALFA1
$IBLDR PROCY.
$IBLDR LNKD1.
$IBLDR LNKI1.
$IBLCR LNKU1.
$IBLDR LNKV1.
$IBLCR LNKY2.
$ORIGIN        BETA1
$IBLDR PRCI1.
$IBLDR PROI2.
$IBLDR LNKI2.
$ORIGIN        ALFA1
$IBLDR PROX1.
$IBLDR PROX2.
$IBLDR LNKX2.
$ORIGIN        BETA1
$IBLDR PROD1.
$IBLDR PROD2.
$IBLDR PROD3.
$IBLDR PROD4.
$IBLDR PROD5.
$IBLDR LNKD2.
$ORIGIN        BETA1
$IBLDR PROCU.
$IBLDR LNKE1.
$IBLDR LNKG1.
$IBLDR LNKH1.
$IBLDR LNKU2.
$ORIGIN        BETAU
$IBLDR PROE2.
$IBLDR PROE3.
$IBLDR PROE4.
$IBLDR PROE5.
$IBLDR PROE6.
$IBLDR LNKE2.
$ORIGIN        BETAU
$IBLDR PROCG.
$IBLDR LNKJ1.
$IBLDR LNKK1.
$IBLDR LNKL1.
$IBLDR LNKN1.
$IBLDR LNKG2.
$ORIGIN        BETA2
$IBLDR PROJ1.
$IBLDR PROJ2.
$IBLDR LNKJ2.
```

To be continued

Continuation (Table A.1, FILE1)

```
$ORIGIN          BETA2
$IBLDR PROCK,
$IBLDR LNKK2,
$ORIGIN          BETA2,REW
$IBLDR PROL1,
$IBLDR PROL2,
$IBLDR LNKL2,
$ORIGIN          BETA2,SYSUT3
$IBLDR PROCN,
$IBLDR LNKN2,
$ORIGIN          BETAU,SYSUT3,REW
$IBLDR PROCH,
$IBLDR LNKH2,
$ORIGIN          BETA1
$IBLDR PROCV,
$IBLDR LNKF1,
$IBLDR LNAG1,
$IBLDR LNAH1,
$IBLDR LNKV2,
$ORIGIN          BETAV
$IBLDR PROCF,
$IBLDR LNKF2,
$ORIGIN          BETAV
$IBLDR PROAG,
$IBLDR LNAJ1,
$IBLDR LNAK1,
$IBLDR LNAL1,
$IBLDR LNAN1,
$IBLDR LNAG2,
$ORIGIN          BETA3
$IBLDR PRAJ1,
$IBLDR PRAJ2,
$IBLDR LNAJ2,
$ORIGIN          BETA3
$IBLDR PROAK,
$IBLDR LNAK2,
$ORIGIN          BETA3,REW
$IBLDR PROAL,
$IBLDR LNAL2,
$ORIGIN          BETA3,SYSUT3
$IBLDR PROAN,
$IBLDR LNAN2,
$ORIGIN          BETAV,SYSUT3,REW
$IBLDR PRCAH,
$IBLDR LNAH2,
$ORIGIN          ALFA1,SYSUT3
$IBLDR PROC2,
$IBLDR LNKA1,
$IBLDR LNKB1,
$IBLDR LNKC1,
$IBLDR LNKS1,
$IBLDR LNAS1,
$IBLDR LNK22,
$ORIGIN          ALFA,SYSUT3
$IBLDR PROCA1
$IBLDR PROCA2
$IBLDR PROCA3
$IBLDR LNKA2,
$ORIGIN          ALFA,SYSUT3
```

Continuation (Table A.1, FILE 1)

```
$IBLCR PROCC.
$IBLDR LNKC2.
$ORIGIN          ALFA,SYSUT3
$IBLCR PROCS1
$IBLCR PROCS2
$IBLCR PROCS5
$IBLDR PROCS6
$IBLDR LNKS2.
$ORIGIN          ALFA,SYSUT3
$IBLDR PROCB.
$IBLDR LNKB2.
$ORIGIN          ALFA,SYSUT3,REW
$IBLDR PROCS3
$IBLDR PROCS4
$IBLDR LNAS2.
```

Table A.2

The RESAB PROGRAMME SYSTEM, FILE 2

Tape preparation

```
$IEDIT           SYSLB2,SCHF2
$IBLDR TRESA.
$IBLDR TPEK1.
$IBLDR TPEB1.
$IBLDR A.L GUN
$ORIGIN          GAMMA1
$IBLDR PTPEB.
$IBLDR TPEB2.
$ORIGIN          GAMMA1
$IBLDR PTPEK.
$IBLDR TPEA1.
$IBLDR TPEC1.
$IBLDR TPED1.
$IBLDR TPEE1.
$IBLDR TPEF1.
$IBLDR TPEG1.
$IBLDR TPEH1.
$IBLDR TPEI1.
$IBLDR TPEJ1.
$IBLDR TPEK2.
$ORIGIN          GAMMA
$IBLDR PTPEA1
$IBLDR PTPEA2
$IBLDR PTPEA3
$IBLDR TPEA2.
$ORIGIN          GAMMA
$IBLDR PTPEC.
$IBLDR TPEC2.
```

To be continued

Continuation (Table A.2, FILE2)

```
$ORIGIN          GAMMA
$IBLDR PTPED.
$IBLDR TPED2.
$ORIGIN          GAMMA
$IBLDR PTPEE.
$IBLDR TPEE2.
$ORIGIN          GAMMA
$IBLDR PTPEF.
$IBLDR TPEF2.
$ORIGIN          GAMMA
$IBLDR PTPEG.
$IBLDR TPEG2.
$ORIGIN          GAMMA
$IEDIT           SYSIN1
$IBLDR PTPEH.
$IEDIT           SYSLB2,SRCH
$IBLDR TPEH2.
$ORIGIN          GAMMA
$IBLDR PTPEI.
$IBLDR TPEI2.
$ORIGIN          GAMMA
$IBLDR PTPEJ1
$IBLDR PTPEJ2
$IBLDR TPEJ2.
```

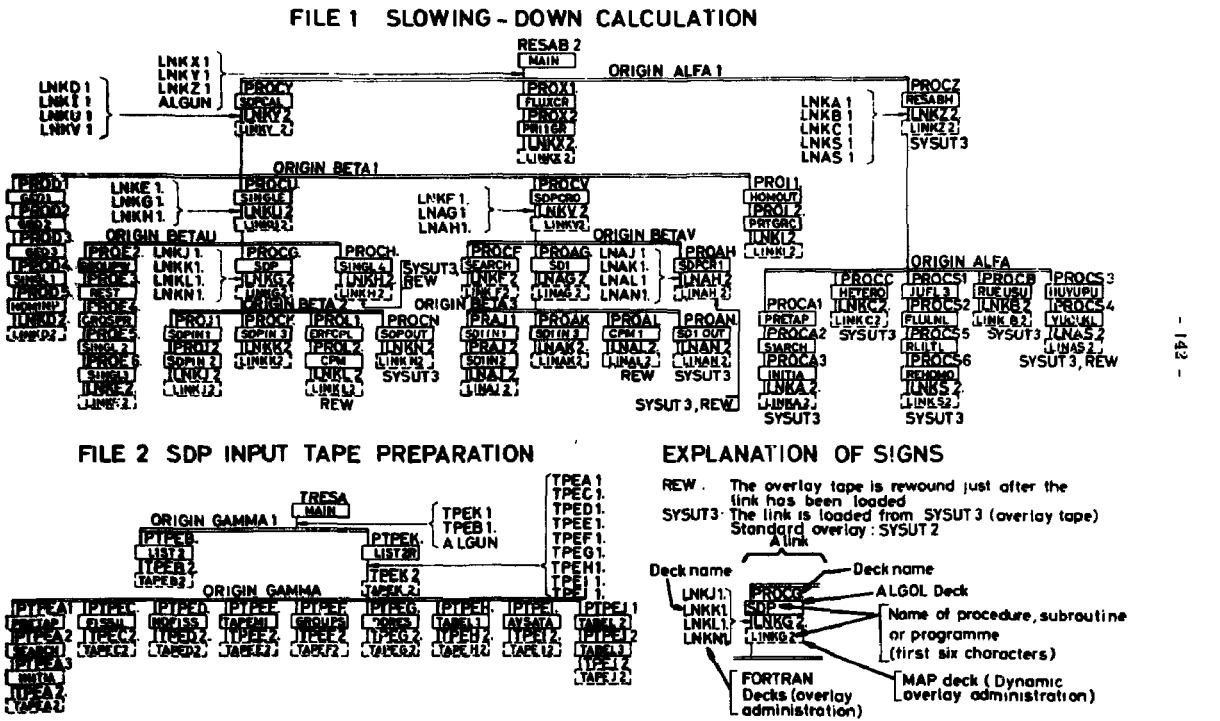

Fig. 2.1. Link structure of the RESAB programme system FILE 1 and FILE 2.

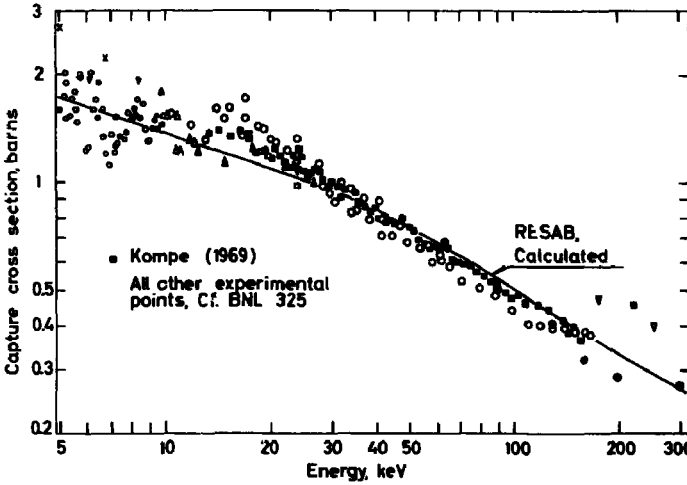

Fig. 3.1. The capture cross section of ^{nat}Ag in the keV region.

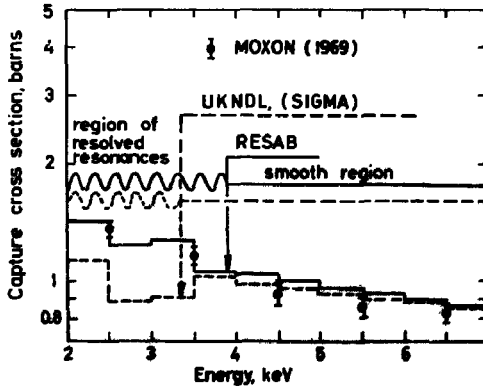

Fig. 3.2. Infinite dilution group average cross section of ^{238}U in the transitional zone between resolved and unresolved resonance region.

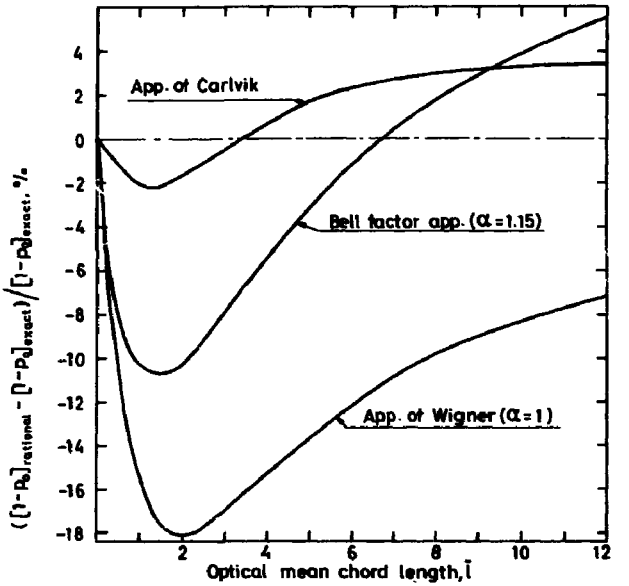

Fig. 4.1. The relative error on the isolated rod escape probability, $1-p_o$, calculated by different rational approximations.

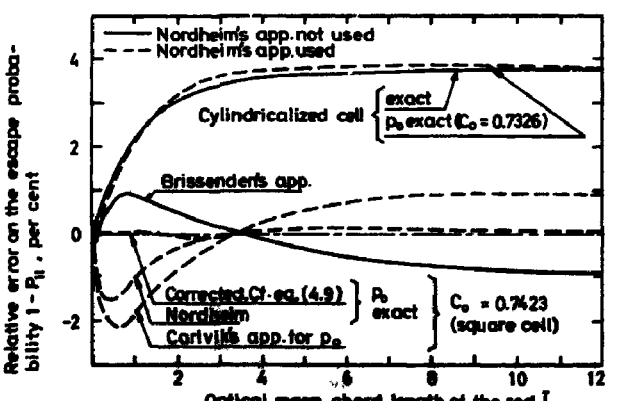

Fig. 4.2. Investigation of approximations for the escape probability $1-P_{11}$ in a square cell with a small optical mean chord length, $\bar{l}_m$, in the moderator region. Rod radius R = 0.2 cm. V_2/V_1 = 1.25. Σ_{t2} = 0.6795 cm^{-1} (Σ_{H_2O}, ρ = 1 g/cm^3 = 1.49 cm^{-1}). $\bar{l}_m = 2R_{t2}/V_2/V_1 = 0.36$.

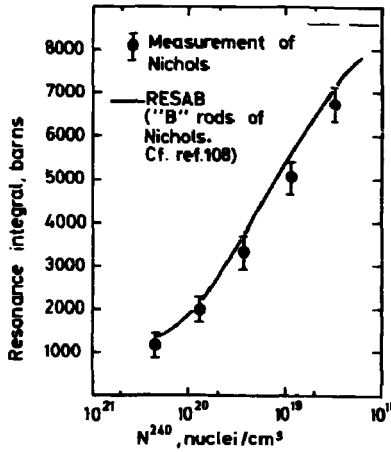

Fig. 4.3. ^{240}Pu resonance integral.

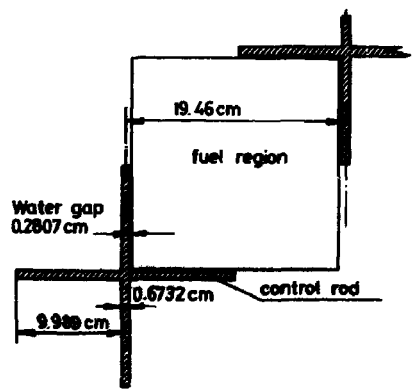

Fig. 4.4. A Yankee reactor assembly.

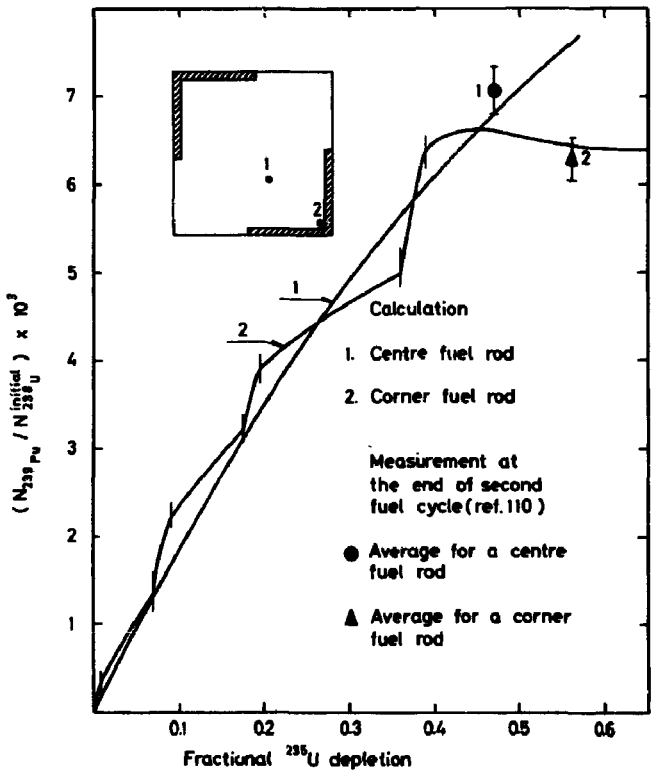

Fig. 4.5. A central assembly depleted during two core cycles in the Yankee reactor. Variation in ^{239}Pu with fuel depletion.

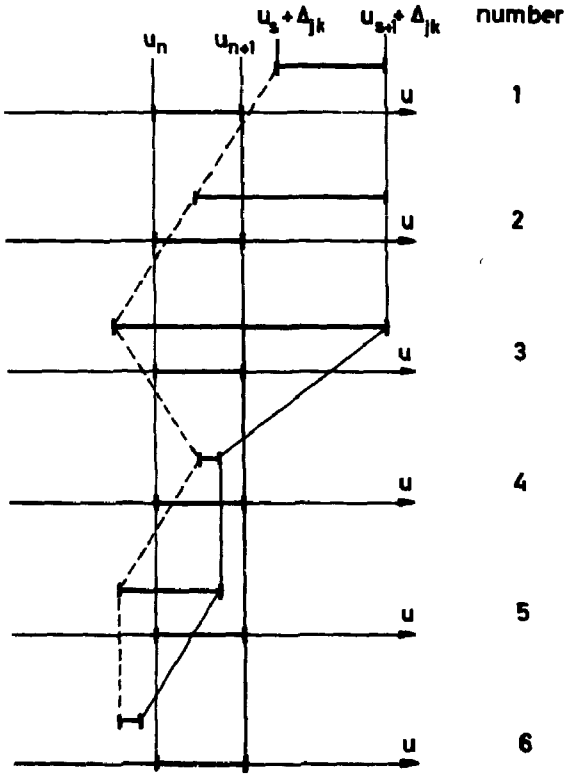

Fig. 5.1. The six possible relative positions of the boundaries of group numbers n and s.

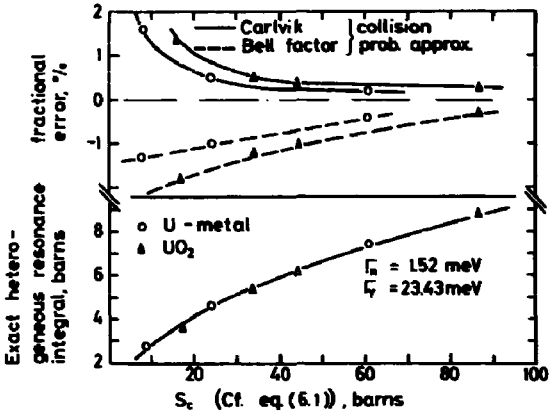

Fig. 6.1. The ^{238}U resonance at 6.68 eV. Investigation of the accuracy of two equivalence principles. "1/v-tail" subtracted.

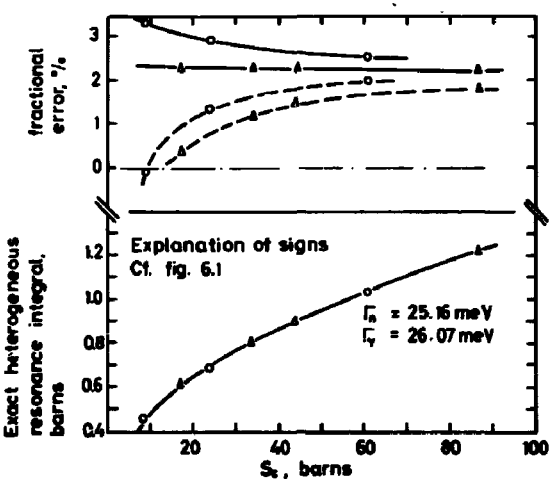

Fig. 6.2. The ^{238}U resonance at 66.90 eV. Investigation of the accuracy of two equivalence principles. "1/v-tail" subtracted.

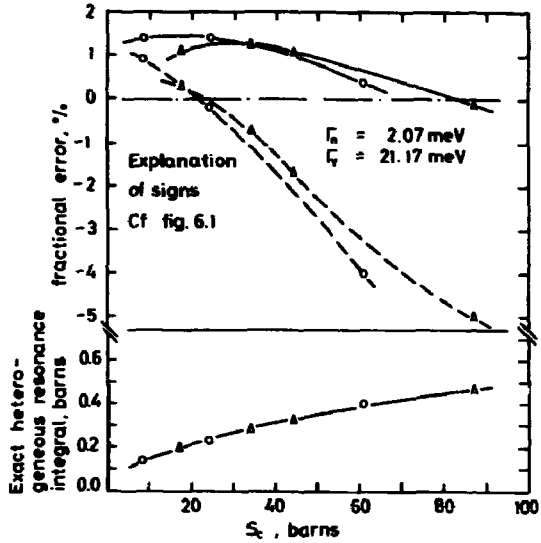

Fig. 6.3. The ^{238}U resonance at 80.77 eV. Investigation of the accuracy of two equivalence principles. "1/v-tail" subtracted.

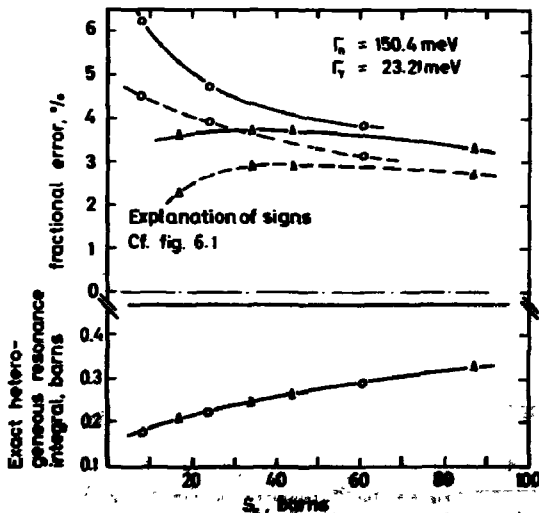

Fig. 6.4. The ^{238}U resonance at 190.36 eV. Investigation of the accuracy of two equivalence principles. "1/v-tail" subtracted.

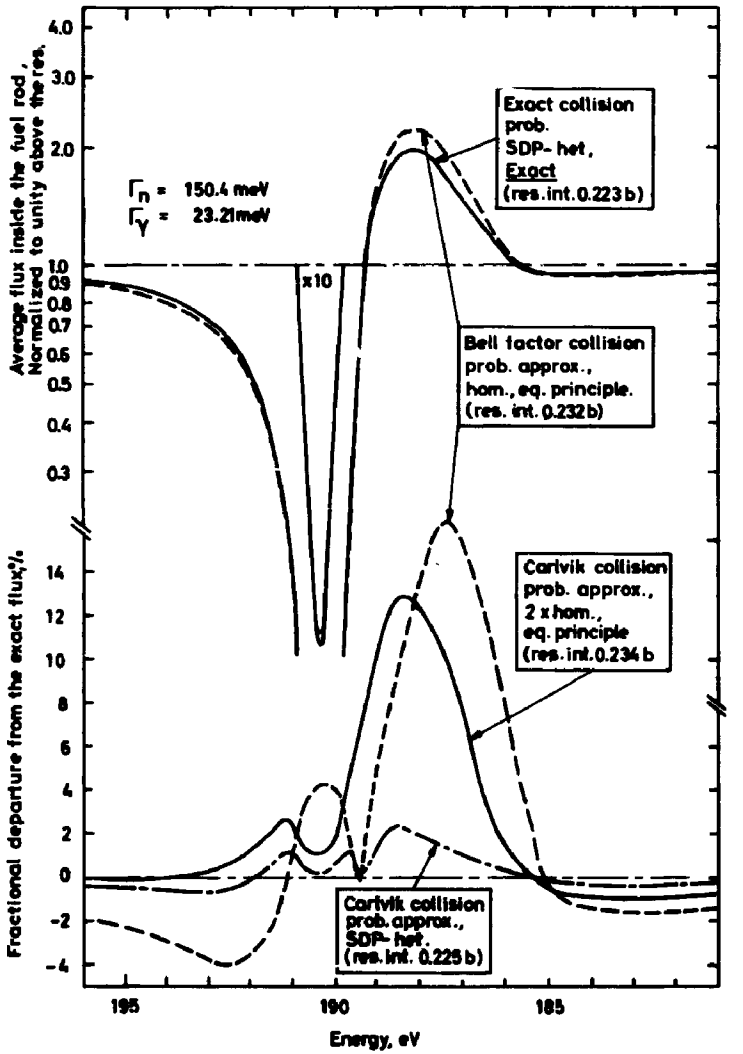

Fig. 6.1. The ^{238}U resonance at 189.84 eV. Investigation of the flux shape involved in different approximations.

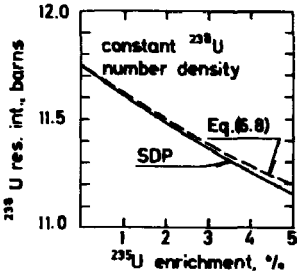

Fig. 6.6. The influence of ^{235}U on the ^{238}U resonance integral. U-metal. Rod radius: 0.5 cm.

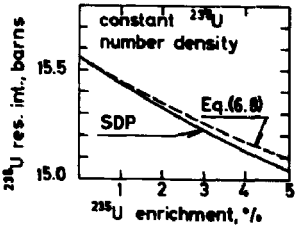

Fig. 6.9. The influence of ^{235}U on the ^{238}U resonance integral. UO_2. Rod radius: 0.625 cm.

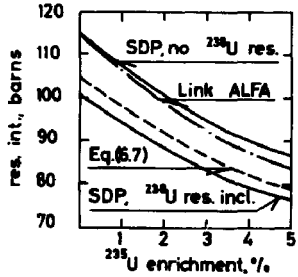

Fig. 6.7. ^{235}U capture resonance integral. U-metal. Rod radius: 0.5 cm.

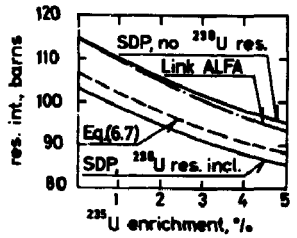

Fig. 6.10. ^{235}U capture resonance integral. UO_2. Rod radius: 0.625 cm.

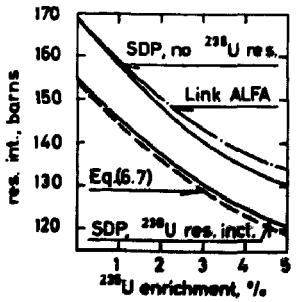

Fig. 6.8. ^{235}U fission resonance integral. U-metal. Rod radius: 0.5 cm.

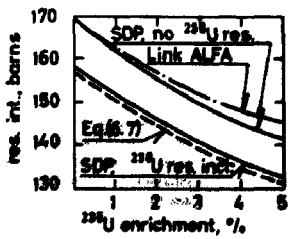

Fig. 6.11. ^{235}U fission resonance integral. UO_2. Rod radius: 0.625 cm.

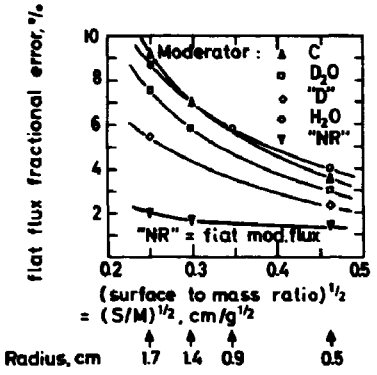

Fig. 7.1. The accuracy of the flat flux approximation. Isolated ^{238}U-metal rods considered in the interval 1200-0.5 eV. Isotropic scattering.

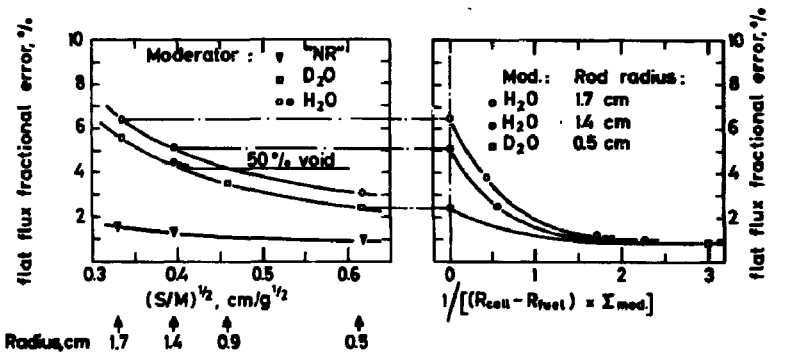

Fig. 7.2. The accuracy of the flat flux approximation. Isolated $^{238}UO_2$ rods considered in the energy interval 1200-0.5 eV. Isotropic scattering. A single point indicates the influence of the external moderator density.

Fig. 7.3. The accuracy of the flat flux approximation. Non-isolated $^{238}UO_2$ rods considered in the interval 1200-0.5 eV. Isotropic scattering.

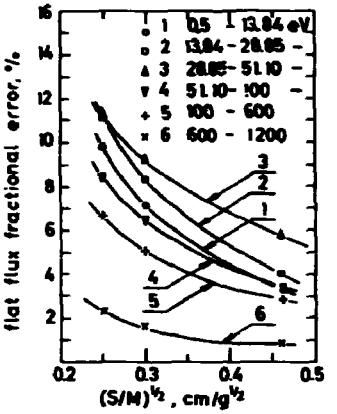

Fig. 7.4. The accuracy of the flat flux approximation in a series of energy intervals. Resonance overlap effects across group boundaries have been taken into account. The rods, which are isolated, consist of ^{238}U-metal, and the moderator is graphite.

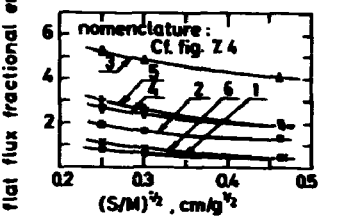

Fig. 7.5. The accuracy of the flat flux approximation inside an isolated absorbing rod. The outer moderator is treated by the NR approximation (flat flux). Rod material: ^{238}U-metal.

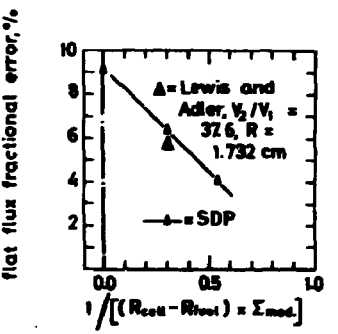

Fig. 7.6. The accuracy of the flat flux approximation in U-graphite lattices. Fuel rod radius r = 1.7 cm in ... (1380-0.5 eV).

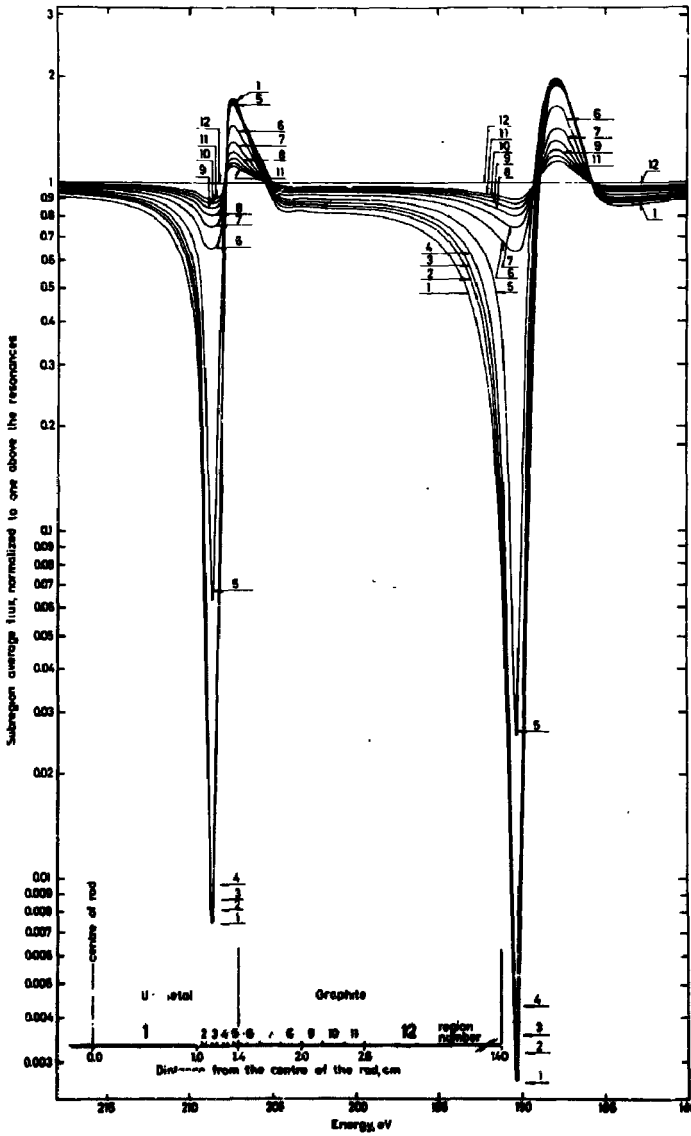

Fig. 7.7. Spatial flux distribution in an energy interval containing two predominantly scattering resonances.

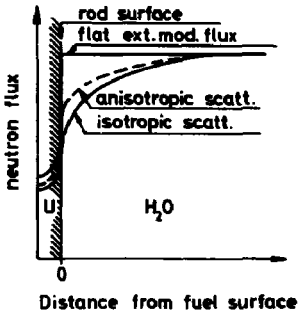

Fig. 7.8. Illustration of the effect of anisotropic external moderator scattering when the rod is isolated. The figure shows the flux profile at an energy where the influence of a neighbouring resonance is still considerable.

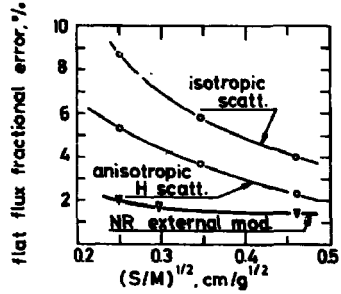

Fig. 7.9. The importance of the anisotropic hydrogen scattering when the external moderator is light-water. The rods considered are isolated ^{238}U-metal rods (1200-0.5 eV).

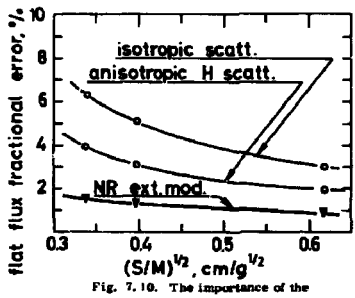

Fig. 7.10. The importance of the anisotropic hydrogen scattering (ext. mod.: H_2O). The rods considered are isolated UO_2 rods (1200-0.5 eV).

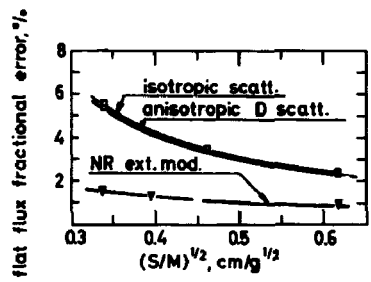

Fig. 7.11. The influence of anisotropic deuterium scattering (ext. mod.: D_2O, rod material: $^{238}UO_2$, 1200-0.5 eV).

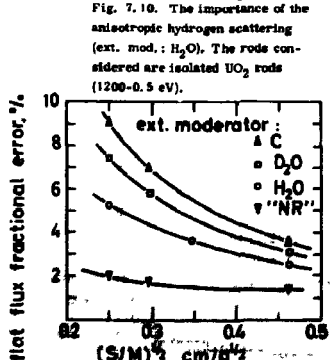

Fig. 7.12. The accuracy of the flat flux approximation if the [illegible] is taken into account. Isolated [illegible] rods (1200-0.5 eV).

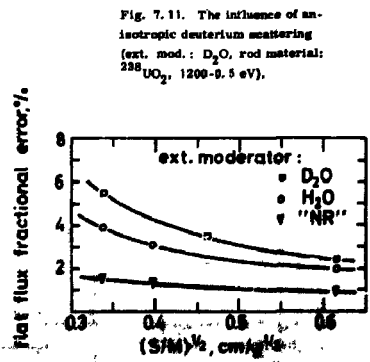

Fig. 7.13. The accuracy of the flat flux approximation if the anisotropic hydrogen scattering is taken into account. Isolated $^{238}UO_2$ rods (1200-0.5 eV).

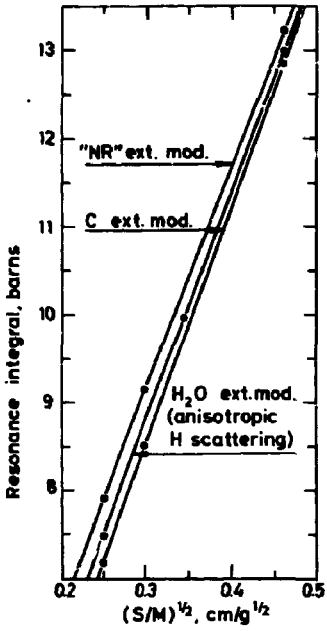

Fig. 7.14. ^{238}U-metal isolated rod resonance integral below 1200 eV (incl. 1/v capture above 0.5 eV).

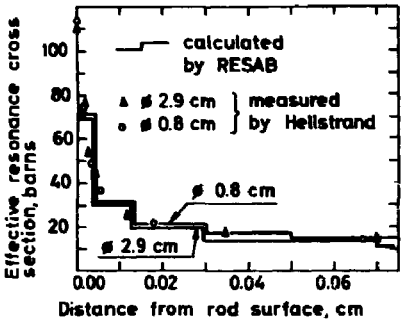

Fig. 7.15. The variation of the ^{238}U-metal resonance integral just below the rod surface.

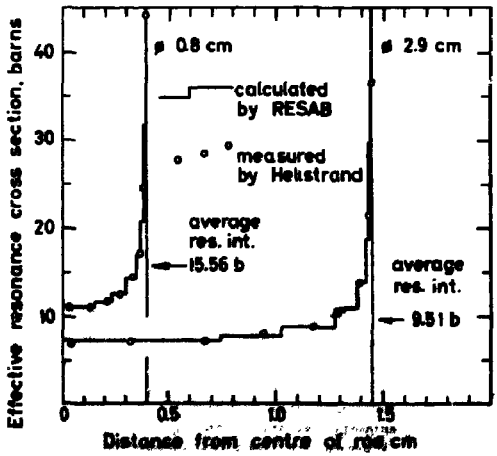

Fig. 7.16. The spatial distribution of the effective resonance absorption for isolated ^{238}U-metal rods.

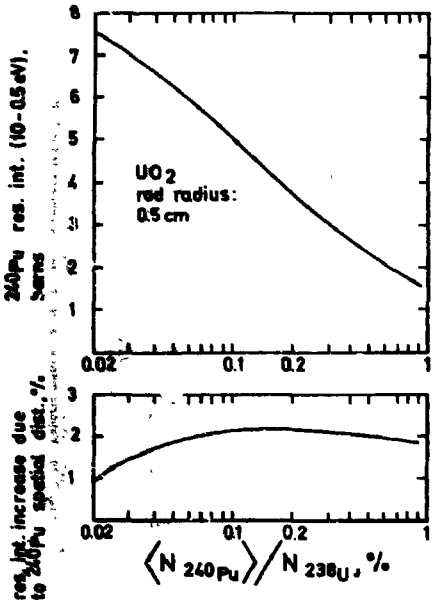

Fig. 7.17. Comparison between the ^{240}Pu resonance integral calculated with non-uniform plutonium distribution and the resonance integral obtained with homogeneous fuel (the first is the greater).

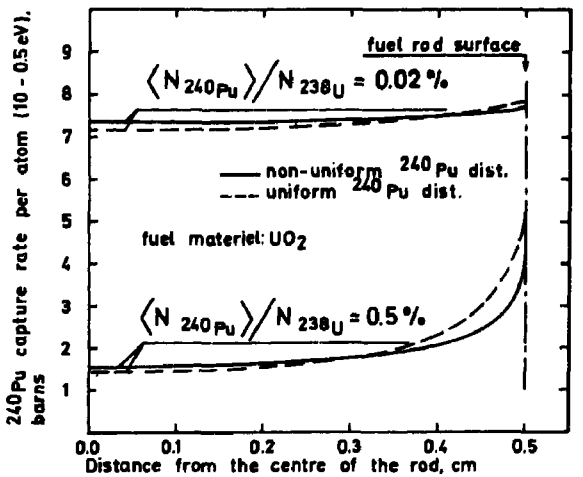

Fig. 7.18. Spatial distribution of ^{240}Pu resonance capture when the fuel material is homogeneous and when the ^{240}Pu concentration is largest at the fuel surface.

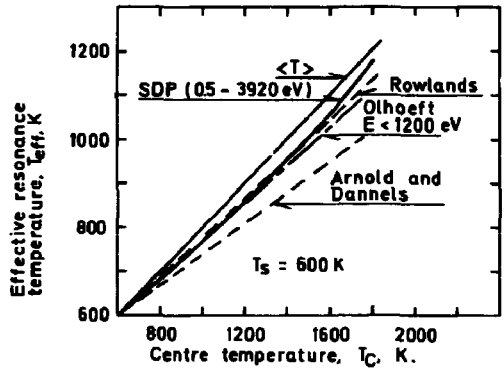

Fig. 7.19. The effective resonance temperature for a UO_2 fuel rod (radius = 0.5 cm). The surface temperature is fixed at 600 K.

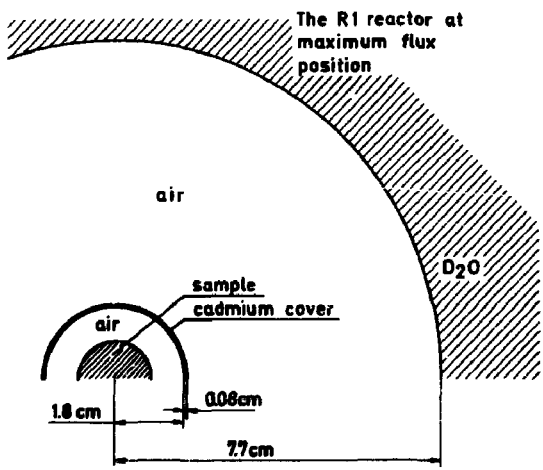

Fig. 7.20. Experimental arrangement as it is represented in SDP.

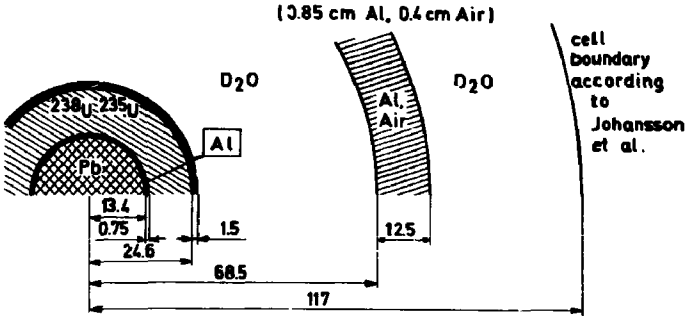

Fig. 8.1. The experimental arrangement of Johansson et al. as it is represented in SDP.

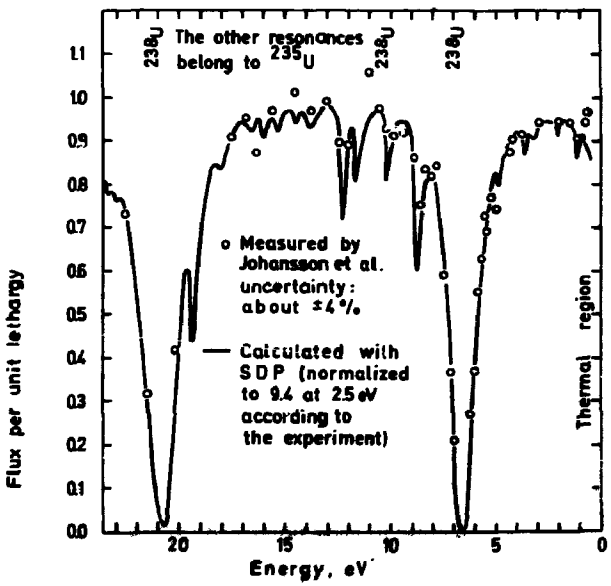

Fig. 8.2. The flux within the lead reflector indicated in fig. 8.1.

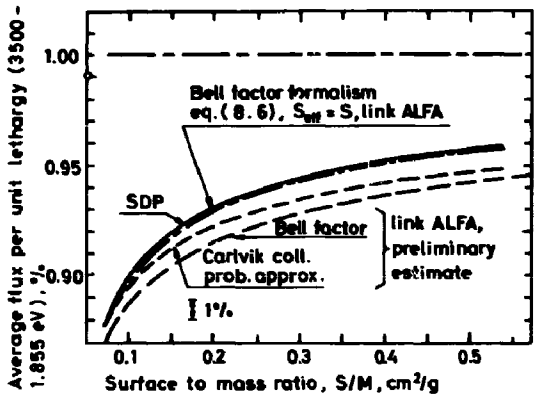

Fig. 8. 3. Different approximations for the average flux within an isolated ^{238}U-metal rod. The flux is normalised to one above the resonance region.

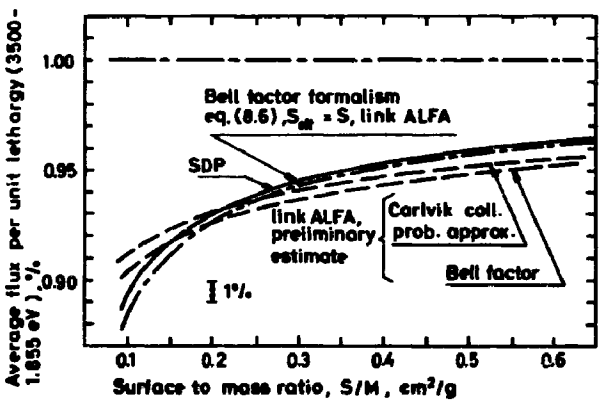

Fig. 8. 4. Different approximations for the average flux within an isolated $^{238}UO_2$ rod. The flux is normalised to one above the resonance region.

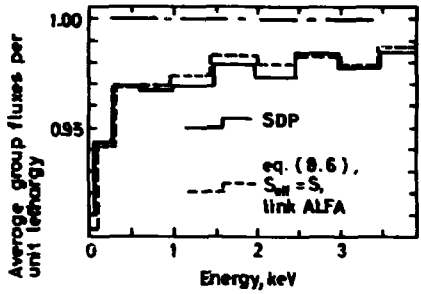

Fig. 8.5. Average group fluxes in the keV region. Only s-wave resonances are included. The rod material is $^{238}UO_2$, and the radius of the rod is 0.85 cm (E > 1.855 eV).

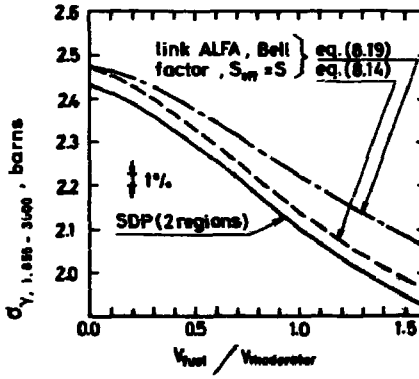

Fig. 8.6. The effective ^{238}U capture cross section in the group 1.855-3600 eV. Rod radius: 0.825 cm. The rod material is UO_2, and the moderator is ^1H_2O (ρ = 1.0 g/cm^3).

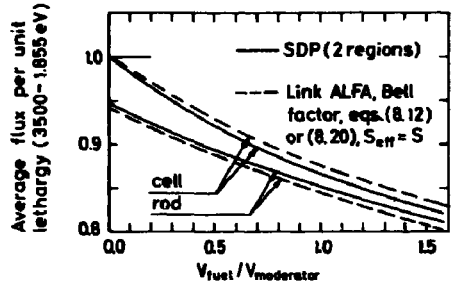

Fig. 8.7. Average flux in cell and rod. Rod radius: 0.625 cm. The rod material is $^{238}UO_2$, and the cell is H_2O moderated ($\rho = 1.0$ g/cm^3). The flux is normalized to one above the resonance region, and only s-wave resonances are considered.

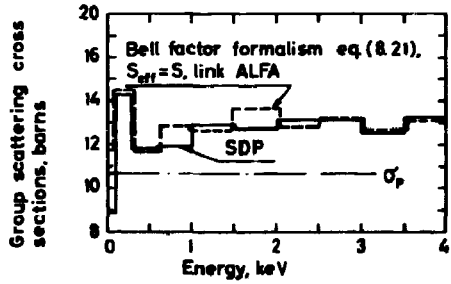

Fig. 8.8. The effective ^{238}U group scattering cross sections. An isolated UO_2 rod with a radius of 0.55 cm is considered. Only s-wave resonances are included ($E > 1.855$ eV).

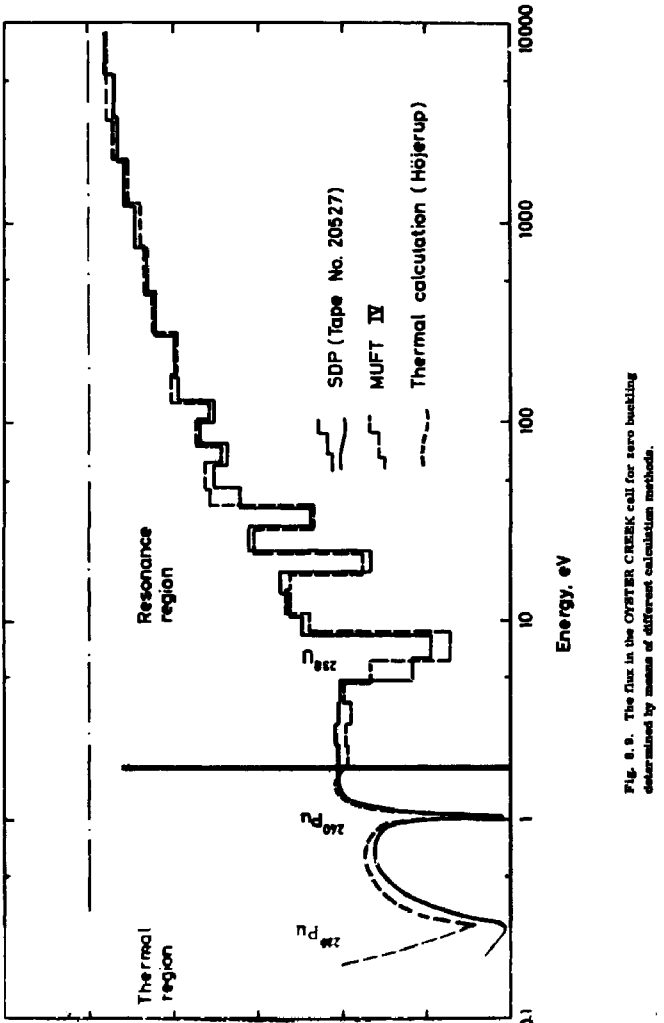

Fig. 8.8. The flux in the OYSTER CREEK cell for zero buckling determined by means of different calculation methods.

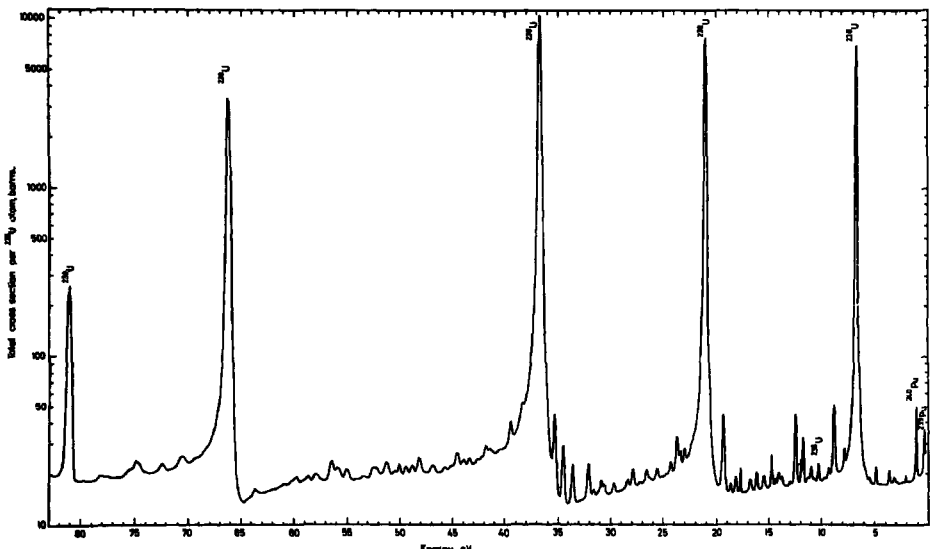

Fig. 8.10. The total cross section per ^{238}U atom of an OYSTER CREEK fuel rod at an irradiation of 5098 MWD/TU initial enrichment: 2.94 %.

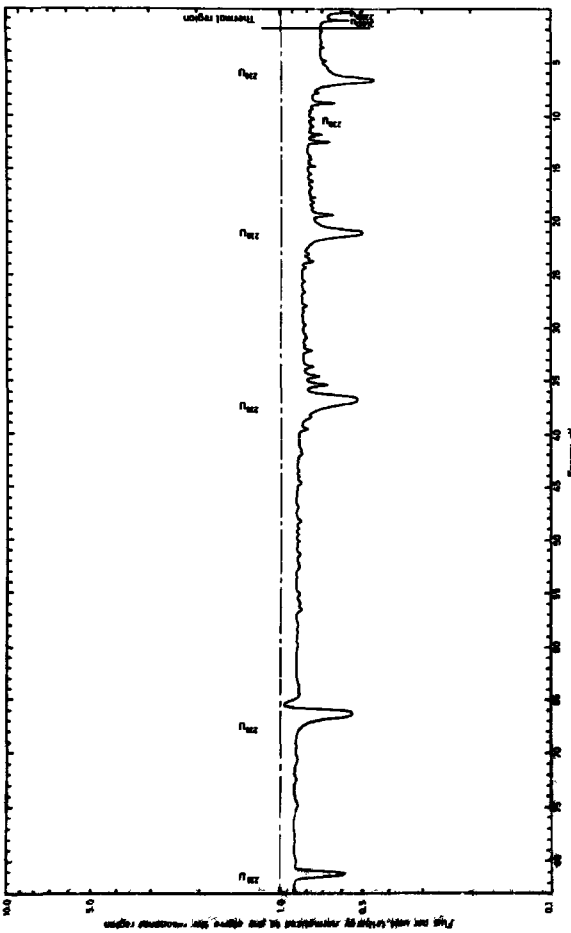

Fig 6.11 The moderator flux spectrum in the reactor cell with the cross section which appears from fig 6.10 (5098 MWD/TU)

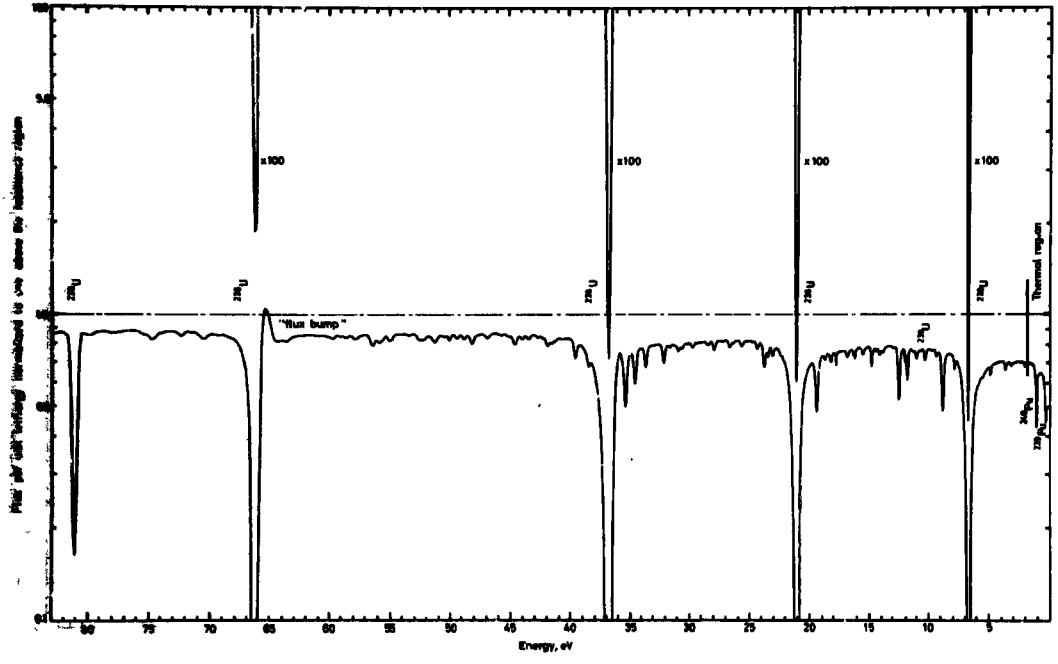

Fig. 8.12. The flux spectrum inside the rod with the cross section shown in fig. 8.10 (5098 MWD/TU).

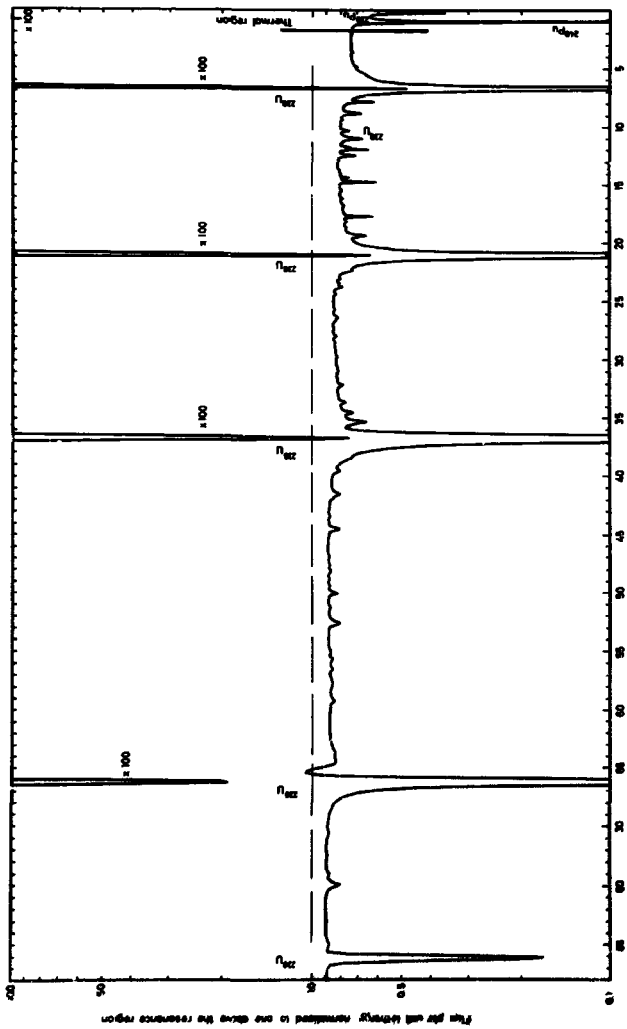

Fig. 6.13. Flux spectrum within the OYSTER CREEK fuel rod at 34000 MWD/TU (initial enrichment : 2.94 % in ^{235}U)